CHARACTERIZATIONS AND DESIGN OF PLANAR OPTICAL WAVEGUIDES AND DIRECTIONAL COUPLERS BY TWO-STEP K^+-Na^+ ION-EXCHANGE IN GLASS

Jacques Albert, M.Sc.

Department of Electrical Engineering
McGill University, Montreal
October 1987

A thesis submitted to the Faculty of Graduate Studies and Research in partial fulfillment of the requirements for the degree of Doctor of Philosophy

Cette thèse est dédiée à François Albert ainsi qu'à ma conjointe Pascale

ABSTRACT

Planar optical waveguides fabricated by K^+-Na^+ ion-exchange in soda-lime glass substrates are investigated.

Experimental characterizations of planar waveguide with respect to a wide range of fabrication conditions have been carried out, including detailed measurements of the refractive index anisotropy resulting from the large induced surface stresses.

Parallel to this, the non-linear diffusion process of ion-exchange was simulated numerically to provide, along with the results of the characterizations, a complete description of the refractive index profile from any set of fabrication conditions.

The magnitude of the maximum surface index change observed was shown theoretically to be almost entirely due to the induced stress at the surface of the substrate, arising from the presence of the larger potassium ions.

Finally, a novel class of single-mode channel waveguides, made by a "two-step" ion-exchange was analyzed. A simple model for these waveguides was developed and used in the design of two directional coupler structures which were fabricated and measured.

The two-step process was conceived because it relaxes waveguides' dimensional control, yielding single-mode guides of larger size, better suited for low-loss connections to optical fibers. It also provides an additional degree of freedom to adjust device properties.

RESUME

La fabrication de guides optiques planaires par échange d'ions potassium-sodium dans un substrat de verre soda-calcique est étudiée.

On a effectué une caractérisation expérimentale des guides planaires dans une gamme de conditions de fabrication, incluant des mesures détaillées de la birefringence causée par les tensions surfaciques induites par ce procédé.

Parallèlement, les equations non-linéaires de diffusion décrivant l'échange d'ions ont été résolues numériquement pour fournir une description complète du profile d'indice en fonction des variables expérimentales.

Il a été démontré que l'augmentation maximale d'indice observée est dûe presque exclusivement aux tensions induites en surface par les différences de taille entre les ions échangés.

Finalement, une nouvelle classe de guides monomodes, fabriqués par un échange à "deux-étapes", a ete analysée. Un modèle simple pour ces guides a été développé et utilisé pour le design de deux structures de couplage directionnel qui ont été fabriquées et mesurées.

Les guides monomodes fabriqués par ce procédé "deux-étapes", conçu pour relaxer les tolérances dimensionnelles de fabrication, peuvent avoir de plus grandes dimensions, facilitant ainsi le couplage avec d'autres guides ou fibres. Cela permet aussi l'ajustement des propriétés des éléments construits grâce au degré de liberté additionnel introduit.

ACKNOWLEDGEMENTS

I wish to thank my supervisor, Professor Gar Lam Yip, for his encouragement and support during the course of this work, and especially for his thoroughness in revising the first draft of this thesis.

I must also mention the contribution of my fellow students, who helped me through many fruitful discussions. In particular, Dr. Michel Belanger, on the technical side, and Mssr. Robert Osborne, Chunmeng Wu and Jingwen Jiang for the theoretical and computational aspects, provided helpful suggestions at various points of this project.

Both the technical and secretarial staff provided me with their usual friendly effectiveness, making my stay at McGill all the more pleasant in the process.

Finally, all of this would certainly not have been possible without the constant support and stimulation of my spouse, Pascale (and of her family, who had to bear with me for extended periods of time during the preparation of the thesis).

Financial support from NSERC, in the form of an Operating Grant, a Strategic Grant, and a Postgraduate Scholarship are also acknowledged.

TABLE OF CONTENTS

LIST OF TABLES AND FIGURES

PRELIMINARY NOTES

References are cited by the last name of the first author only, along with the year of publication (e.g. [Beaulieu 1991]).

Vector quantities are identified by bold type characters, and so are matrices.

CHAPTER 1. INTRODUCTION

1.1 BRIEF HISTORICAL OVERVIEW

With the arrival of low-loss optical fibers in the early seventies [Kapron 1970], a need has developed for optical waveguiding circuits to perform several functions [Tien 1977, Kogelnik 1983]. These functions can be separated into two broad classes.

First, the active devices, in which an externally controlled parameter can modify the function. These include mainly modulators and switches [Hammer 1979, Schmidt 1983], and to some extent, integrated sources and detectors [Garmire 1979]. Then, the passive devices, whose function is fixed and cannot be controlled. Power splitters, waveguide couplers, tapers, and wavelength division (de-)multiplexers belong to that class [Auracher 1983, Tangonan 1983, Schmidt 1983].

In both of these classes, a further distinction must be made between multimode and single-mode systems. Early optical fibers had core areas much larger than the wavelength of light used (typically 50-100 μm core diameters vs 0.5-1.5 μm wavelength). Such waveguides can support many guided modes, each with its own transverse modal field profile and propagation constant. However, due to the limitations in their information-carrying capacity, these are gradually replaced by single-mode fibers, in which only one mode can propagate. This property is achieved

through much smaller core dimension (typically 5-10 μm diameter).

In this work, we will concentrate on single-mode passive waveguiding circuits made by a planar technology in glass.

For recent overviews on these topics, see the references listed at the beginning of the References Section.

1.2 GENERAL GOAL

Glass provides an ideal substrate for waveguiding components to be used in conjunction with optical fibers because of the similarity in material properties (the high transparency of glass and its physical stability being the primary reason for its use in the first place).

Fresnel losses can be minimized between the two types of waveguides and matching of their respective refractive index profiles will eventually lead to very small input/output coupling losses. This is a critical problem because of the small sizes involved and because fibers are circularly symmetric while planar guiding structures are more or less rectangular.

In fact, some of the most successful single-mode devices in recent years have been realized with all-fiber systems, without coupling the light in and out of a separate waveguiding circuit [Bergh 1980, Kawasaki 1977]. However, these approaches are not easy to implement economically for large scale fabrication and the cost of individual devices remain high (20-200$ as of this writing).

On the other hand, the patterning of a circuit on a flat substrate by deposition, photolithography, and diffusion is easily amenable to economical batch production on a large scale, all processes having been well developed for the micro-electronics industry. One of the most successful methods of waveguide fabrication on glass has been ion-exchange, which was initially explored for that purpose by Izawa and Nakagome in 1972 and Giallorenzi et al. in 1973, and recently reviewed in Findakly 1985. A full description is provided in Chapter 2.

1.3 ION-EXCHANGE IN GLASS

The process of ion-exchange lends itself readily to both multimode and single-mode waveguide fabrication although the specific methods differ slightly in each case. For multimode applications, larger sizes (tens of microns) and large index change (>5%) are preferred to increase the numerical aperture of the waveguides [Adams 1981]. The ionic species that satisfy those criterion are silver-sodium (Ag^+-Na^+) and thallium-sodium (Tl^+-Na^+) [Findakly 1985], although they both suffer from some disadvantages related to permanence (for silver) or toxicity (for thallium). To achieve greater thicknesses, an electric field can be used to accelerate the ion-exchange [Izawa 1972, Chartier 1978, Forrest 1986].

On the other hand, for single-mode waveguides, it is preferable to have a slower process, which is more controllable

for layers of the order of a few microns at the most, and a smaller index change. The exchange of potassium for sodium (K^+-Na^+) is a better process in this case although some efforts have been made to adapt the Ag^+-Na^+ process. In one of these, a diluted melt of $AgNO_3$ in $NaNO_3$ was used to reduce the amount of available silver ions [Stewart 1978], while in another, the silver ions were released gradually in the melt by electrolysis [Lagu 1984]. Both of these methods succeeded in reducing the index change and the speed of the process, but they introduce additional complexity in the fabrication, and the question of increased losses with time (due to the formation of atomic silver), has not been completely resolved [Findakly 1985].

In spite of its fairly widespread use for experimental work [Findakly 1982, Honda 1984, Haruna 1984, Yip 1984, Jackel 1985, Okamura 1985, Garmire 1986], very little data has been published on the exact waveguiding properties of waveguides made with the K^+-Na^+ process [Aksenov 1982, Finak 1982, Chartier 1983, Findakly 1985]. This is in contrast with the case of Ag^+-Na^+ exchange which has been the subject of at least two very detailed characterizations of its planar waveguiding properties [Stewart 1977, Griffiths 1981].

When this work was undertaken, such an exhaustive characterization was needed for the K^+-Na^+ exchange. It constituted the starting point of this thesis.

1.4 PRESENTATION OF THE WORK

The goal of a planar waveguide characterization is to determine how waveguiding properties are related to fabrication conditions. The first step is to fabricate a series of planar waveguides in different conditions of duration and temperature, and to measure them (as explained in Chapter 3), using a commonly available type of a substrate glass with a high sodium content. This makes it possible to determine, with the greatest accuracy possible, the magnitude and depth of the refractive index change as a function of the process parameters, in the form of practical design formulas (Chapter 4).

Parallel with this, a theoretical investigation was needed to determine the shape of the induced index change. This is because it is very difficult to measure this profile with the required sub-micron resolution or to infer it from mode index measurements, for these very shallow waveguides supporting at most only a few modes. One of the standard methods of profile reconstruction from mode index measurements is only accurate when many modes are measurable [White 1976], and physical measurement by interferometry [Martin 1974] or with ionic concentration probes [Giallorenzi 1973, Ramaswamy 1986], lack the necessary resolution.

A study, based on the theory of the ion-exchange process, has been made for the Ag^+-Na^+ case [Wood 1976, Stewart 1977], and demonstrated that a second-order polynomial function

provides a good empirical fit to the profile. However, these results were taken by other authors [Okamura 1985] as representative of the potassium case also, while preliminary results of our characterization indicated that a Gaussian function provided an excellent fit of the profile. In order to clear this point, we set out to solve numerically the exact non-linear diffusion equation of ion-exchange and established how the shape of the index change depends on the substrate glass and the ionic species involved (Chapter 2).

In addition to these results, another topic needed clarification with respect to the magnitude of the index change resulting from the K^+-Na^+ exchange. A very accurate model for the refractive index determination from glass composition yielded an index change that was two orders of magnitude lower than measured values [Gortych 1986a,b]. To explain the discrepancy, the effect of induced stress [Kistler 1962], already known to be responsible for the birefringence observed in these waveguides [Zienko 1979, Bradenburg 1986], was calculated (Chapter 5). With the addition of the stress contribution, the experimental values of index change agree very well with the model predictions. In fact, the index change is shown to be almost entirely due to the presence of stress. This is a very significant new development in the understanding of the mechanical and thermal properties of these waveguides.

With the problem of planar waveguides taken care of, the next step is a study of the single-mode channel waveguides in which light is confined laterally as well as in the depth. Such ion-exchanged channels have been used often for device work [Findakly 1982, Walker 1983a, Cullen 1984, Honda 1984, Haruna 1985], but very few analyses of their exact shape and propagation properties have been published [Walker 1983b, Cullen 1986]. All of these used the simple structure consisting of an isolated channel defined by ion-exchange through a narrow aperture.

In this work, it was decided that a more novel structure would be used, fabricated by a two-step ion-exchange method [Yip 1984, and Hinkov 1982 or Chartier 1986 for variants]. With this method, the channel waveguide is surrounded by a slightly shallower planar guide resulting from a second exchange over the whole substrate with the mask removed.

It has two distinct advantages over single-step guides because the lateral index gradient can be diminished at will. Firstly, this allows the fabrication of single-mode guides of much wider dimensions, thereby relaxing fabrication tolerances and facilitating input-output coupling to other waveguides or fibers without the need for tapered matching sections. Secondly, the propagation constant and mode profile can be adjusted by changing the depth of the surrounding planar guide. This allows for the fine tuning of the performance of waveguiding devices to

compensate for design or fabrication inaccuracies. The main advantage of this method of lateral waveguiding control over the alternative approach of depositing a planar cladding on top of the substrate is that it does not require any additional high vacuum processing and is extremely precise.

In order to be able to understand the waveguiding properties of these guides, their exact index profile was calculated numerically from the two-dimensional ion-exchange diffusion equation (Chapter 2). Then, the problem of electromagnetic wave propagation inside these structures could be solved. This is a rather difficult task which has no analytical solutions due to the complicated shape of the index profile. However, various approximate numerical or semi-analytical methods are available.

In Chapter 6, a semi-analytical method is developed to allow a full characterization of channel guides from data derived exclusively from planar guide measurements. A comparison with a matrix variational numerical method, whose precision can be increased by using larger dimensions, confirms the accuracy of the model developed.

But channel guides by themselves serve only limited purposes. The goal of this whole endeavour is the realization of optical circuits using the channel guides. One particularly useful basic structure is the directional coupler [Marcatili 1969, and for its uses: Cochrane 1986]. Besides its basic power

splitting properties, it can be used as a wavelength multi/demultiplexer, or as a very narrow bandpass filter [Kogelnik 1983]. Furthermore, it has the potential to be used as a switch when the substrate glass is doped with semiconductor impurities [Cullen 1986]. Previous work in this area include [Walker 1983c, Yip 1984, Schlaak 1986].

It was therefore decided that a directional coupler would be designed and fabricated. The purpose in doing so is two-fold: first, to verify the accuracy and usefulness of the model developed in chapter 6 for the design of more complex structures; and second, to justify the claims that were made about the advantages of the two-step method for device fabrication.

Chapter 7 presents the analysis of general directional coupler structures as extensions to the single-mode and single waveguide case. The full problem is discussed, including practical input and output sections to the basic coupling element.

Finally, the actual design of two directional couplers is presented in Chapter 8, along with experimental measurements of the fabricated devices.

A brief review of the whole work and prospects for future developments are presented in the conclusion.

1.5 OUTLINE OF ORIGINAL CONTRIBUTIONS

The original contributions of this work to the advancement of knowledge in this fast moving field are summarized below:

- the detailed characterization of planar K^+-ion exchange in glass, including measurements of the refractive index anisotropy [Yip 1985, 1986]

- the quantitative demonstration of the relation between the profile of index change and the individual ion species and substrate glass [Albert 1985]

- the quantitative explanation of the magnitude of the index change resulting from the substitution of potassium for sodium in glass, highlighting the significant contribution of surface induced stress [Albert 1987b]

- the analysis of wide single-mode channel waveguides made by two-step ion-exchange in glass [Albert 1987c]

- the analysis (dispersion curves and modal fields), design and fabrication of a working directional coupler, with adjustable power transfer characteristics [Albert 1987a, 1986].

CHAPTER 2. THE ION EXCHANGE PROCESS

2.1 BASIC PRINCIPLES

2.1.1 Glass composition

A typical soda-lime glass is composed of 71-75% silicon dioxide (SiO_2), 12-16% sodium oxide (Na_2O), 5-15% calcium oxide (CaO), and smaller amounts of various other oxides depending on the exact type of glass (K_2O, Al_2O_3, MgO, etc..)[Pfaender 1983, Doremus 1973, Shand 1955]. It was found a long time ago [Schulze 1913], that, under certain conditions, it is possible to replace some of the ions present in the glass by other ions of equal valence. Sodium in particular has been found to be easily displaced by other monovalent ions (Ag^+, K^+, Li^+). The new ions thus introduced in the glass occupy the same sites as the ions that they replaced since the exchange is on a one-to-one basis. Of course, the properties of glass change in the regions where such exchange has taken place.

More specifically, different ions have different polarizabilities and sizes. This leads, among other effects, to a local change in the refractive index which can be used to guide light by total internal reflection if the exchanged layer has the suitable dimensions and shape. Both the Ag^+-Na^+ and K^+-Na^+ exchanges have been used to make useful optical waveguides in glass by an increase in the refractive index relative to the substrate index. The exact relation between the index change and the concentration of new ions in the glass is

fairly complex but it is generally believed that the two are proportional [Walker 1983b]. This assumption will be used here for the time being, but the derivation of an exact relationship will be discussed in Chapter 5, after the results of our characterization of the K^+-Na^+ process have been presented.

2.1.2 Explanation of the ion-exchange process

Qualitatively, ion-exchange proceeds as follows. A glass substrate containing Na^+ ions is immersed in a molten salt containing chemically similar ions, which will be K^+ here, for example. At the glass-melt interface, both ion concentrations initially drop suddenly from finite values to zero. This is clearly a non-equilibrium situation since K^+ and Na^+ ions are almost perfectly interchangeable in both the melt and the glass. Therefore, thermal agitation at the interface produces random collisions in which one K^+ ion replaces one Na^+ ion, and this process gradually diffuses away from the interface. Of course, in the melt, the Na^+ ions move much more rapidly away from the surface (and are "lost" in what can be considered an infinite reservoir of K^+ ions) than the K^+ ions in the glass, which slowly invade a very thin layer near the surface of the substrate. The process accelerates at higher temperatures because of stronger thermal agitation and also because the glass matrix, through which these ionic motions take place, is less rigid.

When the glass is lifted out of the melt, but kept at a high temperature, the exchange continues without a supply of new K^+ ions. The result is that the ions, which are already in the glass, will tend to redistribute themselves in order to reach equilibrium (i.e. uniform concentration of both K^+ and Na^+ throughout the substrate) by moving in deeper but with decreasing surface concentrations. The process only stops (or rather becomes infinitely slow) when the source of heat is removed and the substrate allowed to cool towards room temperature. Typical exchange temperatures range from 200°C to 550°C and generally do not lie too much above the melting point of the salts used as sources of exchanging ions because excessive heat may lead to damage of the surface of the substrate due to nitrate decomposition and excessive thermal motions [Bartholomew 1980]. The resulting concentration profile has a maximum at the surface and decreases monotonically inside the substrate because of the configuration and nature of the process.

For the specific case of ion-exchange in soda-lime glasses from nitrate melts, it has been established [Doremus 1973] that the preferred ion-exchangers are silver (Ag^+) and potassium (K^+) in that order. In fact, Ag^+-Na^+ exchange occurs significantly faster [Chartier 1983] and yields a larger index change than K^+-Na^+, and is, therefore, more suitable for deep and highly multimoded waveguides [Stewart 1977]. On the

other hand, for single-mode waveguides, the slower exchange rate and lower index change provided by working with potassium allows for easier control and greater repeatability (typical exchange durations for single-mode planar guides: 5-15 minutes for Ag^+ [Zienko 1979], 30 minutes to a few hours for K^+ [see Chapter 4].

Finally, the refractive index is not the only parameter of the glass that is modified by the exchange of ions. Very large stresses are induced near the surface due to the size difference in the ions [Kistler 1962]. These stresses have been known and studied for some time by the glass industry specialists for the purpose of strenghtening sheet glass. Their effect on the waveguiding properties of exchanged layers will be described in Chapter 5.

2.2 MATHEMATICAL MODEL FOR THE ION-EXCHANGE PROCESS

The change in the concentration c (number of ions per unit volume) of a given ionic species can be related to the flux of ions J by:

$$\frac{\partial c}{\partial t} = -\nabla \cdot J \qquad (2-1)$$

For the cases of mixed non-interacting substances diffusing freely and isotropically, the flux obeys Fick's first law [Crank 1956, 1975]:

$$J = -D\nabla c \qquad (2-2)$$

where D, the diffusion coefficient, is a parameter related

to the substances involved and the conditions under which the diffusion is taking place. It can actually depend on c. Substituting (2-2) into (2-1), we get Fick's second law:

$$\frac{\partial c}{\partial t} = \nabla\cdot(D\nabla c) \qquad (2-3)$$

which can be solved for c, given suitable initial and boundary conditions if D is known.

In the ion-exchange process, diffusion is no longer free but restricted by the condition that each incoming ion replaces an outgoing ion in a one-to-one fashion to preserve the global neutrality of the glass [Helfferich 1958]. Locally, however, since the two types of ions have different mobilities within the glass, one may tend to outrun the other. An electric field results which has the effect of restoring neutrality by equalizing the fluxes of the two ions. The contribution of this electric field to the flux can be evaluated as follows [Frederikse 1981]:

The ratio of the speed of the ions to the magnitude of the driving electric field is given by the mobility μ,

$$v_E = \mu E \quad \text{m/sec} \qquad (2-4)$$

and the mobility is related to the diffusion coefficient D by:

$$\mu = \frac{eD}{kT} \quad \text{m}^2/\text{Volt}\cdot\text{sec} \qquad (2-5)$$

where e is the elementary charge (1.6×10^{-19} Coul),

k is Boltzmann constant (1.38×10^{-23} J/^{o}K),

T is the temperature in ^{o}K.

Then,

$$J_E = cv_E = c\frac{eD}{kT}E \quad (m^2 \cdot sec)^{-1} \tag{2-6}$$

The total fluxes of ions become (with the subscripts a and b denoting K^+ and Na^+ ions respectively):

$$J_a = -D_a(\nabla c_a - \frac{e}{kT} c_a E) \tag{2-7}$$

$$J_b = -D_b(\nabla c_b - \frac{e}{kT} c_b E) \tag{2-8}$$

Neutrality requires:

$$J_a = -J_b \tag{2-9}$$

and

$$c_a + c_b = c_0 = \text{constant} \tag{2-10}$$

The constant c_0 is the concentration of Na^+ ions present in the glass prior to the exchange. Since K^+ ions replace Na^+ ions on a one-to-one basis the total concentration of $Na^+ + K^+$ remains c_0.

Substituting (2-10) into (2-8) and using (2-9) we get:

$$J_a = -D_a \left(\frac{c_a D_b + c_b D_b}{c_a D_a + c_b D_b}\right) \nabla c_a \tag{2-11}$$

From (2-11), we can define an effective diffusion coefficient D' by:

$$D' = \frac{D_a D_b (c_a + c_b)}{c_a D_a + c_b D_b} = \frac{D_a}{1-\left(1-\frac{D_a}{D_b}\right)\hat{c}_a} \quad m^2/sec$$

$$D' = \frac{D_a}{1 - \alpha \hat{c}_a} \tag{2-12}$$

with

$$\hat{c}_a = \frac{c_a}{c_a + c_b} \; ; \; \hat{c}_b = \frac{c_b}{c_a + c_b} = 1 - \hat{c}_a \tag{2-13}$$

and

$$\alpha = 1 - \frac{D_a}{D_b} = 1 - \frac{\mu_a}{\mu_b} \tag{2-14}$$

for the flux of K^+ ions from a KNO_3 melt into a glass where

they replace Na^+ ions. This leads to :

$$\frac{\partial \hat{c}_a}{\partial t} = \nabla\cdot(D' \nabla \hat{c}_a) = \nabla\cdot\left(\frac{D_a}{1-\alpha\hat{c}_a}\nabla\hat{c}_a\right) \qquad (2-15)$$

as our partial differential equation (PDE) describing ion-exchange.

2.3 SOLUTION OF THE ION-EXCHANGE DIFFUSION EQUATIONS

2.3.1 Planar ion-exchange: analytical solutions.

For the case of planar, or slab, waveguides, the exchange is performed without masking the substrate to define channels or desired structures. Since the diffusion reaches only a few microns' depth in a substrate of at least a few square millimeters, the process is essentially one-dimensional along the depth direction, labeled x. Setting the derivatives with respect to y and z to zero in (2-15), we get:

$$\frac{\partial \hat{c}_a}{\partial t} = \frac{\partial}{\partial x}\left(\frac{D_a}{1 - \alpha\hat{c}_a}\frac{\partial \hat{c}_a}{\partial x}\right) \qquad (2-16)$$

This is a non-linear PDE of second order in x and first order in t. Therefore, we need two boundary conditions in x and an initial condition in time. The spatial domain of integration is the substrate. At time zero, the concentration of new ions is zero.

$$\hat{c}_a(x,0) = 0 \qquad (2-17)$$

For the boundary conditions [Frischat 1975], we used a zero concentration at infinity and a fixed value of concentration at the surface since the mobility of the ions in the melt is sufficient to maintain a homogeneous and constant supply of new

ions, in spite of the temporary presence of the outdiffusing ions. It was observed [Doremus 1969, Frischat 1975, Cullen 1986] that for the K^+-Na^+ exchange, the maximum concentration of exchanged ions (occurring at the surface) is only a fraction h (around 0.9) of the total concentration of available Na^+:

$$\hat{c}_a(0,t) = h = \text{constant} \tag{2-18}$$

$$\hat{c}_a(\infty,t) = 0 \tag{2-19}$$

The constant "h" appearing in (2-18) represents the fraction of acceptor sites (Na^+) that are effectively participating in the exchange because of:

$$\hat{c}_a(0,t) = \frac{c_a(0,t)}{c_0} = h \tag{2-20}$$

and

$$c_0 = c_b(0,0) \tag{2-21}$$

so that

$$c_a(0,t) = hc_b(0,0)$$

Note that the last equation is only valid for $t > 0$, since $c_a(0,0) = 0$. It takes a short time for $c_a(0,t)$ to reach its equilibrium value, but it is negligible compared to the diffusion times used.

This completes the formulation of the problem. In order to begin its solution, we use a transformation, due to Boltzmann, to reduce (2-16) to an "ordinary differential equation" [Crank 1956, p. 148]:

$$\gamma = \frac{x}{2\sqrt{D_a t}} \tag{2-22}$$

then

$$\frac{\partial}{\partial x} = \frac{\partial}{\partial \gamma}\frac{\partial \gamma}{\partial x} = \frac{1}{2\sqrt{D_a t}}\frac{\partial}{\partial \gamma} \tag{2-23}$$

$$\frac{\partial}{\partial t} = \frac{\partial}{\partial \gamma}\frac{\partial \gamma}{\partial t} = \frac{-x}{4\sqrt{D_a t^3}}\frac{\partial}{\partial \gamma} \tag{2-24}$$

and (2-16) becomes:

$$-2\gamma\frac{d\hat{c}_a}{d\gamma} = \frac{d}{d\gamma}\left(\frac{1}{1-\alpha\hat{c}_a}\frac{d\hat{c}_a}{d\gamma}\right) \tag{2-25}$$

with

$$\hat{c}_a(\gamma = 0) = h \quad (t>0) \tag{2-26}$$

and

$$\hat{c}_a(\gamma = \infty) = 0 \quad (0<t<\infty) \tag{2-27}$$

Furthermore, let us renormalize $\hat{c}_a$ to have a more convenient boundary condition at $\gamma = 0$.

Putting

$$c = \frac{\hat{c}_a}{h} \; ; \; c(\gamma=0) = 1 \; ; \; c(\gamma=\infty) = 0 \tag{2-28}$$

and (2-25) becomes:

$$-2\gamma\frac{dc}{d\gamma} = \left(\frac{1}{1 - \alpha h c}\frac{dc}{d\gamma}\right) \tag{2-29}$$

where we see that (2-28) is equivalent to scaling α by h. In the following, $\hat{\alpha} = \alpha h$.

A parametric solution of equation (2-29) is presented in [Crank 1956, Ch.9] and detailed in Appendix A of this thesis. The result of the solution is shown below so that it can be used as a starting point for a more convenient power series expression for $c(\gamma)$, originally proposed by [Wood 1976]. In this solution, both c and γ are expressed as functions of a common parameter θ:

$$\gamma(\theta) = \frac{-1}{\sqrt{2\mu}}(\theta-(\theta^2-\mu\ln\theta^2)^{\frac{1}{2}})\exp\left(\int_0^{\theta}(\phi^2 - \mu\ln\phi^2)^{\frac{-1}{2}}\,d\phi\right) \tag{2-30}$$

$$c(\theta) = \frac{1}{\hat{\alpha}}\left(1 - \exp\left(-2\int_0^{\theta}(\phi^2 - \mu\ln\phi^2)^{\frac{-1}{2}}\, d\phi\right)\right) \qquad (2\text{-}31)$$

where μ is found by solving:

$$\ln(1 - \hat{\alpha}) = -2\int_0^{1}(\phi^2 - \mu\ln\phi^2)^{\frac{-1}{2}}\, d\phi \qquad (2\text{-}32)$$

Now since we are interested in a solution for $c(\gamma)$ in a very shallow layer below the surface of the substrate, we will seek for it in the form of a Taylor's series expansion near $\gamma = 0$:

$$c(\gamma) = c(0) + \left.\frac{dc}{d\gamma}\right|_{\gamma=0}\gamma + \frac{1}{2}\frac{d^2c}{d\gamma^2}\gamma^2 + \frac{1}{6}\frac{d^3c}{d\gamma^3}\gamma^3 + \ldots \qquad (2\text{-}33)$$

where the derivatives are evaluated with the help of (2-30) and (2-31):

$$\frac{dc}{d\gamma} = \frac{dc}{d\theta}\frac{d\theta}{d\gamma} = \frac{dc}{d\theta}\left(\frac{d\gamma}{d\theta}\right)^{-1} \qquad (2\text{-}34)$$

where

$$\frac{dc}{d\theta} = \frac{2}{\hat{\alpha}}(\theta^2 - \mu\ln\theta^2)^{\frac{-1}{2}}\exp\left(-2\int_0^{\theta}(\phi^2 - \mu\ln\phi^2)^{\frac{-1}{2}}\, d\phi\right) \qquad (2\text{-}35)$$

and

$$\frac{d\gamma}{d\theta} = -\frac{1}{\theta}\sqrt{\frac{\mu}{2}}(\theta^2-\mu\ln\theta^2)^{\frac{-1}{2}}\exp\left(\int_0^{\theta}(\phi^2-\mu\ln\phi^2)^{\frac{-1}{2}}\, d\phi\right) \qquad (2\text{-}36)$$

yielding finally:

$$\frac{dc}{d\gamma} = \left(\frac{-2\sqrt{2}\theta}{\hat{\alpha}\sqrt{\mu}}\right) \exp\left(-3\int_0^{\theta}(\phi^2-\mu\ln\phi^2)^{\frac{-1}{2}}\, d\phi\right) \qquad (2-37)$$

A similar calculation gives:

$$\frac{d^2c}{d\gamma^2} = \frac{4\theta}{\hat{\alpha}\mu}\left((\theta^2-\mu\ln\theta^2)^{\frac{1}{2}}\right) \exp\left(-4\int_0^{\theta}(\phi^2-\mu\ln\phi^2)^{\frac{-1}{2}}\, d\phi\right) \qquad (2-38)$$

and

$$\frac{d^3c}{d\gamma^3} = \frac{4\sqrt{2}\gamma}{\hat{\alpha}\mu\sqrt{\mu}}\left((4\theta - (\theta^2-\mu\ln\theta^2)^{\frac{1}{2}})((\theta^2-\mu\ln\theta^2)^{\frac{1}{2}} - 3\theta) - (\theta^2-\mu) - 3\right) *\ldots$$

$$\ldots * \exp\left(-5\int_0^{\theta}(\phi^2-\mu\ln\phi^2)^{\frac{-1}{2}}\, d\phi\right) \qquad (2-39)$$

The expressions (2-37) to (2-39) must be evaluated at $\gamma=0$. Therefore, the value of $\theta(\gamma=0)$ is needed. This is found by using formulae (A-33), (A-34) and (A-40) in Appendix A, yielding:

$$\theta(\gamma\rightarrow 0) \rightarrow 1 \tag{2-40}$$

and also by (2-32):

$$\int_0^{\theta=1} (\phi^2 - \mu\ln\phi^2)^{\frac{-1}{2}}\, d\phi = \frac{-1}{2}\ln(1-\hat{\alpha}) \tag{2-41}$$

Using these results, we get:

$$c(\gamma) = 1 + \left(\frac{-2\sqrt{2}}{\hat{\alpha}\sqrt{\mu}}(1-\hat{\alpha})^{\frac{3}{2}}\right)\gamma + \left(\frac{-4}{\hat{\alpha}\mu}(1-\hat{\alpha})^2\right)\gamma^2 + \left(\frac{2\sqrt{2}}{3\hat{\alpha}\mu\sqrt{\mu}}(1-\hat{\alpha})^{\frac{5}{2}}(\mu-4)\right)\gamma^3 + \ldots \tag{2-42}$$

which, along with the definition of γ:

$$\gamma = \frac{x}{2\sqrt{D_a t}} \tag{2-43}$$

fixes $c(x,t,D_a,\hat{\alpha})$, the normalized concentration profile. It is not necessary to know c_0, which would determine the magnitude of $c_a(0,t)$ because $\Delta n(x=0)$ is measured independently. This means that $\Delta n(x)$ can be obtained as $\Delta n(0)*c(x)$ since $c(x)$ is normalized to 1.

This result will be used in section 2.3.2 when we compare the profiles obtained for K^+-Na^+ ion-exchange with those resulting from Ag^+-Na^+ with the help of exact numerical solutions.

2.3.2 Planar ion-exchange: numerical solutions.

Starting again from (2-29) with conditions (2-28) (repeated here for convenience):

$$-2\gamma\frac{dc}{d\gamma} = \frac{d}{d\gamma}\left(\frac{1}{1-\hat{\alpha}c}\frac{dc}{d\gamma}\right) \qquad (2\text{-}44)$$

$$= \frac{1}{1-\hat{\alpha}c}\frac{d^2c}{d\gamma^2} - \frac{\hat{\alpha}}{(1-\hat{\alpha}c)^2}\left(\frac{dc}{d\gamma}\right)^2$$

$$c(0) = 1 \quad ; \quad c(\infty) = 0 \qquad (2\text{-}45)$$

One way of solving (2-44) numerically is to transform it into a system of first order equations [Conte 1980]:

$$\frac{dc}{d\gamma} = g \qquad (2\text{-}46)$$

$$\frac{dg}{d\gamma} = -2g\gamma(1-\hat{\alpha}c) - \frac{\hat{\alpha}g^2}{(1-\hat{\alpha}c)} \qquad (2\text{-}47)$$

with $c(0) = 1 \quad ; \quad c(\infty) = 0$ (2-48)

This system is fully determined (although non-linear) and can be solved. One problem remains, that of the boundary at infinity. It is handled by a mapping which transforms the $\gamma = [0,\infty]$ domain into a bounded region in $\rho = [0,1]$. The mapping is:

$$\rho = \frac{\gamma}{1+\gamma} \quad ; \quad \gamma = \frac{\rho}{1-\rho} \qquad (2\text{-}49)$$

and the derivative with respect to "γ" becomes:

$$\frac{d}{d\gamma} = (1-\rho)^2\frac{d}{d\rho}$$

so that (2-46)-(2-48) become:

$$\frac{dc}{d\rho} = \frac{g}{(1-\rho)^2} \qquad (2\text{-}50)$$

$$\frac{dg}{d\rho} = -2g(1-\hat{\alpha}c)\frac{\rho}{(1-\rho)^3} - \frac{\hat{\alpha}g^2}{(1-\hat{\alpha}c)(1-\rho)^2} \qquad (2\text{-}51)$$

with $c(0) = 1 \quad ; \quad c(1) = 0$ (2-52)

The system (2-50)-(2-52) is solved using a commercially available subroutine called DVCPR from the IMSL package on a grid of 60 points in the interval $\rho = [0,0.99]$ (corresponding to $\gamma = 0$ to 99). The program uses an implicit finite difference algorithm which is unconditionally stable (regardless of the grid spacing $\Delta\rho$).

The only parameter of the system is $\hat{\alpha}$. For K^+-Na^+ ion-exchange in soda-lime glass, the ratio of the mobilities of the two ions and the fraction of sodium participating in the exchange are respectively [Doremus 1969]:

$$\frac{\mu_{Na^+}}{\mu_{K^+}} \cong 500 \; ; \; h \cong 0.9 \quad (T=374°C)$$

which gives $\hat{\alpha} = 0.898$. On the other hand, for Ag^+-Na^+ exchange, the value of $\hat{\alpha} = 0.56$ was found [Stewart 1977].

The effect of varying $\hat{\alpha}$ on the solution for $c(\gamma)$ is rather important, as can be seen in Figure 2-1. This sheds some light on the controversy which surrounds the choice of an approximate function to model the refractive-index profile resulting from ion-exchange. In the case of Ag^+-Na^+, an extensive study showed that the best fit is provided by a second-order polynomial [Stewart 1977], prompting some people to use the same function when dealing with potassium exchange [Okamura 1985]. Others [Chartier 1980, Giallorenzi 1973, Gortych 1986a,b] have proposed and used Gaussian functions and "erfc"

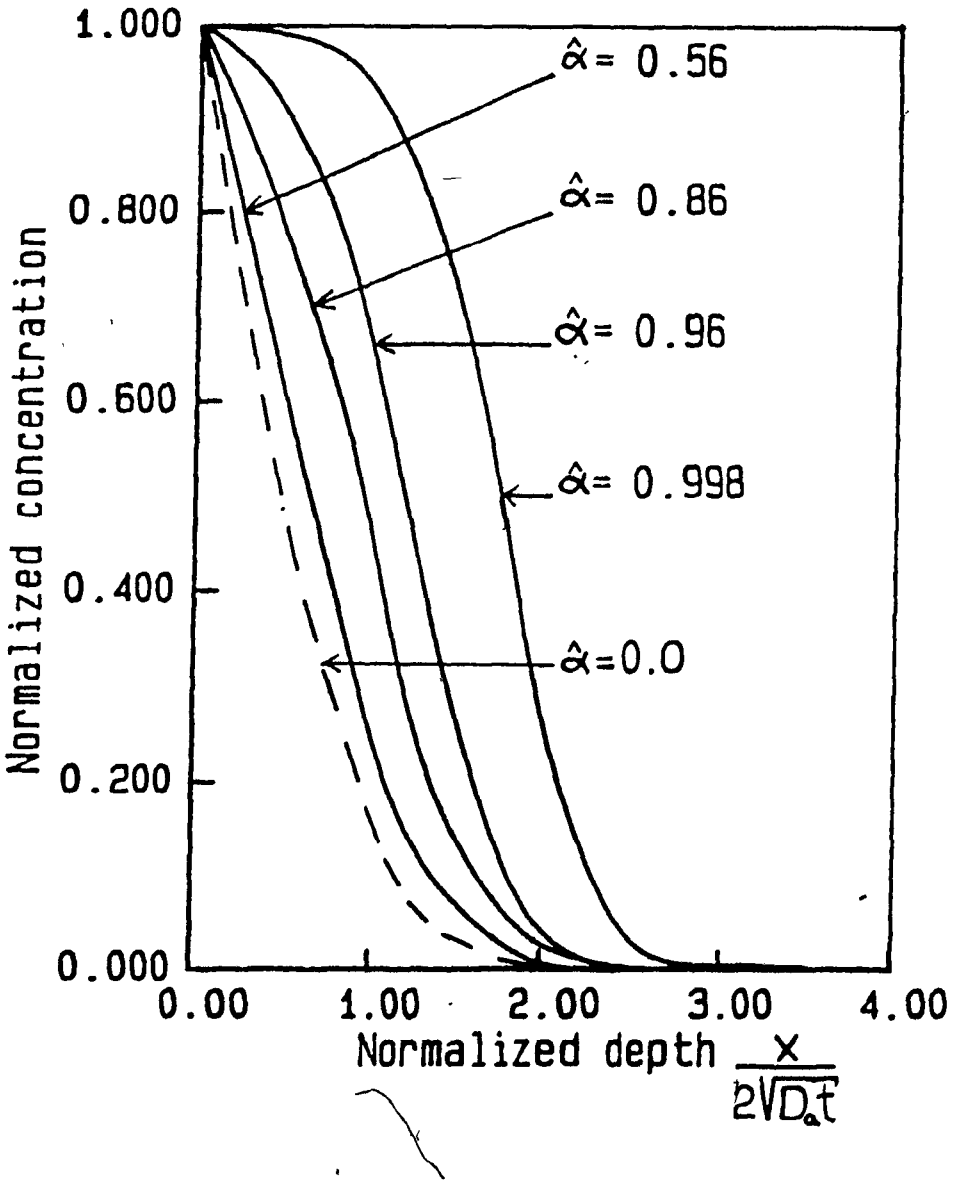

Figure 2-1. Effect of the value of $\hat{\alpha}$ on the profile of the exchanged ion concentration.($\hat{\alpha}=0 \rightarrow$ erfc)

functions (i.e. one minus the error funtion, or "complementary error function"), for various types of exchange, usually basing their arguments on classical diffusion theory, for which these two functions represent standard solutions. It is now clear, from Figure 2-1, that the exact shape depends critically on $\hat{\alpha}$, which in turn varies widely with the exchanging species and substrate glass [Doremus 1969].

In order to clarify the question between the silver and potassium cases, Figures 2-2 and 2-3 show the numerical solutions for the two previously cited values of $\hat{\alpha}$, along with the best Gaussian fit to it and also with the analytical power series solution derived in the previous section (taking its first three terms, up to second order). On Figure 2-2 (K^+), the Gaussian fit follows quite well the exact result over its whole range while the power series does not remain accurate far away from the origin.

On the other hand, in Figure 2-3 (Ag^+), while the Gaussian fit is relatively poor over the whole range, the power series is very accurate over a domain that extends almost to the nominal depth ($y = 1$) of the profile. This explains the good fit obtained by [Stewart 1977] since waveguides made from Ag^+-Na^+ are much more strongly guiding (their index change is ten times larger) than those made with potassium, and most of the optical power propagates in a very shallow layer near the surface ($y=0$). In the K^+-Na^+ case however, the optical

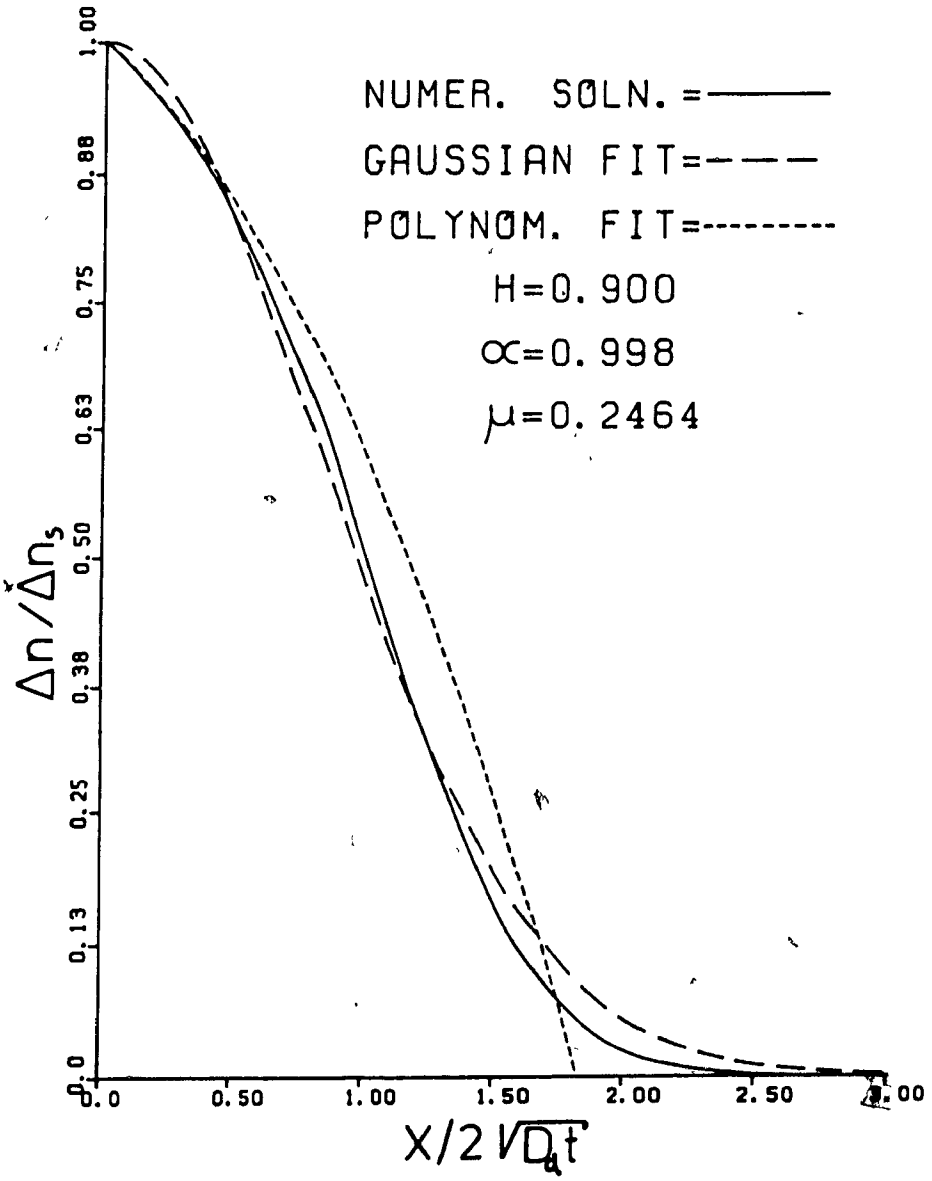

Figure 2-2. Variation of refractive index change with normalized depth for K^+-Na^+ exchange. Comparison of the numerical result with the approximate solutions.

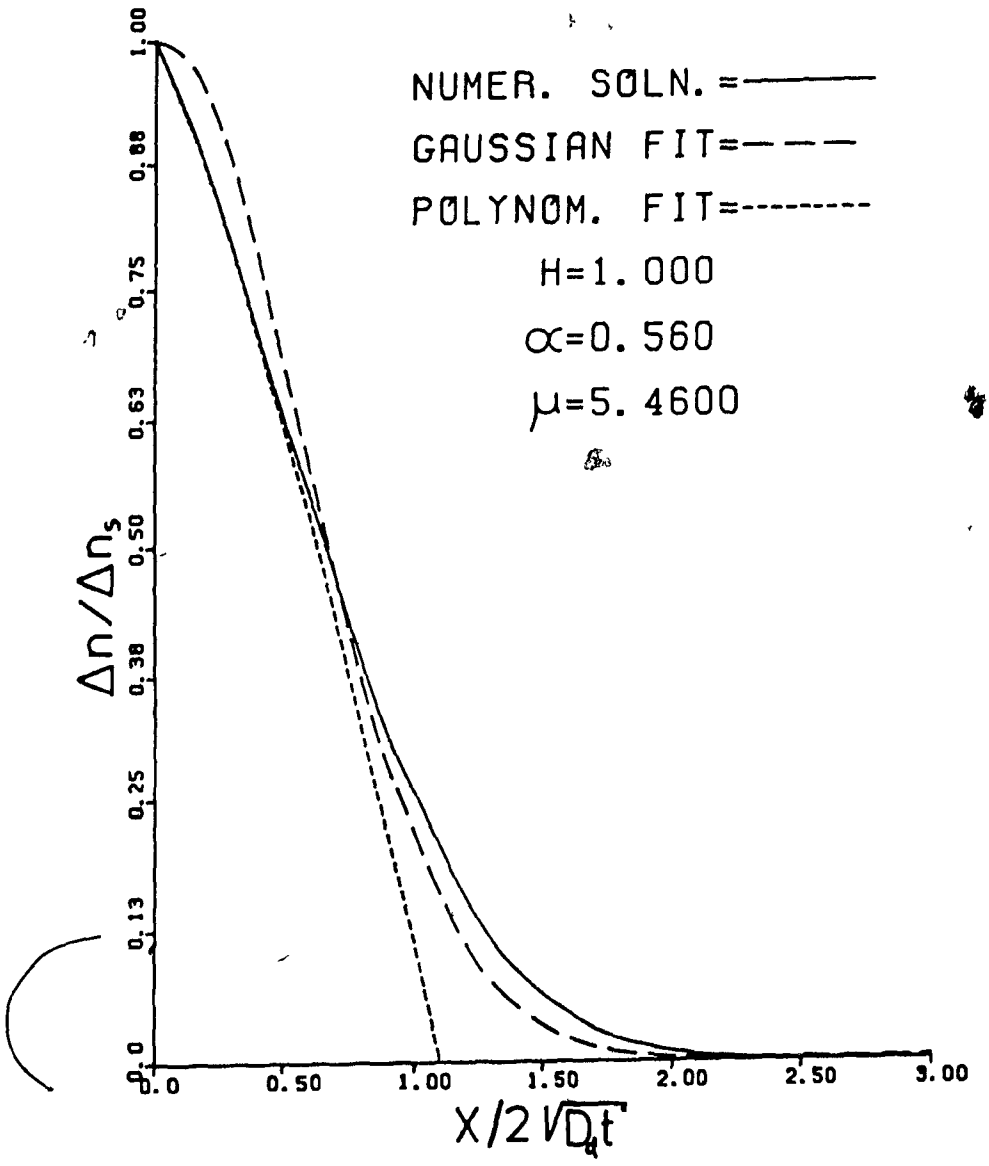

Figure 2-3. Variation of refractive index change with normalized depth for Ag^+-Na^+ exchange. Comparison of the numerical result with the approximate solutions.

power is less confined and good agreement of the model function is necessary over the whole profile for it to be successful in predicting waveguiding properties. As far as the erfc function is concerned, its behaviour near the origin (a large negative slope), is totally inconsistent with the numerical solutions obtained for $\hat{\alpha}$ values larger than 0.5, which are much more rounded at $\gamma=0$ (see Figure 2-1).

These conclusions are confirmed by our own characterization of the K^+-Na^+ process in soda-lime glass (presented in chapter 4), where we use a Gaussian function of the form:

$$\Delta n(x) = \Delta n_s \, e^{-\frac{x^2}{d^2}} = \Delta n_s \, e^{-\frac{x^2}{D_e t}} \qquad (2\text{-}53)$$

to model the index profile with very good accuracy, with "D_e", an effective diffusion coefficient, and "t", the duration of the exchange. In Figure 2-2, the best Gaussian fit is obtained for

$$c(x) = e^{-\frac{\gamma^2}{\delta^2}} = e^{-\frac{x^2}{4D_a t \delta^2}} \qquad \text{with } \delta = 1.17 \qquad (2\text{-}54)$$

which allows for the determination of D_a (needed in the next section) from a measurement of D_e.

2.3.3 Numerical solutions for channel waveguides.

It is possible to obtain very accurate solutions to partial differential equations by using numerical methods on a computer. These solutions can be used to check the accuracy and the range of validity of approximate methods (as was done in the previous section) and are applicable to the more general case of two-

dimensional diffusion through an aperture. It is from these results that the waveguides obtained by ion-exchange will be analyzed in later chapters.

The 2-D implementation of the numerical solution is described below, in more details than in the previous section because no commercial subroutines were used.

Starting again from (2-15), in two dimensions:

$$\frac{\partial c}{\partial t} = \frac{\partial}{\partial x}\left(\frac{D_a}{1-\hat{\alpha}c}\frac{\partial c}{\partial x}\right) + \frac{\partial}{\partial y}\left(\frac{D_a}{1-\hat{\alpha}c}\frac{\partial c}{\partial y}\right) \qquad (2-55)$$

where the normalizations (2-28) and $\hat{\alpha} = h\alpha$ have been used again. To "standardize" somewhat the numerical procedure, the following transformation is made [Heifferich 1958]:

$$f = \ln(1 - \hat{\alpha}c) \qquad (2-56)$$

$$\frac{\partial f}{\partial x} = \frac{-\hat{\alpha}}{1-\hat{\alpha}c}\frac{\partial c}{\partial x} \qquad (2-57)$$

and similarly for $\frac{\partial f}{\partial y}$ and $\frac{\partial f}{\partial t}$ to arrive at:

$$(1-\hat{\alpha}c)\frac{\partial f}{\partial t} = e^f \frac{\partial f}{\partial t} = D_a\left(\frac{\partial^2 f}{\partial x^2} + \frac{\partial^2 f}{\partial y^2}\right) \qquad (2-58)$$

$$\frac{\partial f}{\partial t} = e^{-f} D_a\left(\frac{\partial^2 f}{\partial x^2} + \frac{\partial^2 f}{\partial y^2}\right) . \qquad (2-59)$$

The spatial domain of integration is shown on Figure 2-4 for the case of ion-exchange through an opening of width D. This allows for an explicit formulation of the other boundary conditions:

$$c(0,|y|<\tfrac{D}{2}) = 1 \qquad (2-60)$$

$$c(0,|y|\geq\tfrac{D}{2}) = 0 \qquad (2-61)$$

$$c(\infty,y) = 0 \qquad (2-62)$$

$$c(x,\pm\infty) = 0 \qquad (2-63)$$

Note that condition (2-61) is dependent on the experimental procedure [Wilkinson 1978]. In principle, nothing prevents lateral diffusion to occur along x=0, just under the mask. However, in the case of metal (aluminium) masks (as will be the case here), the exchange along y is prevented because no electric field can exist in that direction at the interface with the conductor. Mathematically, this corresponds to setting $E_y = 0$ in (2-7) and (2-8). Then, when we impose conditions (2-9) and (2-10), the result is that $\partial c/\partial y$ must be equal to zero. Furthermore, no flux is possible in the x direction at $x = 0$ because of the mask, which means that $\partial c/\partial x = 0$. Since the net total fluxes are zero at $x = 0$, then the concentration of new ions remains at its initial value there, i.e. remains zero. When the mask is non-conducting, the first restriction (E_y=0) does not apply and the appropriate boundary condition is one of zero resultant normal flux (outward or inward)*:

$$\frac{\partial c}{\partial x}\left(0,|y|>\frac{D}{2}\right) = 0 \qquad (2-64)$$

In terms of f the boundary conditions become:

$$f\left(0,|y|<\frac{D}{2}\right) = \ln(1-\hat{\alpha}) \qquad (2-65)$$

$$f\left(0,|y|\geq\frac{D}{2}\right) = 0 \qquad (2-66)$$

$$f(\infty,y) = 0 \qquad (2-67)$$

$$f(x,\pm\infty) = 0 \qquad (2-68)$$

The numerical solution of (2-59) is based on replacing the derivatives by finite differences on a discrete space-time

---

* The above considerations are only approximative near the mask edge because the electric fields and gradients are not uniform there

grid. The spacing of the grid points must be such that we have a reasonably high resolution in the main region of interest. At the same time, the grid must extend far enough in the spatial domain to allow the use of boundary conditions that should be at infinity. All of this contributes to making computing time extremely large if steps are not taken to reduce the problem in some way.

First, we can halve the computing time by solving only one half of the problem. As can be seen from Figure 2-4, and the fact that ion-exchange in glass is isotropic, it is obvious that the concentration profile will be symmetric about y = 0. Therefore, a new boundary can be used at y = 0 and calculations limited to the positive values of y. The boundary condition is:

$$\frac{\partial c}{\partial y}(x,0) = 0 = -\frac{\partial f}{\partial y}(x,0) \qquad (2\text{-}69)$$

which follows from the symmetry of c with respect to y:

$$c(x,y) = c(x,-y) \qquad (2\text{-}70)$$

Another time and space saving measure consists of using a variable grid on which to calculate the finite differences, in the same manner that was done in the previous section. This new grid is obtained by mapping the semi-infinite x and y axes onto finite intervals by the following change of variables:

$$\xi = \frac{x}{x+a} \quad ; \quad x = \frac{a\xi}{1-\xi} \qquad (2\text{-}71)$$

$$\eta = \frac{y}{y+b} \quad ; \quad y = \frac{b\eta}{1-\eta} \qquad (2\text{-}72)$$

By this transformation, an evenly spaced grid in the ξ-η coordinate system corresponds to an x-y grid which begins very

fine near (0,0) and gradually becomes coarser away from the origin, yielding the desired high resolution in the rectangle defined by x = (0,a) and y = (0,b), and also coverage of the regions outside of it extending to infinity. Note that:

$$\xi,\eta \rightarrow 1 \quad \text{as} \quad x,y \rightarrow \infty \tag{2-73}$$

$$\xi,\eta \rightarrow 0 \quad \text{as} \quad x,y \rightarrow 0 \tag{2-74}$$

The central part of the x-y grid is shown on Figure 2-4. The outermost points are left out because it would not be possible to distinguish the central portion on the same scale. The total grid consists of 11 equally spaced points in ξ (located at 0.0, 0.1, 0.2,...,1.0) and 16 points in η (0.0, 0.067, 0.133, 0.200,...,1.0). The corresponding values of x and y are listed on the sample outputs from program DDFUS (Tables 2-1 to 2-3), and they are shown graphically on Figure 2-4. With the new variables, equation (2-59) is transformed in the following manner:

$$\frac{\partial}{\partial x} = \frac{\partial \xi}{\partial x}\frac{\partial}{\partial \xi} = \frac{(1-\xi)^2}{a}\frac{\partial}{\partial \xi} \tag{2-75}$$

$$\frac{\partial^2}{\partial x^2} = \frac{(1-\xi)^3}{a^2}\left(-2\frac{\partial}{\partial \xi} + (1-\xi)\frac{\partial^2}{\partial \xi^2}\right) \tag{2-76}$$

and similarly for "y", to yield finally:

$$\frac{\partial f}{\partial t} = D_a e^{-t}\left[\frac{(1-\xi)^3}{a^2}\left(-2\frac{\partial f}{\partial \xi} + (1-\xi)\frac{\partial^2 f}{\partial \xi^2}\right) + \frac{(1-\eta)^3}{b^2}\left(-2\frac{\partial f}{\partial \eta} + (1-\eta)\frac{\partial^2 f}{\partial \eta^2}\right)\right] \tag{2-77}$$

To solve the problem numerically, an explicit finite-

difference scheme was chosen because of its convenience and simplicity [Gerald 1970]. Also the accuracy of that method can be controlled relatively easily by changing the resolution of the time and spatial steps used in the finite differences, as long as the time step is small enough to ensure the stability of the computation [Gerald 1970]. Stability means that errors do not grow exponentially with successive iterations in time (i.e. do not start to oscillate wildly). A criterion for stability is derived below.

The finite differences which correspond to the partial derivatives are listed below. $f_0(I,J)$ is the value of f at grid point (I,J) (ξ and η coordinate respectively), and time t_0, while $f_1(I,J)$ is the value at time $t_0 + \Delta t$.

$$\left(\frac{\partial f}{\partial \xi}\right)_{I,J} = \frac{f_0(I+1,J) - f_0(I-1,J)}{2\Delta\xi} \qquad (2\text{-}78)$$

$$\left(\frac{\partial f}{\partial \eta}\right)_{I,J} = \frac{f_0(I,J+1) - f_0(I,J-1)}{2\Delta\eta} \qquad (2\text{-}79)$$

$$\left(\frac{\partial^2 f}{\partial \xi^2}\right)_{I,J} = \frac{f_0(I+1,J) + f_0(I-1,J) - 2f_0(I,J)}{(\Delta\xi)^2} \qquad (2\text{-}80)$$

$$\left(\frac{\partial^2 f}{\partial \eta^2}\right)_{I,J} = \frac{f_0(I,J+1) + f_0(I,J-1) - 2f_0(I,J)}{(\Delta\eta)^2} \qquad (2\text{-}81)$$

$$\left(\frac{\partial f}{\partial t}\right)_{I,J} = \frac{f_1(I,J) - f_0(I,J)}{\Delta t} \qquad (2\text{-}82)$$

The set of equations (2-78)-(2-82), when replaced in (2-77), determines uniquely the values of f_1 in terms of those of f_0. The calculation proceeds as follows: first the matrix $f_0(I,J)$ is initialized with zeros, except at the unmasked sur-

face (I=1,J depends on the mask aperture) where the values are fixed at $\ln(1 - \hat{\alpha})$. Then, the finite-difference equation is calculated for the values of f_1 at all the "interior" grid points (remember that on the boundaries I=11 and J=16 the values remain constant, equal to zero). On the boundary y = 0, J=1 and formulae (2-79) and (2-81) contain terms for which J=0, which are outside the calculation domain. Fortunately, we know that the value of f(I,0) must be equal to the value of f(I,2) because of the symmetry of the problem about y = 0. Therefore we use:

$$f_0(I,0) = f_0(I,2) \tag{2-83}$$

in (2-79) and (2-81). Once f_1 is known everywhere, it replaces f_0 and the process is repeated for another time step.

Before proceeding with the results of these calculations, the parameters a, b, D_a, $\hat{\alpha}$, and Δt must be chosen. The spatial scale of the problem is fixed by a and b since, by equations (2-71) and (2-72), x=a and y=b correspond to ξ,η= 0.5 and separate the region where the grid is finest from the outside, where it is coarser. In this work, masks with apertures of 10 μm were used, so that b was fixed at 5 μm to correspond to the edge of the mask. The depth of the waveguides would vary from 0 to 2 μm and the value of a was fixed at 1 μm.

The diffusion parameters, $\hat{\alpha}$ and D_a were calculated as mentioned in the last section. For K^+-Na^+ exchange in soda-lime glass, they are:

$$\hat{\alpha} = 0.898$$

$$D_a = \frac{D_e}{4(1.17)^2} = 1.95 \times 10^{-16} m^2/sec$$

The value of D_e for T=385°C was used (see Chapter 4).

Finally, the time step Δt must be small enough to ensure stability. For parabolic differential equations in two dimensions, similar to (2-59) without the exponential factor, the criterion is [Gerald 1970]:

$$\Delta t \leq \frac{(\Delta x)^2+(\Delta y)^2}{8D_a} \qquad (2\text{-}84)$$

As an hypothesis, we assume that the presence of the exponential factor can be accounted for by considering it "locally constant" around each grid point and including it in (2-84) as such:

$$\Delta t \leq \frac{((\Delta x)^2+(\Delta y)^2)(1 - \hat{\alpha}c)}{8D_a} \qquad (2\text{-}85)$$

To find a lower bound for Δt_{max}, we take the largest value of c (i.e. c=1), which occurs where the grid is finest (i.e. smallest Δx and Δy, equal to 0.1 μm and 0.35 μm), and the numerical values of D_a and $\hat{\alpha}$ for K^+, giving finally:

$$\Delta t \leq \frac{(1 \times 10^{-14}+1 \times 10^{-13} m^2)(1 \times 10^{-1})}{8(2 \times 10^{-16} m^2/sec)} \cong 6 \text{ sec.} \qquad (2\text{-}86)$$

The final choice for Δt is 4.2 seconds, but other values have been tried to verify the stability of the result.

An example of the concentration profile obtained for an exchange of 1 hour at 385°C through a 10 μm wide opening is shown on Figure 2-5 (with the corresponding data in Table 2-1). Also, Tables 2-2 and 2-3 show the results of the same calculation but executed with time steps of 2.1 and 8.4 seconds,

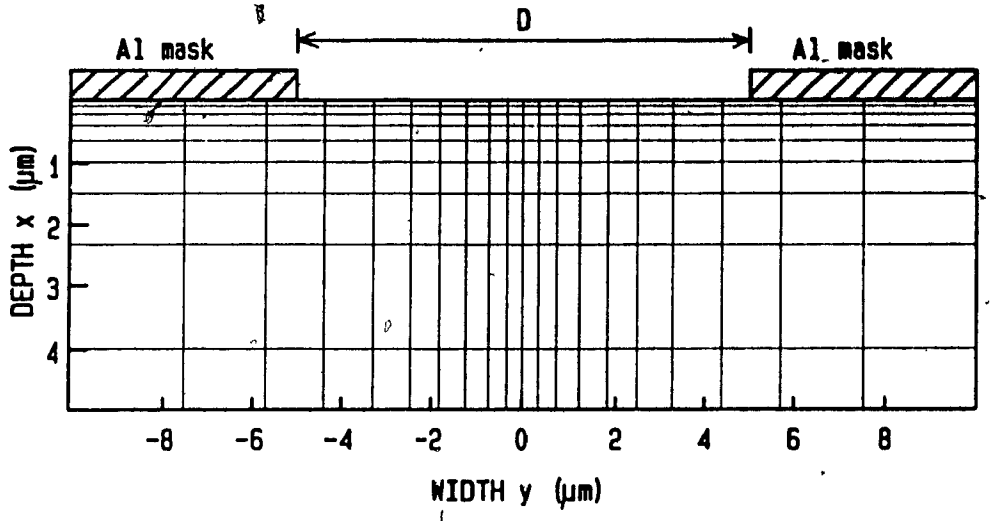

Figure 2-4. Calculation grid for the solution of the exchange diffusion equations.

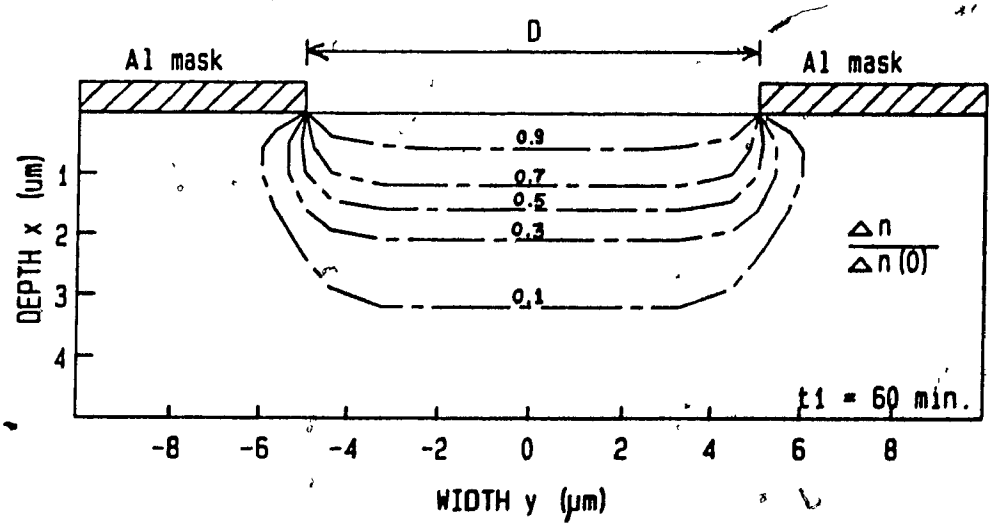

Figure 2-5. Constant concentration contours resulting from a single exchange of one hour at 385°C. D=10 μm.

t_1 = 3600.0 Δt = 4.20 D_a = 0.195D-15 and $\hat{\alpha}$ = 0.898

y ↓ / x =	0.000	0.111	0.250	0.429	0.667	1.000	1.500	2.333	4.000	9.000
0.000	1.000	0.986	0.965	0.934	0.882	0.787	0.590	0.199	0.010	0.000
0.357	1.000	0.986	0.965	0.934	0.882	0.787	0.590	0.199	0.010	0.000
0.769	1.000	0.986	0.965	0.933	0.882	0.787	0.590	0.199	0.010	0.000
1.250	1.000	0.986	0.965	0.933	0.881	0.786	0.589	0.199	0.010	0.000
1.818	1.000	0.985	0.965	0.933	0.881	0.785	0.587	0.198	0.010	0.000
2.500	1.000	0.985	0.964	0.931	0.878	0.780	0.580	0.194	0.010	0.000
3.333	1.000	0.984	0.961	0.926	0.868	0.764	0.558	0.183	0.009	0.000
4.375	1.000	0.976	0.942	0.893	0.817	0.692	0.475	0.145	0.007	0.000
5.714	0.000	0.054	0.101	0.138	0.158	0.152	0.107	0.031	0.002	0.000
7.500	0.000	0.002	0.004	0.007	0.009	0.009	0.007	0.002	0.000	0.000
10.000	0.000	0.000	0.000	0.000	0.000	0.000	0.000	0.000	0.000	0.000
13.750	0.000	0.000	0.000	0.000	0.000	0.000	0.000	0.000	0.000	0.000
20.000	0.000	0.000	0.000	0.000	0.000	0.000	0.000	0.000	0.000	0.000
32.500	0.000	0.000	0.000	0.000	0.000	0.000	0.000	0.000	0.000	0.000
70.000	0.000	0.000	0.000	0.000	0.000	0.000	0.000	0.000	0.000	0.000

Table 2-1 Output of program to calculate the concentration profile of exchanged ions T=385°C , D=10μm

t_1 = 3600.0 Δt = 2.10 D_a = 0.195D-15 and $\hat{\alpha}$ = 0.898

y ↓ / x =	0.000	0.111	0.250	0.429	0.667	1.000	1.500	2.333	4.000	9.000
0.000	1.000	0.986	0.965	0.934	0.882	0.787	0.590	0.199	0.010	0.000
0.357	1.000	0.986	0.965	0.934	0.882	0.787	0.590	0.199	0.010	0.000
0.769	1.000	0.986	0.965	0.933	0.882	0.787	0.589	0.199	0.010	0.000
1.250	1.000	0.986	0.965	0.933	0.881	0.786	0.589	0.199	0.010	0.000
1.818	1.000	0.985	0.965	0.933	0.881	0.785	0.587	0.198	0.010	0.000
2.500	1.000	0.985	0.964	0.931	0.878	0.780	0.580	0.194	0.010	0.000
3.333	1.000	0.984	0.961	0.926	0.868	0.764	0.558	0.183	0.009	0.000
4.375	1.000	0.976	0.942	0.893	0.817	0.692	0.475	0.145	0.007	0.000
5.714	1.000	0.127	0.101	0.138	0.158	0.152	0.107	0.031	0.002	0.000
7.500	1.000	0.075	0.004	0.007	0.009	0.009	0.007	0.002	0.000	0.000
10.000	1.000	0.073	0.000	0.000	0.000	0.000	0.000	0.000	0.000	0.000
13.750	1.000	0.073	0.000	0.000	0.000	0.000	0.000	0.000	0.000	0.000
20.000	1.000	0.073	0.000	0.000	0.000	0.000	0.000	0.000	0.000	0.000
32.500	1.000	0.073	0.000	0.000	0.000	0.000	0.000	0.000	0.000	0.000
70.000	1.000	0.073	0.000	0.000	0.000	0.000	0.000	0.000	0.000	0.000

Table 2-2. Same conditions as Table 2-1, except Δt=2.1 sec.

t_1 = 3600.0 Δt = 8.40 D_a = 0.195D-15 and $\hat{a}$ = 0.898

y ↓ / x =	0.000	0.111	0.250	0.429	0.667	1.000	1.500	2.333	4.000	9.000
0.000	1.000	0.887	0.937	0.874	0.827	0.733	0.545	0.186	0.010	0.000
0.357	1.000	0.991	0.890	0.887	0.829	0.734	0.546	0.186	0.010	0.000
0.769	1.000	0.910	0.944	0.884	0.834	0.738	0.548	0.187	0.010	0.000
1.250	1.000	0.994	0.907	0.898	0.839	0.743	0.552	0.188	0.010	0.000
1.818	1.000	0.925	0.952	0.896	0.845	0.747	0.555	0.189	0.010	0.000
2.500	1.000	0.996	0.918	0.906	0.847	0.749	0.554	0.187	0.009	0.000
3.333	1.000	0.935	0.955	0.899	0.844	0.740	0.539	0.178	0.009	0.000
4.375	1.000	0.987	0.923	0.884	0.805	0.680	0.466	0.143	0.007	0.000
5.714	0.000	0.053	0.099	0.136	0.156	0.150	0.105	0.031	0.002	0.000
7.500	0.000	0.002	0.004	0.007	0.009	0.009	0.007	0.002	0.000	0.000
10.000	0.000	0.000	0.000	0.000	0.000	0.000	0.000	0.000	0.000	0.000
13.750	0.000	0.000	0.000	0.000	0.000	0 000	0.000	0.000	0.000	0.000
20.000	0.000	0.000	0.000	0.000	0.000	0.000	0.000	0.000	0.000	0.000
32.500	0.000	0.000	0.000	0.000	0.000	0.000	0.000	0.000	0.000	0.000
70.000	0.000	0.000	0.000	0.000	0.000	0.000	0.000	0.000	0.000	0.000

Table 2-3 Output of program to calculate the concentration profile of exchanged ions.
Same conditions as Table 2-1, except Δt=8 4 sec

Numerical instability is seen as oscillations in the results, especially in columns x=0.111 and x=0 250.

showing no change in the first case and instability in the second (evidenced by oscillations in the results, particularly at $x = 0.25\mu m$).

2.3.4 Two-step ion-exchange

Another possibility, which is studied more specifically, in this work, is to perform a double exchange by removing the mask at some point and allowing the exchange to resume over the whole plane of the substrate. Mathematically, it means changing the boundary condition (2-61) to:

$$c(0,y \geq \frac{D}{2}) = 1 \qquad (2-87)$$

after a given time t_1

The purpose of doing this is to control the lateral waveguiding properties of the channels defined by the first exchange. As we will see in later chapters, a wide range of possibilities is offered by adjusting the relative durations of the masked (t_1) and unmasked (t_0) exchanges.

To have a point of reference in the study, the total time $t_1 + t_0$ was kept constant at 1 hour, the temperature was always 385°C, and the mask opening always 10 μm. This way, all the channels have the same depth (1.97μm) in the central part (which was unmasked during both t_1 and t_0) and it is the depth variation outside of the channel (in its lateral "cladding") that provides control over the optical modes and their propagation constants. The 10 μm width was chosen to demonstrate the possibility of making wide single-mode channel

waveguides by this method so that fabrication tolerances would be reduced and that dimensional compatibility with single-mode fibers would be increased (at least in one dimension). For comparison, single-mode channel waveguides in $LiNbO_3$ are limited to lateral dimensions on the order of 2-3 μm and many single-mode fibers have diameters between 5 and 10 μm. Finally, by fine-tuning t_1 (and t_0), it is possible to compensate design or fabrication inaccuracies with a given mask layout without having to re-design it.

Some results of two-step ion-exchange are illustrated in Figures 2-6 and 2-7. The fabrication of such structures will be discussed in chapter 3, and their waveguiding properties analyzed in chapter 6 and 7.

As a final note for this chapter, the computer program described is fairly general and can be adapted easily to other types of boundary conditions, parameter values, etc... Its usefulness has yet to be exploited fully to explore new types of waveguide fabrication by ion-exchange.

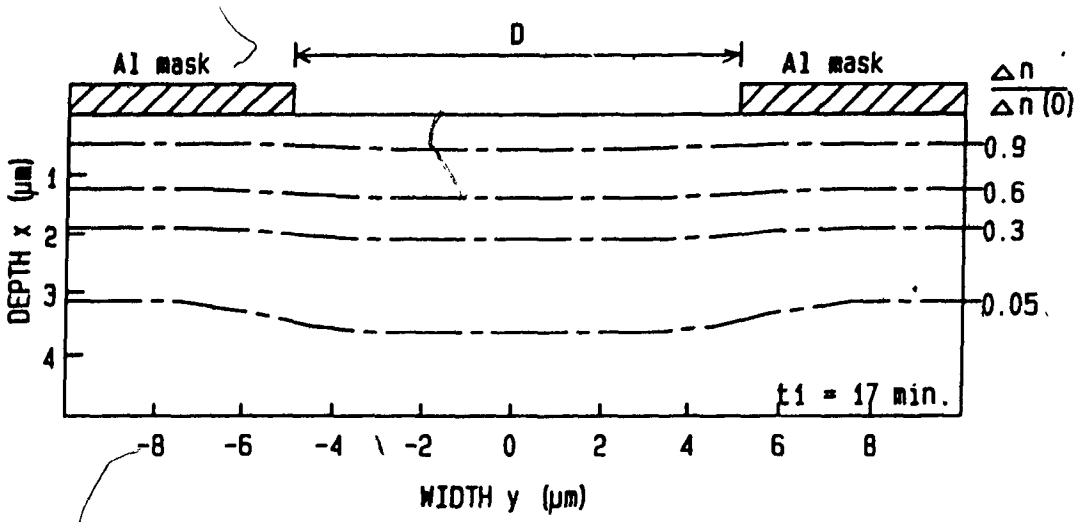

Figure 2-6. Constant concentration contours resulting from a two-step exchange at 385°C. t_1=17 min., D=10μm.

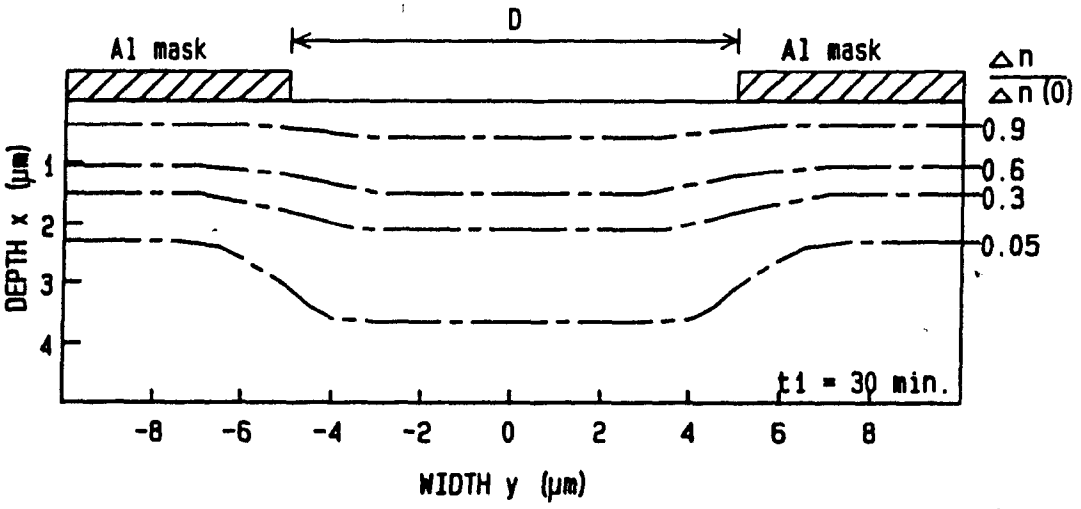

Figure 2-7. Constant concentration contours resulting from a two-step exchange at 385°C. t_1=30 min., D=10μm.

CHAPTER 3. FABRICATION AND MEASUREMENT TECHNIQUES.

3.1 INTRODUCTION

In this chapter, the fabrication and measurement of optical waveguides made by ion-exchange in glass are described. The procedures are adapted from those used in other laboratories, with minor adjustments made to satisfy the particular needs of this study.

3.2 FABRICATION

3.2.1 General considerations

The substrate used in the experiments is an ordinary microscope slide (Fisher Scientific Co.) made of soda-lime glass. It has a high sodium content and a good surface quality resulting from a flame polish [Zernike 1979]. Of course, the main advantage in using such a substrate is the fact that it can be bought in large quantities at very low cost (compared with specially prepared optical glasses such as BK-7, or with single crystals such as $LiNbO_3$). This is ideal for use in exploratory research where many waveguides need to be fabricated and evaluated, such as is the case here.

The microscope slides are shipped "pre-cleaned" in hermetically sealed boxes. Careful handling with gloves helps in preventing additional contamination (especially organic) but a very thorough cleaning is necessary for their use as optical waveguides. This is because the substrate must be free from

defects even as small as a fraction of the wavelength of the light used (tenths of microns) over the whole propagation path (tens of millimeters).

The cleaning steps are as follows:

First of all, the slide is inspected for any visible damage, rinsed in flowing deionized water, blown dry with nitrogen, and inspected again. Imperfect slides are eliminated at this point. The good ones are then placed in a substrate holder made of aluminium so that they will not be touched again until the end of the whole process. The remainder of the cleaning steps are:

a- A 5 minutes' wash in an ultrasonic bath where a few grains of Sparkleen (Fisher Sci. Co.) detergent have been dissolved (too much detergent will scratch the surface).

b- Rinse in flowing deionized (D.I.) water.

c- 5 minutes ultrasonic rinsing in D.I. water.

d- Repeat steps b and c.

e- 30 minutes in a "degreaser". This is a closed vessel containing a small quantity of isopropyl alcohol, placed on a heating plate so that much of the alcohol is vaporized. When the cool substrate is inserted in the vessel, rapid condensation occurs on its surfaces, resulting in a very active rinsing effect and removal of any organic contamination.

f- Rinse in flowing D.I. water, blow-dry with nitrogen.

To evaluate the cleanliness of the slide, a small amount of

D.I. water is spread over it. The water spreads evenly on a clean surface and evaporates away gradually, showing interference fringes (and highlighting defects) as it gets thinner and thinner.

As a final step, the slides are blown dry and placed in an oven kept at about 80°C to make sure that all the water is gone before either ion-exchange (for planar guides) or high-vacuum Aluminium deposition and photolithography (for channel guides).

Other cleaning steps have been tried (such as rinses and ultrasonic cleaning with methanol and/or acids) but they did not lead to better results and were abandoned. In fact, a cleaning process that is too aggressive may do more harm than good by damaging the surface polish on a scale too small to be observed.

3.2.2 Description of the ion-exchange environment

The furnace (Lindberg Crucible Furnace) has a vertical core and can be used in the 20 to 1200°C range. The temperature is fixed by a temperature controller to within 1°C. The potassium nitrate (KNO_3) crystals are placed in a steel crucible inside the furnace which is closed at the top with an asbestos cover. A small hole in the cover allows the insertion of a brass rod terminating in a steel clip, which is used to hold two substrates and to lower them into the melt without opening the cover.

The fact that the process takes place in a liquid (approximately 150 ml of it) smoothes out any temperature gradient along the length of the substrate (because of convection currents arising from slightly non-uniform heating) and also any temporal temperature fluctuations. (Note: there is a certain debate in the ion-exchange litterature over the use of stirred melts to ensure a constant concentration of exchanging ions at the surface of the substrate by removal of the outgoing ions from that area. This stirring may occur naturally because of convection in the melt and comparisons between the two methods become difficult to establish with certainty).

3.2.3 Planar waveguide fabrication

Using gloves, or small metallic tweezers, the substrate is taken from the drying oven and placed in the steel clip that is to hold it in the furnace. The whole assembly is suspended over the melt for a heating period of 10 minutes to bring the entire substrate to the exchange temperature and then lowered in the KNO_3 melt. The heating ensures that the exchange begins immediately at the right temperature. After the desired period of time, the substrate is removed from the melt, and also from the furnace, the whole process lasting about 15 seconds until the residual KNO_3 recrystallizes on the glass, indicating that the exchange has "practically" ended (the exchange diffusion coefficient is an exponentially decaying function of the inverse of the temperature and drops rapidly to negligible values once

the heating stops). Care must be taken in handling the slide at this point because it is still extremely hot and susceptible to breakage when in contact with a cool object. It is better to leave it in the clip until well cooled.

Finally, the slide is washed clean of the crystallized salt in running D.I. water and the waveguide is ready to be measured.

3.2.4 Fabrication of channel waveguides (and other patterned circuits).

The procedure used in this work involves a two-step ion-exchange in which the channels are defined first by masking selected areas of the substrate, followed by an exchange over the whole area of the substrate, after removal of the mask, to modify the waveguiding properties of the channels in a controlled fashion. The fabrication steps are illustrated in Figure 3-1.

The aluminium (Al) deposition is performed in a vacuum station at a pressure of 2×10^{-6} Torr by heating a tungsten wire on which four one centimeter long Al hooks (formed from a high purity (Marz grade) wire furnished by MRC Corp.) have been suspended. Upon heating the tungsten wire (by passing a high current through it), the Al evaporates in the vacuum enclosure. A part of it condenses on the glass slide as a very uniform film of 100-150 nanometers (the exact thickness is not critical as long as it is larger than about 100 nm [Tsutsumi

FABRICATION STEPS

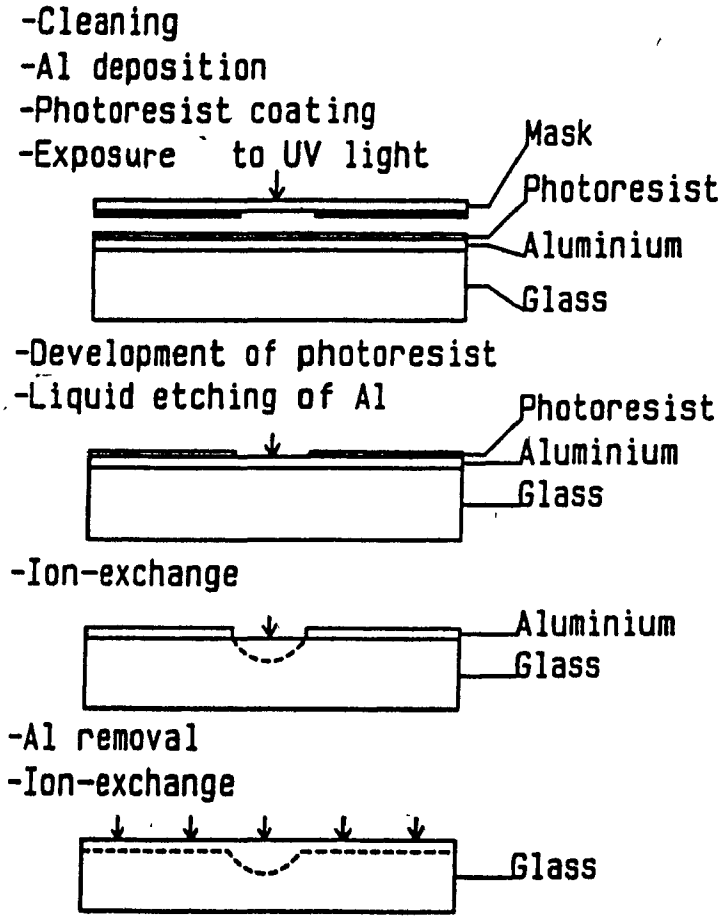

Figure 3-1. Diagram of fabrication procedure for two-step ion-exchanged channels.

1986]).

To remove the Al film from the areas where the exchange is to take place, photolithography is used. First, a 1:1 mixture of photoresist (Shipley 1450J) and thinner (Shipley AZ) is deposited on the Al surface by spinning the substrate at 4000 RPM for 20 seconds and baking the resulting film for 30 minutes at 80°C. Then, a master mask is brought in contact with the photoresist layer and a U.V. lamp is used to expose the resist through the mask openings for 5-10 seconds. Development of the resist is done in a 1:1 mixture of Microposit developer (Shipley) and D.I. water for 30-45 seconds and results in removal of the resist from the exposed areas.

After that, the substrate is baked for 1 hour at 120°C to harden the resist pattern. Finally, the Al is etched away from the areas where the resist has been removed by immersion in a solution of 32:2:6 parts of phosphoric acid, nitric acid, and D.I. water for 1-3 minutes. The exact times of development and etching are determined by inspecting the process until the channels become visually clear of resist or Al. Then, the substrate is dipped in a D.I. water bath and blown dry gently. The patterns are observed under a microscope to make sure that they are free of residual particles and well defined. After the completion of the etching and before proceeding to the ion-exchange, the photoresist which was used as a mask for the etchant is removed by dissolution in acetone.

The first step of ion-exchange, to define the waveguiding channels, is carried out in the same manner as was described in 3.2.3, except that the glass substrate is now partially masked. After the first step, the Al mask is removed with the etching solution and the substrate cleaned in D.I. water.

The second step of exchange is also done as in 3.2.3 except for one thing: the heating time of the substrate prior to the insertion in the melt is reduced to 5 minutes. This represents a compromise between the need to bring the substrate in thermal equilibrium with the melt and that to prevent the index profile obtained in the first exchange from being modified by this heating in the absence of a source of ions (thereby increasing the difficulty of modelling the profile theoretically for design purposes).

3.3 MEASUREMENT PROCEDURES

3.3.1 Introduction

The method chosen to characterize the planar waveguide properties is called modal spectroscopy. In this method, the measured propagation constants of all the modes that can be excited in a given guide are used to determine its refractive-index profile.

The way to measure the propagation constant of each mode is to selectively excite them with a prism-coupler. The theory of

operation of this coupler has been described often (see [Tamir 1979] and [Zernike 1979] for instance), and only its main features are presented here (in section 3.3.2) for brevity. The actual measurement set-up is described in 3.3.3 along with the methods used to enhance the accuracy of the measured propagation constants.

A prism-coupler is also used to launch light into channel waveguides. In that case, the methodology (described in 3.3.4) is different because the goal is no longer a high sensitivity in mode selection but rather to get as much power as possible in the single-mode guide and as little as possible in the planar guide which surrounds it.

Output coupling is also drastically different for the two cases, again because of their different purposes.

3.3.2 Operation of the prism-coupler

A right-angle prism of refractive index higher than that of the waveguide is brought in close contact with it as shown in Figure 3-2. A beam of light enters the prism and is totally reflected at the prism-air interface. The evanescent field caused by the reflection propagates along the base of the prism with the same wavevector component k_z (parallel to both the plane of incidence and the plane of the substrate) as that of the incoming lightwave for continuity of the fields at the interface. Also, in the plane of incidence, but perpendicular to the guide surface (i.e. direction $\hat{x}$), the fields decay

exponentially. When the waveguide is sufficiently close to the prism, the evanescent field acts as a source of electromagnetic radiation in the guiding layer (i.e. a polarization source term in the wave equation). And when the k_z component of the incident beam matches the propagation constant β (which is also a k_z component) of a mode, this mode is excited efficiently. Therefore, by gradually changing the angle of incidence of the beam at the entrance face of the prism, the values of k_z are scanned continuously, allowing the launching of each mode separately. This concludes the explanation of the principle of operation. In practice however, several factors have to be considered.

A right-angle prism is used to prevent the coupling of energy back from the waveguide to the prism by bringing the input beam as close as possible to the edge of the prism. Therefore, just after the excitation point, the evanescent wave of the waveguide mode "sees" nothing but an infinite cladding of air, instead of a high index layer separated from the guide by a thin low index layer through which it could tunnel energy. In fact, we can use a prism as a very efficient output coupler at the other end of the waveguide.

The refractive index of the prism should be at least as high, preferably higher than the maximum index of the guide (n_s). This is because in the prism, $k_z = n_p k_0 \sin \theta_p$

$< n_p k_0$ while in the guide k_z is smaller than but almost equal to $n_s k_0$ (for the fundamental mode). Therefore, to have θ_p reasonably smaller than 90 degrees (grazing incidence) at the prism base, we need $n_p > n_s$.

3.3.3 Measurement set-up for planar guides

To measure β with the greatest accuracy, the coupling angle θ_i must be very precisely known. A few precautions must be taken to that effect. First, the pressure holding the prism and waveguide together must be light so that the propagation constants of the guide are not significantly changed by the presence of this additional superstrate of high index. Second, as little focusing as possible must be used on the entrance beam. This is because a focused beam has significant energy entering the prism at a large spread of angles, making it difficult to determine the angle for which the coupling is maximum.

To determine this angle for a given mode, light exited at the end of the waveguide is observed on a viewing screen. To get a better radiation pattern the waveguides are cut near the end to expose their cross-section. This is because at the end of the uncut substrate, ion-exchange has also taken place on the sides of the glass slide, thereby ending the planar guide in an abrupt horn as the exchanged layer "turns" around the inside faces of the substrate as shown on Figure 3-3.

The far-field radiation pattern of a mode is well

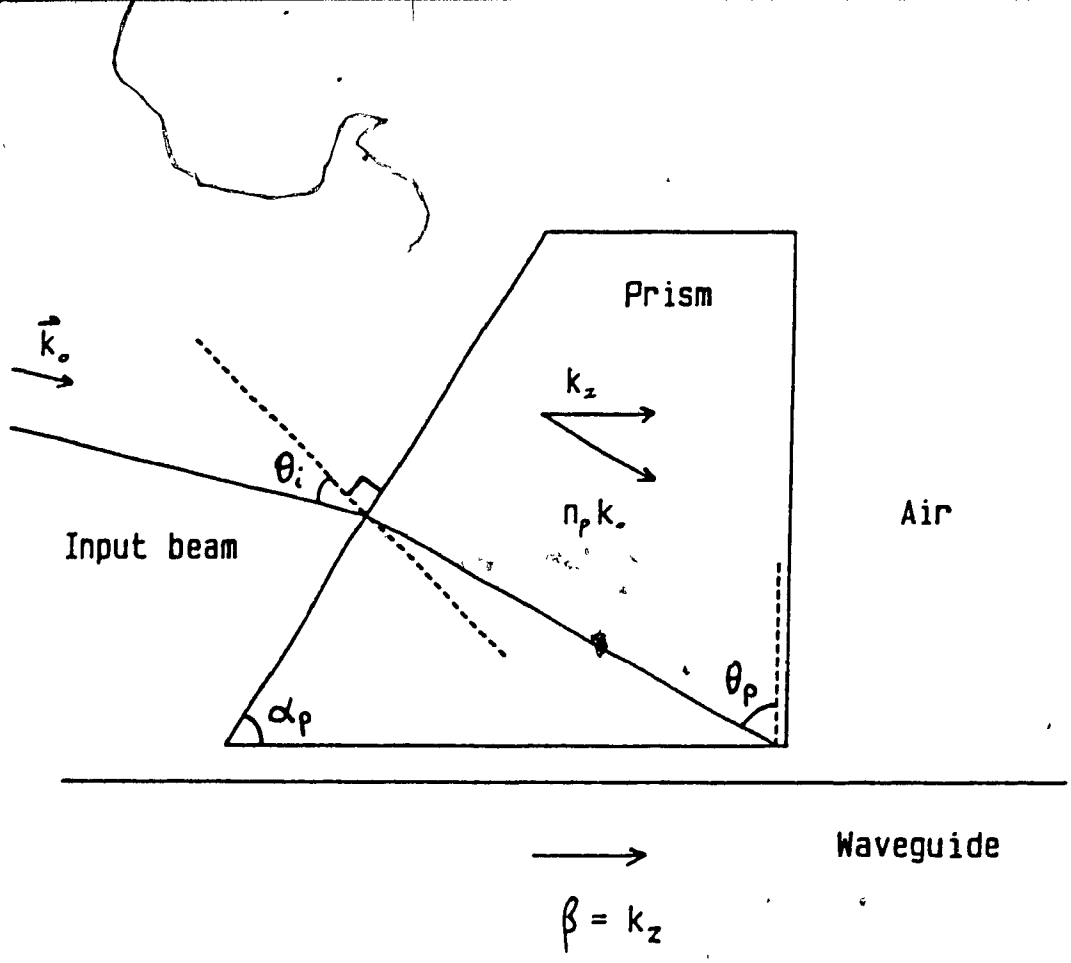

Figure 3-2. Geometry of prism coupler.

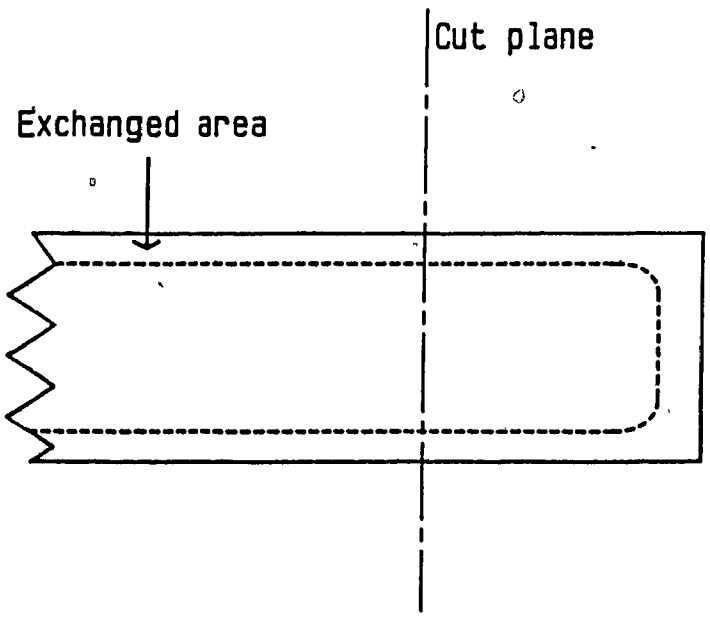

Figure 3-3. Location of the cut plane to expose the waveguide cross-section.

identifiable (see Figure 3-4) and, once such an identification has been made, the output of the guide is refocused and imaged onto a detector (an avalanche photodiode) to help in accurately finding the angle of entry yielding the maximum input power in the mode.

To facilitate input coupling, the prism-waveguide holder is mounted on a 3-axis micropositioner, which is itself mounted on a precise goniometer (accuracy of 5 arc-seconds). A polarizer is used to select TE and TM modes and the output of the photodetector is connected to an analog voltmeter to facilitate the visual identification of the point of maximum power. The lens system used to image the waveguide end onto the detector is to de-magnify so that when the angle is scanned, and the end of the guide moves laterally, its smaller image stays within the area of the detector! The light source used is a 5 mW He-Ne laser (Spectra-Physics) operating at 632.8 nm. The whole system is shown on Figure 3-5.

To get the propagation constants from the angle of incidence of the incoming beam, the following formula (derived using geometrical optics) is used [Zernike 1979]:

$$N_e = \frac{\beta}{k_0} = n_p\left(\sin\left(\alpha_p + \sin^{-1}\left(\frac{\sin\theta_i}{n_p}\right)\right)\right) \qquad (3-1)$$

where n_p = refractive index of the prism

α_p = base angle of prism

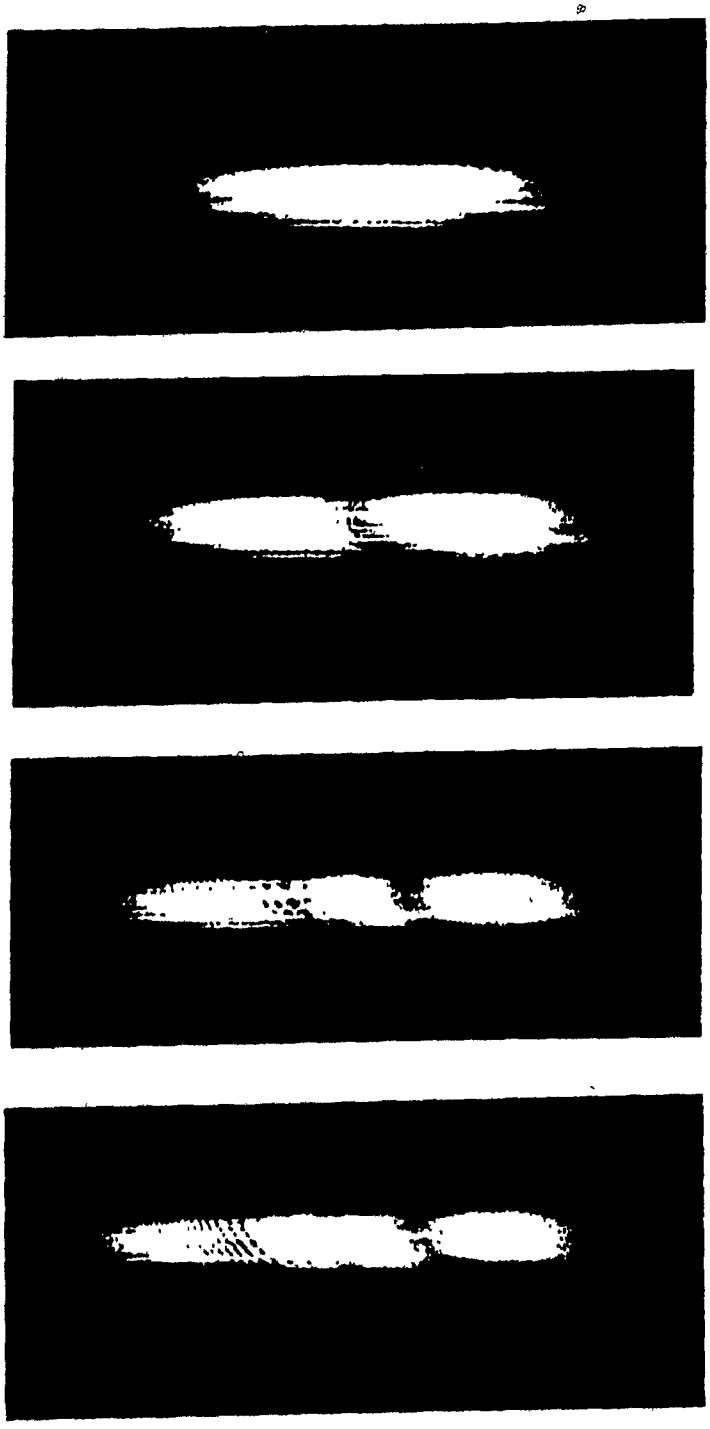

Figure 3-4. Photographs of the far field of the radiated power from the output of a planar guide.

θ_i - angle of the incoming beam relative to the normal to the face of the prism.

In practice, the reference angle (θ_i - 0), is measured by rotating the prism until the incoming beam is reflected back on itself. Series of measurements are made for each individual mode of one waveguide, until the value found for θ_i becomes certain to within 1 arc-minute (i.e. 30 arc-seconds each for θ_i itself and the reference angle which is remeasured for each set of modes). The prism angle α_p, was measured on the goniometer by successively reflecting a beam off two of its faces. The result is α_p - 50°00'20" ± 1'. Finally, the index of the prism, made of SF11 glass has been interpolated from the Schott catalogue (p.82) as n_p - 1.7786 for the wavelength of the light that is used (632.8 nm).

The uncertainty in θ_i leads to a measurement error of $\pm 2 \times 10^{-4}$ on the normalized propagation constant (also called N_e, the "effective index" of the mode). The errors in the values of α_p and n_p have the same effect on all the measurements and lead to an additional uncertainty of about $\pm 3 \times 10^{-4}$.

Another variable that needs to be determined is n_b, the index of the glass substrate prior to the exchange. Since the slides that we used were not made specifically to optical standards, their refractive index is not catalogued and has to

be measured in-house. The simplest method to do this is to use the set-up described above and to find the angle of incidence at which the waveguide becomes cut-off by observing the end of the substrate. It is easy to see the point where the light is no longer confined and starts leaking into the substrate. At this point, $N_e = n_b$, the cut-off condition. The result of many such measurements on different slides yielded a value of $n_b = 1.513$ with a standard deviation of $\pm 2 \times 10^{-4}$.

Results of the effective index measurements are presented in the next chapter.

3.3.4 Measurement set-up for channel guides and circuits

Here, the main problem is to get as much power as possible into the input channel and as little as possible in the planar guide which surrounds it. This is not an easy task because the channels are at the same time small (2 by 10 microns) and very weakly defined (the lateral index-change gradient is very small in the single mode regime, as will be seen in chapter 6)*.

A prism-coupler is used again at input, but this time it is strongly pressed against the guide and the input beam is focused (with a lens of 10 cm focal length). The lens is placed on a 3-axis micropositioning stage to adjust the position of the input beam relative to the 10 micron wide channel. Furthermore, the prism-guide assembly is mounted on the same goniometer as before but with an additional rotational axis perpendicular to the plane of the guide so that the axes of the entrance beam and of

---

* Note: It is not possible to measure the individual propagation constants of the modes of channel guides with an output prism because the small value of Δn_s (in this case) leads to very small angular differences between the "m-lines".

the channel can be aligned in that plane.

At the output, what is needed is a measure of the amount of light power in the output channels and also to see if there is any power that has radiated out in the planar guide. A prism is used to couple out the light, but, instead of observing the far field pattern, a microscope is used to image the base of the prism, where the light is coupled out of the channels, onto a screen. The image thus formed is shown in Figure 3-6 for the case of output from two adjacent channels. The abrupt edge of the light traces corresponds to the position of the right angle corner of the prism, where the coupling out begins. Evanescent coupling is gradual and takes place over a finite length as the light wave moves rightward in the picture. The vertical axis of the picture represents a direction parallel to the plane of the substrate but perpendicular to the channels, allowing the observation of the lateral distribution of power in the whole waveguide.

Quantitatively, we are not concerned with absolute values, but with the relative distribution of power in the output channels and with the power scattered (lost) laterally in the planar surrounding guide. Most of the unwanted scattering induced by the bends and irregularities in the devices will occur laterally because the confinement is much weaker in that direction ($\Delta N_e \cong 5 \times 10^{-4}$ while $\Delta n_s \cong 1 \times 10^{-2}$).

In practice, the quantitative measurements were obtained

by replacing the viewing screen (or photographic camera) by a power meter (United Detector Technology model UDT-21A) with a large aperture but masked by a fine slit aligned parallel to the horizontal axis of Figure 3-6. By scanning the detector vertically while directing its analog output to a graphic plotting device, a lateral output profile was obtained where the total power escaping from the prism at any position was integrated by the specially configured detector. A typical scan is shown in Figure 3-6, and more will be presented in Chapter 8.

As a final note on this measurement procedure, we must consider how meaningful numbers can be obtained from these scan traces. The channels are presumably identical and they are single-moded or very nearly so. Therefore, we can assume that their lateral power profile is identical, except for an arbitrary amplitude factor:

$$P_b(y) = A_b^2\, P(y) \quad ; \quad P_a(y) = A_a^2\, P(y) \tag{3-2}$$

Furthermore, the slit through which the measurement is done has a finite width. This means that the scanning of the slit across a channel ("a" for instance) yields the convolution of the mode profile with the slit function S(y) (a square "pulse" in y):

$$P_a^{meas.}(y) = A_a^2 \int_{-\infty}^{+\infty} P_a(y')S(y'-y)\, dy' = A_a^2\, Q(y) \tag{3-3}$$

A similar result holds for the other channel and we see that the maximum height of the traces is a direct measurement of

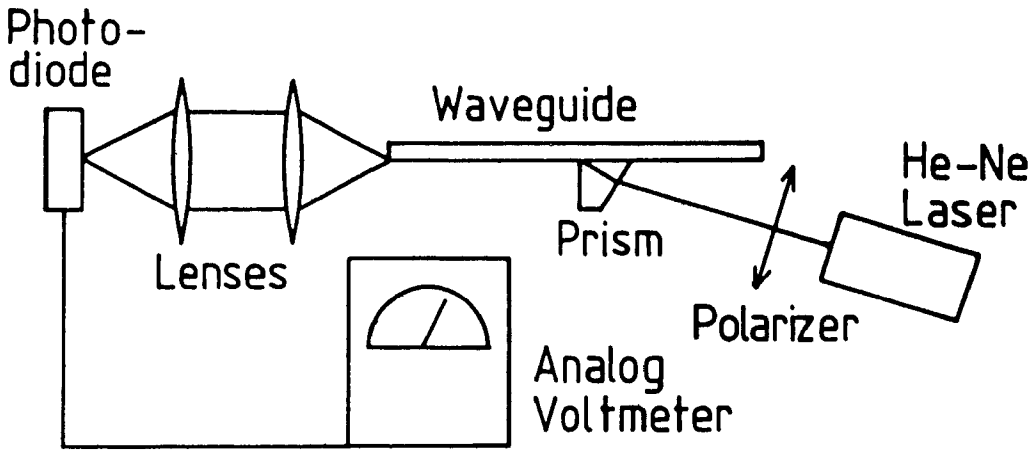

Figure 3-5. Experimental set-up to measure the effective indices of planar guides.

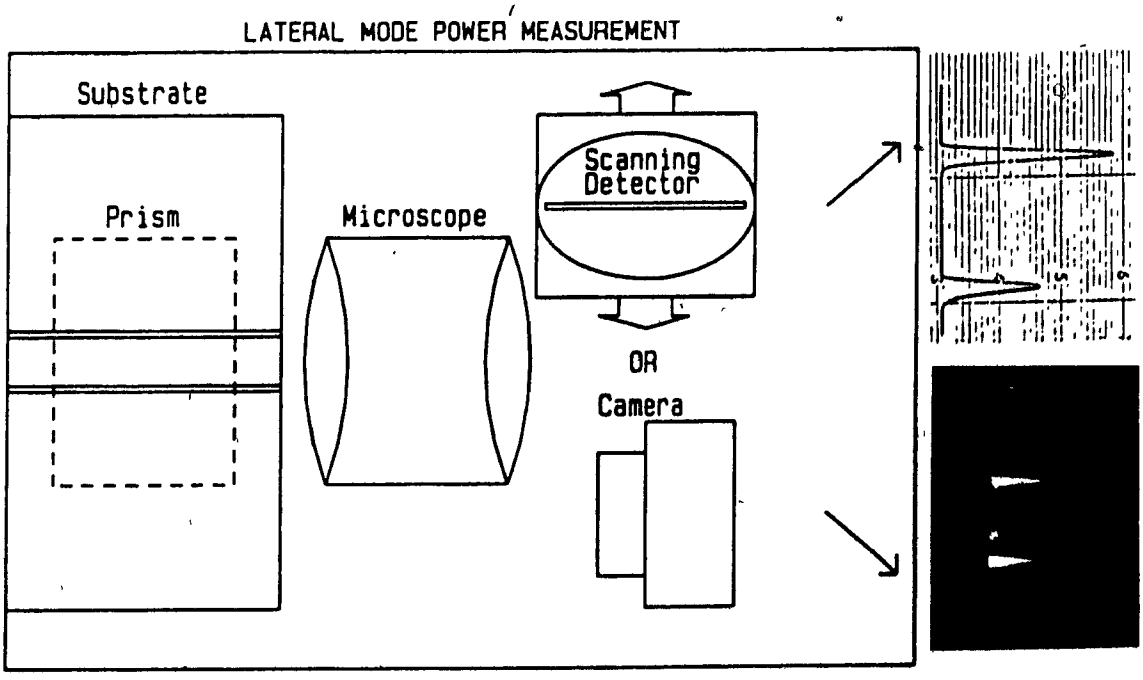

Figure 3-6. Diagram of measurement procedure for the lateral distribution of power in a multichannel device made by two-step ion-exchange. The camera and photodetector can be used interchangeably.

output power, except for a constant factor, which is the same for both channels and cancels out of any relative measurements. This is true regardless of the actual shape of the mode profile function or the slit width!

This completes the description of the experimental facilities and methods used in this work. Results, along with their reduction and analysis, are presented in the following chapters.

CHAPTER 4. CHARACTERIZATION OF PLANAR WAVEGUIDES.

4.1 INTRODUCTION

This extensive characterization was undertaken in order to establish the process parameters that correspond to given waveguide properties. Similar studies have been carried out for the case of Ag^+-Na^+ ion-exchange (both thermal and electric field assisted) in glass, but, for K^+-Na^+, only very sparse and fragmented data were available before our publication of these results. Since then, our work has been extended to other types of glass by another group [Gortych 1986a,b].

The parameters that can be varied for thermal ion-exchange are the temperature of the process and its duration. Additional refractive-index profile modifications, such as heating an already exchanged layer outside a source of ions, have not been considered.

The melting point of KNO_3 being 337°C [Bartholomew 1980], the lowest exchange temperature should be significantly higher to have a reasonably strong thermal agitation in the melt to avoid stagnation of the outgoing ions near the interface. This stagnation effect restricts ion-exchange by limiting the supply of new ions at the boundary. The other end of the temperature range is chosen to be high enough to have a significantly faster rate of exchange but not so high as to lead to surface damage by excessive thermal agitation of the ions near the interface. The following temperatures were used: 370,

385, 400, 425°C, for various time durations. Additionally, one waveguide was made at both 360 and 440°C to extend the range of the characterization.

4.2 RESULTS AND DATA REDUCTION

The normalized propagation constants N_e (also called "effective indices") which have been measured are presented in Tables 4-1a and 4-1b.

From these, the refractive-index profile giving rise to the waveguiding can be obtained. There are two approaches to do this. In the so-called Inverse WKB method [White 1976], the profile is reconstructed by using straight line segments to connect discrete values of index calculated at various depths from the modal measurements. The usefulness and accuracy of this method diminish rapidly with the number of modes supported by the guide. The other approach is statistical and involves finding a refractive index profile for which a solution to the dispersion equation yields effective indices that fit as closely as possible the measured ones. The disadvantage of this method is that the shape of the profile must be chosen a priori to reduce the number of variables in the best fit search (for it to become a tractable problem with reasonable effort). The choice can be based on physical arguments, and then justified by the aptitude of the chosen profile shape in successfully reproducing

the measured data. In this work, a Gaussian function is used to model the index profile of planar waveguides for the reasons which have been developed in chapter 2. The depth coordinate "x" increases from 0 at the surface towards the interior of the substrate:

$$n(x) = n_b + \Delta n_s \, e^{-\frac{x^2}{d^2}} \qquad (4-1)$$

$$\Delta n_s = n_s - n_b \qquad (4-2)$$

where n_s = the index at the surface

n_b = the index of the substrate

d = an effective depth (depth at which $n(x) = \Delta n_s \, e^{-1}$

For this graded-index 1-D waveguiding problem, the effective indices N_e are calculated from the well-known WKB dispersion relation [Hocker 1975]:

$$\frac{2\pi d}{\lambda}\int_0^{\hat{x}_t}\sqrt{n^2(\hat{x}) - N_e^2}\, d\hat{x} = (m + \tfrac{1}{4})\pi + \phi_s \qquad (4-3)$$

$$\phi_s = \tan^{-1}\left(\frac{n_s}{n_c}\right)^p\left(\frac{N_e^2 - n_c^2}{n_s^2 - N_e^2}\right)^{\frac{1}{2}} \qquad (4-4)$$

p = 2 (TM)

0 (TE)

m = 0,1,2,3,... the mode order

λ = free-space wavelength of the light

$\hat{x} = x / d$

x_t = the "turning point" defined by $n(x_t) = N_e$

i.e.

$$\hat{x}_t = \left(\frac{x_t}{d}\right) = \left(-\ln\left(\frac{N_e - n_b}{\Delta n_s}\right)\right)^{\frac{1}{2}} \qquad (4-5)$$

Assuming that n_b is known, n(x) contains two unknowns (Δn_s and d). Therefore, putting two values of N_e with their

mode order m for a given guide in equation (4-3), yields a fully determined problem of two equations and two unknowns. These equations are transcendental and do not form a linear system. To solve them, one of the unknowns is eliminated by using the normalized coordinate $\hat{x}$ and taking the ratio of a pair of equations (4-3) corresponding to a given pair of modes. The resulting equation can be root-searched numerically for Δn_s.

After this is completed, d is found by replacing Δn_s in one equation from the pair. When a waveguide supports more than two modes of a given polarization, the problem is over-determined and the values of d and Δn_s that are retained are the average of the values obtained from all the possible pairings of modes. For single-mode guides, the fact that Δn_s does not depend on the duration of exchange is used and d is calculated from (4-3) by taking the Δn_s found for the other waveguides fabricated at the same temperature. The values found for each waveguide are also listed on Tables 4-1a, 4-1b and the corresponding dispersion curves plotted on Figures 4-1 to 4-4 along with the measured N_e.

4.3 FINDING MODELS FOR (Δn_s, d) vs (T, t)

The results of the previous section show that the individual profiles found for each waveguide can model accurately the effective indices of their modes. However, a deterministic relation between temperature and duration on one side (T,t), and

TABLE 4-1a

Mode index measurements with calculated profile parameters.
TE MODES

T (°C)	#	t (min)	√t (√min)	TE0	TE1	TE2	TE3	TE4	TE5	d (μm)	n_s
360	37	1440	38.0	1.5200	1.5171	1.5150				6.5	1.5223
370	36	126	11.2	1.5161						2.3	1.5222
	34	360	19.0	1.5182	1.5145					4.6	1.5220
	35	631	25.1	1.5188	1.5156	1.5135				5.6	1.5218
	33	1090	33.0	1.5201	1.5174	1.5153				7.0	1.5223
	32	1420	37.7	1.5206	1.5180	1.5162	1.5144			7.9	1.5227
385	31	120	11.0	1.5173						3.1	1.5219
	39	240	15.5	1.5183	1.5148					4.3	1.5218
	17	331	18.2	1.5189	1.5155	1.5132				4.6	1.5222
	20	592	24.3	1.5195	1.5168	1.5146				5.3	1.5220
	19	1036	32.2	1.5200	1.5176	1.5157	1.5142			7.0	1.5219
	18	1440	37.9	1.5202	1.5180	1.5163	1.5149			9.1	1.5218
	38	1440	37.9	1.5203	1.5181	1.5164	1.5150			9.3	1.5218

T (°C)	#	t (min)	√t (√min)	TE0	TE1	TE2	TE3	TE4	TE5	d (μm)	n_s
400	24	60	7.8	1.5162						2.4	1.5221
	22	121	11.0	1.5183	1.5147					4.1	1.5219
	23	180	13.4	1.5188	1.5153	1.5133				4.6	1.5220
	5	250	15.8	1.5191	1.5158	1.5137				5.2	1.5220
	21	355	18.9	1.5198	1.5171	1.5149				6.0	1.5222
	8	520	22.8	1.5201	1.5175	1.5152	1.5141			7.2	1.5222
	6	1066	32.7	1.5200	1.5181	1.5164	1.5150	1.5138		9.6	1.5217
	7	1351	36.8	1.5202	1.5187	1.5172	1.5159	1.5148	1.5137	11.6	1.5217
425	30	30	5.5	1.5173						3.2	1.5219
	28	60	7.8	1.5184	1.5148					4.5	1.5220
	25	150	12.3	1.5196	1.5169	1.5148				5.6	1.5219
	27	240	15.5	1.5201	1.5178	1.5157	1.5142			7.0	1.5223
	10	324	18.0	1.5199	1.5177	1.5159	1.5146			8.0	1.5215
	29	330	18.2	1.5201	1.5180	1.5163	1.5149			9.3	1.5217
	26	420	20.5	1.5203	1.5186	1.5171	1.5156	1.5146		11.1	1.5217
440	13	281	16.8	1.5198	1.5183	1.5167	1.5152			10.6	1.5215

TABLE 4-1b

Mode index measurements with calculated profile parameters.

TM MODES

T (°C)		t (min)	√t (√min)	TM0	TM1	TM2	TM3	TM4	TM5	d (μm)	n_s
360	37	1440	38.0	1.5217	1.5183	1.5158				6.3	1.5244
370	36	126	11.2	1.5173						2.4	1.5238
	34	360	19.0	1.5196	1.5153					3.9	1.5238
	33	631	25.1	1.5202	1.5163	1.5138				4.7	1.5236
	33	1090	33.0	1.5216	1.5184	1.5159	1.5142			6.7	1.5239
	32	1420	37.7	1.5219	1.5188	1.5166	1.5148			7.5	1.5240
385	31	120	11.0	1.5187	1.5139					3.0	1.5241
	39	240	15.5	1.5199	1.5156					4.0	1.5241
	17	331	18.2	1.5205	1.5166	1.5139				4.7	1.5241
	20	592	24.3	1.5213	1.5180	1.5155	1.5132			6.0	1.5242
	19	1036	32.2	1.5217	1.5188	1.5168	1.5151	1.5135		7.9	1.5237
	18	1440	37.9	1.5220	1.5196	1.5175	1.5158	1.5143		8.9	1.5240
	38	1440	37.9	1.5218	1.5195	1.5177				9.7	1.5235

T (°C)		t (min)	√t (√min)	TM0	TM1	TM2	TM3	TM4	TM5	d (μm)	n_s
400	24	60	7.8	1.5175						2.4	1.5241
	22	121	11.0	1.5199	1.5155					3.9	1.5242
	23	180	13.4	1.5204	1.5164	1.5139				4.8	1.5238
	5	250	15.8	1.5207	1.5170	1.5144				5.2	1.5239
	21	355	18.9	1.5216	1.5185	1.5158				6.4	1.5245
	8	520	22.8	1.5219	1.5189	1.5166	1.5151			7.6	1.5240
	6	1066	32.7	1.5215	1.5194	1.5176	1.5159	1.5143		9.6	1.5233
	7	1351	36.8	1.5217	1.5204	1.5185	1.5169	1.5156	1.5145	11.5	1.5234
425	30	30	5.5	1.5185						3.2	1.5236
	28	60	7.8	1.5197	1.5155					4.0	1.5238
	25	150	12.3	1.5210	1.5179	1.5154				6.3	1.5237
	27	240	15.5	1.5214	1.5190	1.5166	1.5147			7.7	1.5239
	10	324	18.0	1.5214	1.5190	1.5171	1.5152	1.5140		8.7	1.5233
	29	330	18.2	1.5214	1.5191	1.5172	1.5155	1.5143		9.2	1.5232
	26	420	20.5	1.5217	1.5197	1.5179	1.5161	1.5152		10.4	1.5234
440	13	281	16.8	1.5214	1.5194	1.5179	1.5164	1.5149		10.8	1.5231

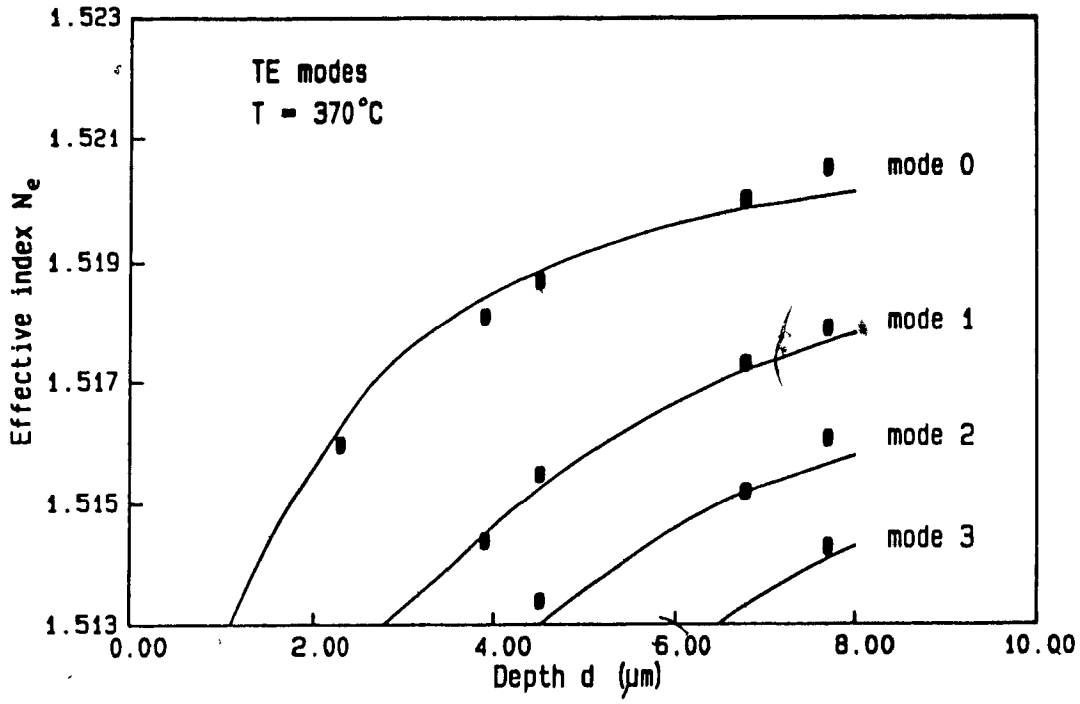

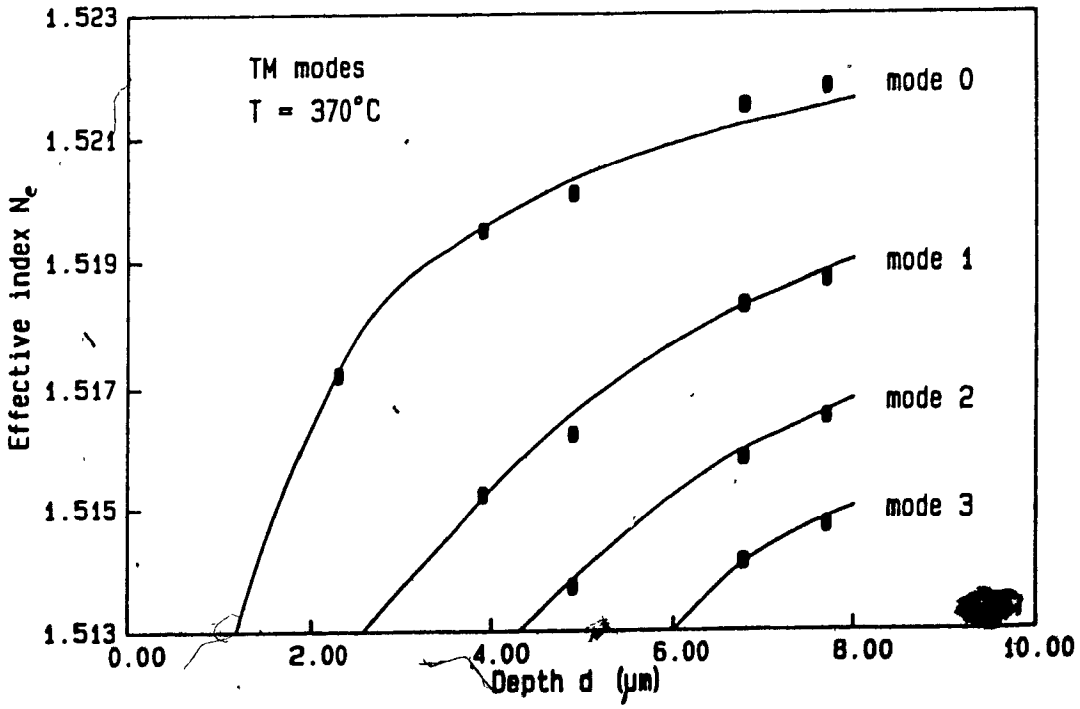

Figure 4-1. Theoretical dispersion curves for planar guides, calculated with best fit value of Δn_s, along with measured values of effective indices. T=370°C. a) TE modes. b) TM modes.

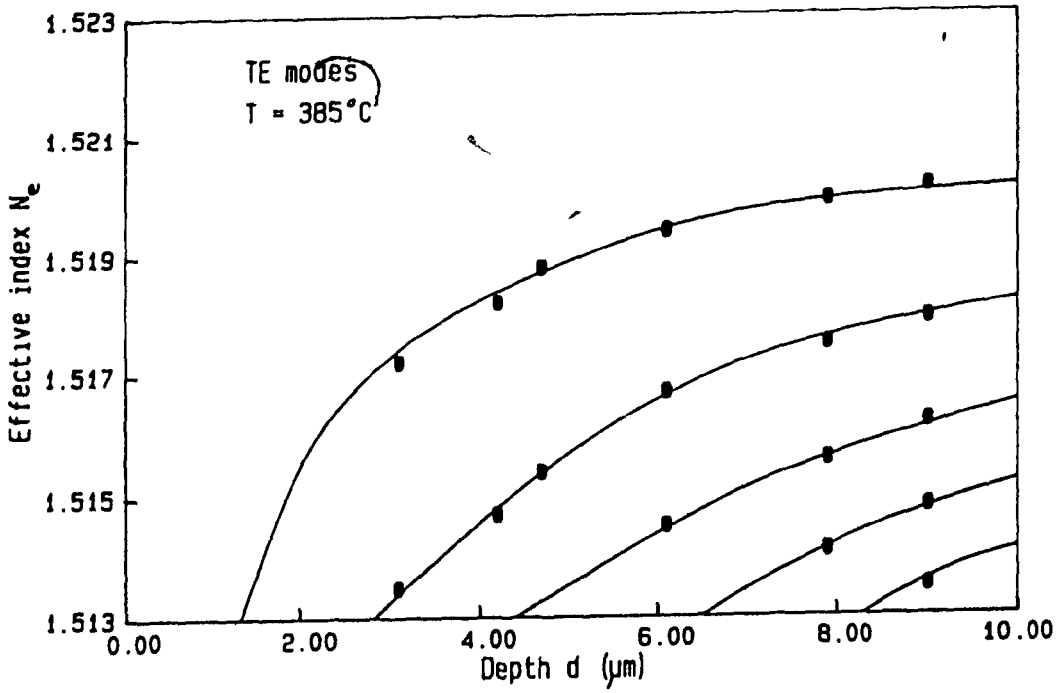

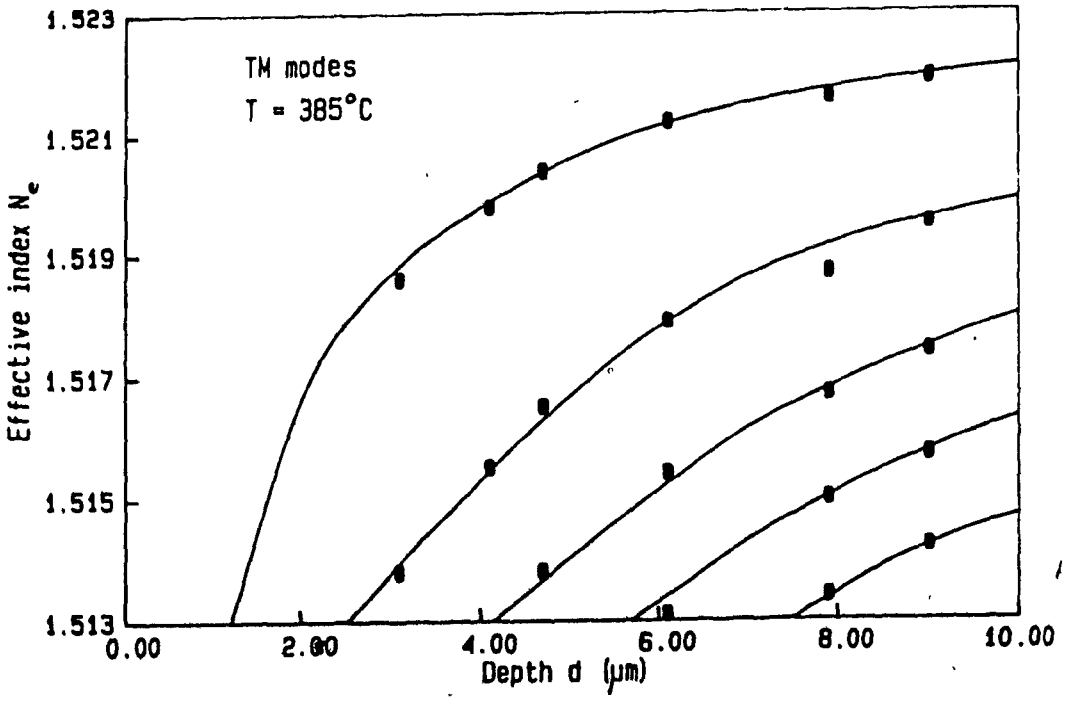

Figure 4-2. Theoretical dispersion curves for planar guides, calculated with best fit value of Δn_s, along with measured values of effective indices. T=385°C. a) TE modes. b) TM modes.

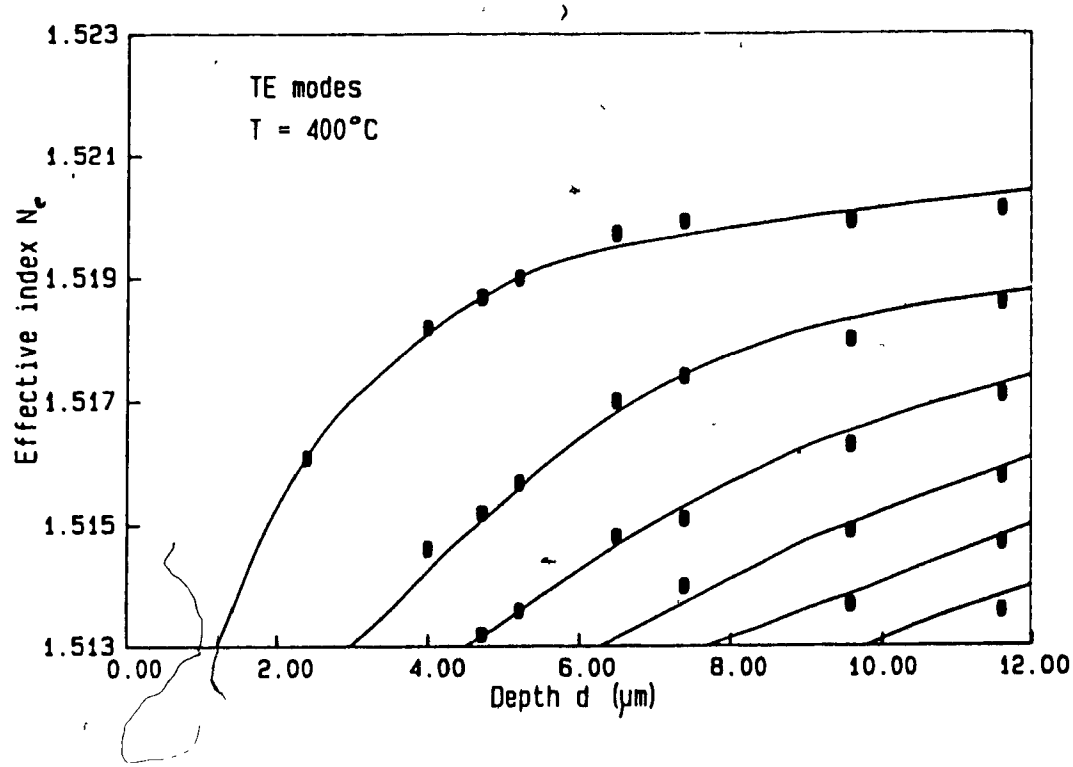

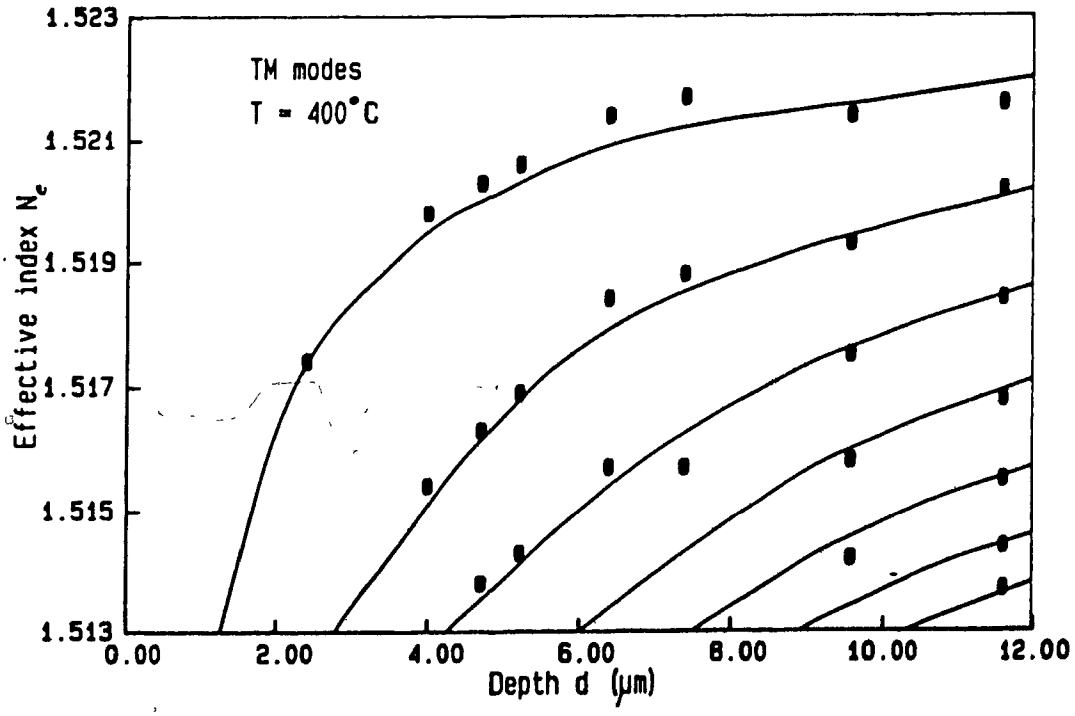

Figure 4-3. Theoretical dispersion curves for planar guides, calculated with best fit value of Δn_s, along with measured values of effective indices. T=400°C. a) TE modes. b) TM modes.

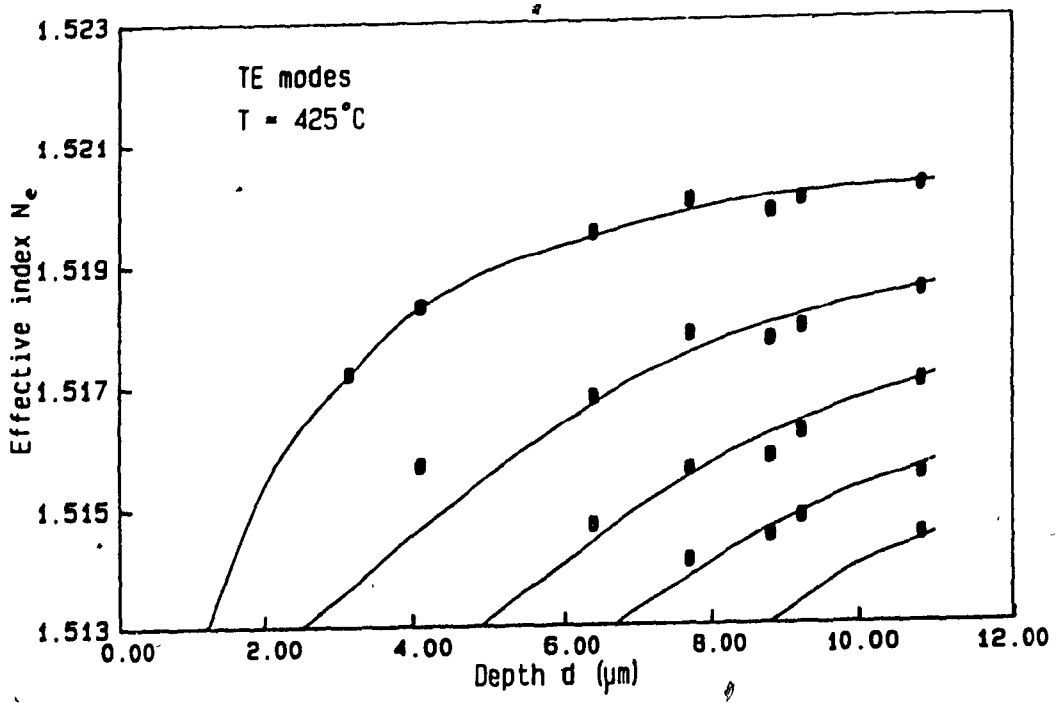

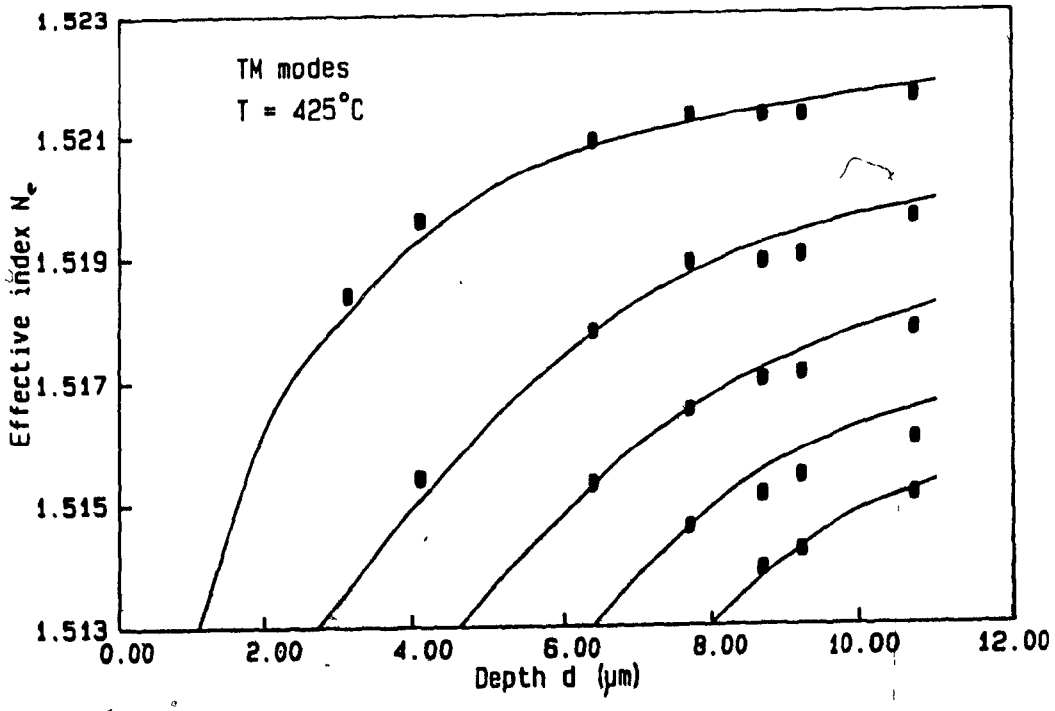

Figure 4-4. Theoretical dispersion curves for planar guides, calculated with best fit value of Δn_s, along with measured values of effective indices. T=425°C. a) TE modes. b) TM modes.

(Δn_s,d) on the other side is needed to enable the specification of waveguide parameters from arbitrary fabrication conditions. In Chapter 2, we did find that the depth of the index profile (as defined in eqn.(4-2)) is proportional (see 2-54)) to the square root of the duration (at a given temperature):

$$d = \sqrt{D_e t} \qquad (4-6)$$

We introduce here the concept of an "effective diffusion coefficient" D_e that includes all the proportionality factors and depends on the profile and the actual definition of d that is used.

It is easy to verify the validity of (4-6) by plotting d against $\sqrt{t}$ for all the guides measured. This is done on Figure 4-5. On these plots, straight lines (forced through the origin) are fitted to the data points by a least-squares procedure to yield the coefficients $D_e(T)$. Finally, to model the relation between D_e and T, the similarity of ion-exchange with classical diffusion is exploited by looking for an Arrhenius [Chartier 1983] type of equation:

$$D_e = D_0 \, e^{\frac{-\Delta H}{RT}} \qquad (4-7)$$

where D_0 - constant to be determined

ΔH - an activation energy (also to be determined)

R - molar gas constant (8.31 Joules-mole^{-1}-°K^{-1})

The values of D_0 and $\Delta H/R$ are found by fitting straight lines to plots of $\ln(D_e)$ vs (1/T). This is illustrated in

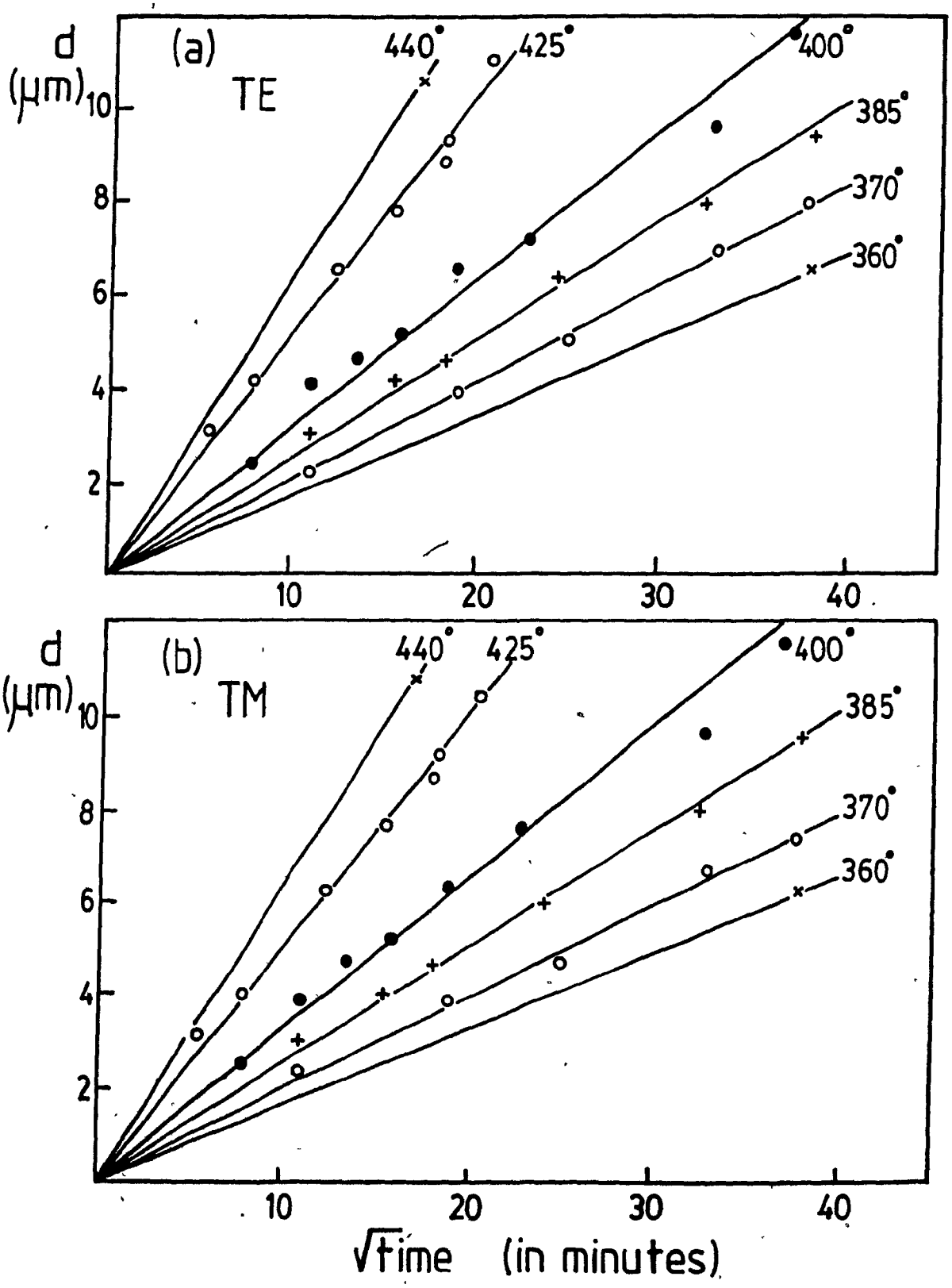

Figure 4-5. Guide depth d versus the square root of the exchange time, for various temperatures (labeled in °C). a) TE modes. b) TM modes.

Figure 4-6 where the validity of equation (4-7) is clearly demonstrated.

Table 4-2 summarizes all the results of this characterization. The information contained therein allows for the calculation of the index profile of K^+-Na^+ ion-exchanged waveguides fabricated in soda-lime glass for any temperature or duration.

4.4 DISCUSSION OF ERRORS

In this sort of work, it is not so much the absolute accuracy in Δn_s and d that counts but rather how accurate the effective indices calculated from them are. In order to answer that question, the average difference between the measured N_e's (167 data points) and the values calculated from the results of section 4.3 has been found to be equal to 1.6×10^{-4} ($\pm$ 1.2×10^{-4}), smaller than the measurement uncertainty on N_e. The single largest difference is 6×10^{-4}.

The problem of estimating the correctness of the choice of the profile and of the values of Δn_s and d by another independent measurement is far from trivial and is addressed in the next section.

Another question of interest, which relates more to the quality of the fabrication procedure, is about the reproducibility of the results. To evaluate that property, two waveguides were made, more than 5 months apart, in the same

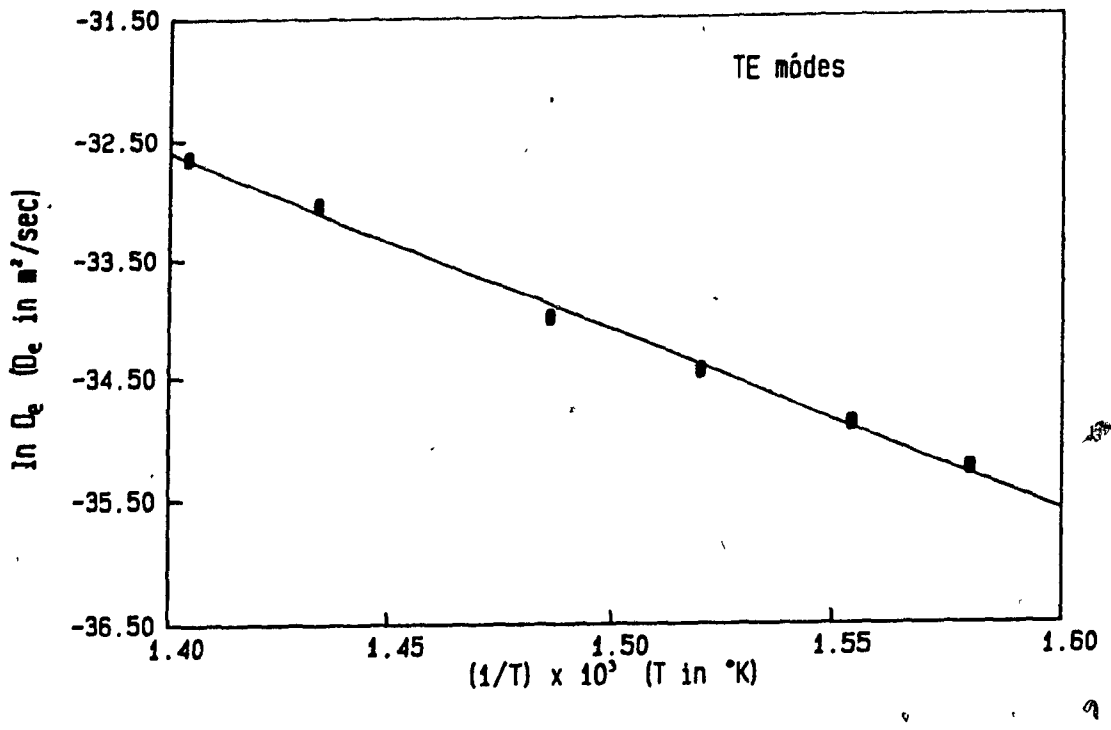

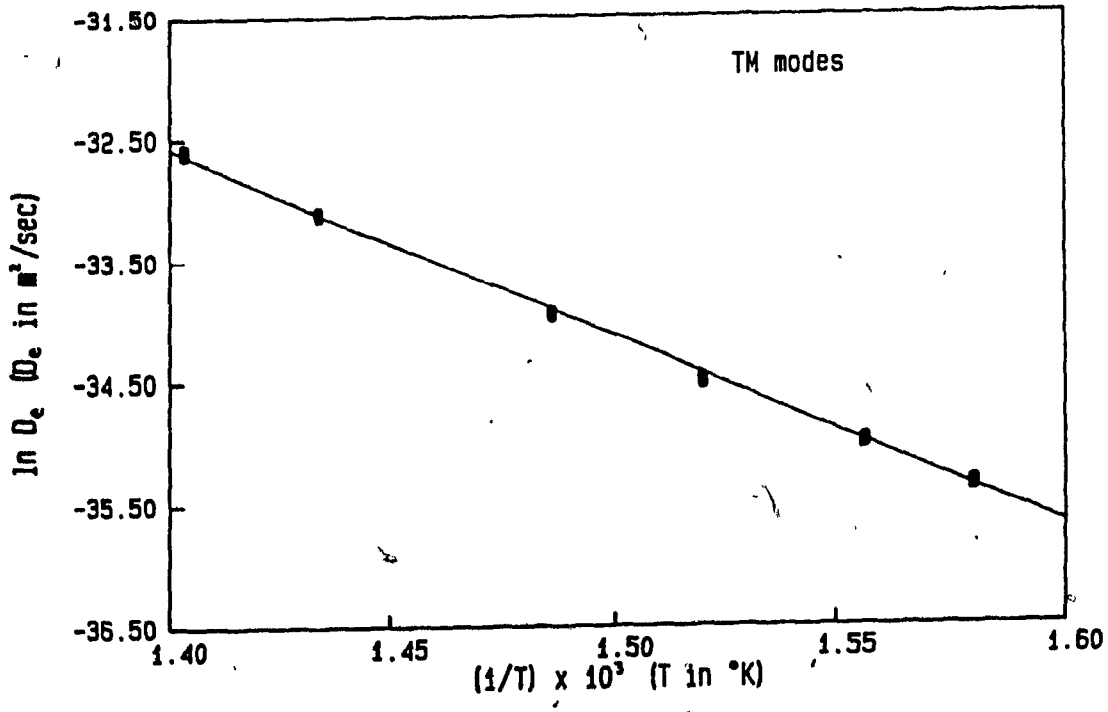

Figure 4-6. Natural logarithm of the effective diffusion coefficient D_e versus the inverse of the temperature in Kelvins. The straight line is a best fit to the individual points.
a) TE modes. b) TM modes.

TABLE 4-2

Summary of results for the characterization of planar waveguides made by K^+-ion exchange in soda-lime glass.

T (°C)	$\Delta n_s^{TE} \times 10^3$	$\Delta n_s^{TM} \times 10^3$	$D_e^{TE} \times 10^{16}$ (m^2/sec)	$D_e^{TM} \times 10^{16}$ (m^2/sec)
360	9.2 ± 0.3	11.3 ± 0.3	4.91	4.53
370	9.1 ± 0.5	10.7 ± 0.4	7.18	6.50
385	8.8 ± 0.2	10.8 ± 0.4	10.82	10.61
400	8.7 ± 0.3	10.5 ± 0.5	17.14	18.02
425	8.7 ± 0.3	10.4 ± 0.4	45.21	42.16
440	8.4 ± 0.5	10.0 ± 0.6	66.78	68.81

$$D_e^{TE} = 7.82 \times 10^{-6} \exp\left(\frac{-1.49 \times 10^4}{T}\right) \ (m_2/sec) \pm 2\%$$

$$D_e^{TM} = 1.60 \times 10^{-5} \exp\left(\frac{-1.54 \times 10^4}{T}\right) \ (m_2/sec) \pm 2\%$$

$$d = \sqrt{D_e t}$$

conditions (time and temperature). Their measured effective indices, along with the resulting profile parameters, are presented in Table 4-1a as numbers 18 and 38 for T = 385°C. The agreement is better than 5% for Δn_s, 10% for d, and within experimental error for N_e, which is not bad considering the absolute size of the quantities involved (difficulties prevented the measurement of high order TM modes.

4.5 INTERPRETATION OF THE RESULTS

Although a certain number of assumptions were made in the process of modelling the different parameters involved in this characterization, the experimental results did follow the various relationships that were introduced somewhat arbitrarily. Also, the models introduced for $(\Delta n_s, d)$ vs (T, t) have been shown to succeed in reproducing the experimentally determined values of effective indices, within measurement accuracy. However, the evidence for, among other things, the Gaussian shape of the profile, is indirect and probably inconclusive. In an extension of our work on K^+-Na^+ exchange to other types of substrate glass, another group [Gortych 1986a,b] has used successfully a different profile (an error function complement) in the fitting procedure of section 4.2. Although their fabrication methods are different from ours and also that the exact profile does vary with the type of glass (see Chapter 2),

such a fundamental change of shape may seem surprising.

An explanation of that observation is that there is a certain degree of insensitivity to the exact shape of the profile in the solution of (4-3) (especially near the origin), and that other means of measurement are needed to conclusively determine the shape of the profile. However, these methods would need a depth resolution of the order of a tenth of a micron (because the differences between the erfc and Gaussian functions occur on such a scale) along with a high sensitivity to very small quantities of K^+ ions (a few percent) in the glass. This is clearly not an easy experimental problem, and for the purpose of designing optical waveguide structures, the model that we have used is more than sufficiently accurate to be useful, and well justified physically (Chapter 2).

Also, it seems that the types of glass used in those studies may have a much lower value of $\hat{\alpha}$ than soda-lime glass, which has the highest value of the glasses compiled in [Doremus 1969]. In that case the better fit with the erfc function is not surprising, as can be seen in Figure 2-1.

CHAPTER 5. THE ORIGIN OF THE INDEX CHANGE FOR K^+-Na^+ EXCHANGE.

5.1 INTRODUCTION

The fabrication process for optical waveguides by ion-exchange usually involves a silicate glass substrate containing soda (Na_2O) and various other oxides (CaO, K_2O, Al_2O_3, etc...). This process has been known for a long time [Schulze 1913], for purposes different from waveguide fabrication, and has been used successfully to strengthen glass by inducing a high compression layer at the surface to prevent crack formation and propagation [Bartholomew 1980].

The explanation for the index change resulting from ion-exchange is based on the fact that the ions participating in the exchange have different electronic polarizabilities and that they occupy a different volume in the glass. An index increase results from ions of higher polarizability and/or of smaller volume. The relevant parameters are presented in Table 5-1 [Findakly 1985].

TABLE 5-1

ion	Polarizability ($Å^3$)	Ionic Radius (Å)	Exp. Δn
Na^+	0.41	0.95	-
Ag^+	2.40	1.26	~10%
K^+	1.33	1.33	~1%

Qualitatively, it appears that in both cases the increase

in the polarizability is the dominant effect and that it is somewhat correlated to the resultant Δn. However, an attempt to calculate the index change simply from the compositional change, based on a model due to [Huggins 1940] and refined by [Fantone 1983], yields the correct value for the Ag^+-Na^+ case (see below), but fails completely in the case of K^+-Na^+ [Fantone 1983, Gortych 1986a,b], underestimating Δn by 2 orders of magnitude. It would appear that in the latter case the increase due to the polarizability is almost exactly cancelled by the decrease due to the volume change; and yet we do get a Δn of 1% experimentally.

We present here a quantitative explanation of this discrepancy based on the effect of the large induced stresses at the surface through the photoelastic effect. Apart from its interest as a basic phenomenon, the theory behind the stress-induced index change may lead to a better understanding of how the fabrication procedures affect the properties of the optical waveguides.

In the following section, the Huggins-Fantone (H-F) model is described and its predictions compared with the experimental results. Then, in the third section, we will discuss how stresses develop in the exchanged layer and how they influence the index change calculated from the H-F model. Finally the implications and applications of our calculations will be discussed.

5.2 THE HUGGINS-FANTONE MODEL

The derivation presented here follows that of [Fantone 1983]. The refractive index n of a silicate glass can be expressed in terms of its composition by:

$$n = 1 + \frac{R_0}{V_0} \qquad (5-1)$$

where R_0 is the refraction per mole of oxygen ions and V_0 is the volume of glass per mole of oxygen ions.

[Huggins 1940] showed that both V_0 and R_0 can be calculated directly from the composition of the glass through a set of empirically determined coefficients in the following linear relationships:

$$V_0 = cte + \sum b_M N_M \qquad (5-2)$$

$$R_0 = \sum a_M N_M \qquad (5-3)$$

where N_M is the number of moles of ion I contributed by the molecular component M = $I_m O_n$ (K_2O or Al_2O_3 for instance) per mole of oxygen ions contributed by all the components of the glass. It is calculated from the compositional data in weight fractions by the following formula:

$$N_M = \frac{m_M f_M / W_M}{\sum n_M f_M / W_M} \qquad (5-4)$$

where W_M is the molecular weight (weight of one mole) of the component M, f_M its weight fraction in the glass, m_M the number of ions I and n_M the number of oxygen (O) ions in the molecular formula. Relevant coefficients are listed in Table 5-2 (from [Fantone 1983], Table II for b and Table V for a):

TABLE 5-2

Ion	a*	b
Na^+	6.02	8.7
Ag^+	15.97	12.72
K^+	9.54	15.5

All units in cm^3/mole of ion

* The value of a is wavelength-dependent. Its value for 656 nanometers is used here although our working wavelength is 633 nanometers (differences in "a" are fairly insensitive to wavelength in that region).

Let us examine what happens to R_0 and V_0, and consequently to n, when we exchange a fraction χ of Na^+ ions with K^+ (or Ag^+) ions:

$$V_0^* = cte + \sum' b_M N_M + (1-\chi) b_{Na} N_{Na} + \chi b_K N_{Na} \qquad (5-5)$$

$$R_0^* = \sum' a_M N_M + (1-\chi) a_{Na} N_{Na} + \chi a_K N_{Na} \qquad (5-6)$$

where $\sum'$ indicates summation over all components except sodium and potassium (recall that N_{Na} refers to the initial concentration of sodium ions).

Then:

$$V_0^* - V_0 = \chi \Delta V = \chi N_{Na} (b_K - b_{Na}) \qquad (5-7)$$

$$R_0^* - R_0 = \chi \Delta R = \chi N_{Na} (a_K - a_{Na}) \qquad (5-8)$$

yielding:

$$\Delta n = n^* - n = \frac{R_0^*}{V_0^*} - \frac{R_0}{V_0} = \frac{R_0 + \chi \Delta R}{V_0 + \chi \Delta V} - \frac{R_0}{V_0} \qquad (5-9)$$

and, neglecting terms of order 2 in Δ:

$$\Delta n \approx \frac{\chi}{V_0}(\Delta R - \frac{R_0}{V_0}\Delta V) \qquad (5\text{-}10)$$

Equation (5-10) constitutes a demonstration that the index change resulting from ion-exchange is in fact proportional to the amount of exchange χ, and therefore to the concentration of new ions (because $\chi = N_K/N_{Na}$). This is a result often used but rarely proved.

In order to calculate Δn from (5-10) we need to know the N_{Na} of the substrate. Using a typical compositional data for ordinary soda-lime glass (given in Table 5-3) [Shand 1958, Gortych 1986a], we get $N_{Na} = 0.155$. For $K^+ - Na^+$ exchange, this values gives:

$$\Delta V = 1.054 \text{ cm}^3/\text{mole } O^- \text{ ions}$$

$$\Delta R = 0.546 \text{ cm}^3/\text{mole } O^- \text{ ions}$$

$$\Delta n \approx 3\times10^{-4}\chi$$

TABLE 5-3

	n	m	f(%)	W(gr/mole)
SiO_2	2	1	72	60.1
Na_2O	1	2	14	62.0
CaO	1	1	9	56.1
MgO	1	1	4	40.3
Al_2O_3	3	2	1	102.0

$n(\lambda=633 \text{ nm}) = 1.513$

$V_0 \approx 15. \text{ cm}^3/\text{mole of } O^- \text{ ions [Fantone 1983]}$

Since χ lies between 0 and 1, the last result is two orders of magnitude too small (see Chapter 4). A similar conclusion holds for BK-7 glass [Gortych 1986a,b and Fantone 1983]. Using the same N_{Na} for $Ag^+ - Na^+$ exchange, we get $\Delta n \approx .08\chi$,

in good agreement with the measured value of 0.09 [Stewart 1977].

What is so peculiar about K^+-Na^+ that makes the H-F model fail? We will show in the next section that this process, known as 'ion stuffing' for surface strenghtening in the glass industry [Bartholomew 1980], does not allow free expansion of the glass to accommodate the larger K^+ ions. Therefore, the value of ΔV to be used in (5-10) is smaller than the calculated one and results in a larger value of Δn. The same effect occurs for Ag^+-Na^+ exchange but in that case its magnitude is 10 times smaller than the index change calculated without it. It is the almost exact cancellation of the two terms of (5-10) which makes it significant for the potassium case.

5.3 CORRECTIONS DUE TO SURFACE-INDUCED STRESS

The build-up of stress by ion-exchange is a well-known fact in the glass industry. [Kistler 1962] observed measurable bending of thin (1 mm) glass plates by exchanging various types of ions on one side only of the plates. When the ratio of exchanged depth (d) to substrate thickness (b) is very small, as is generally the case with optical waveguides, the amount of stress relaxation due to bending and stretching of the whole substrate becomes negligible (of the order of (d/b) away from the edges to be precise, see [Timoshenko 1951], with [Richmond

1964] for the analogy between thermal stress and chemical exchange stress). In that case, it is as if the newly exchanged glass, with its larger volume, had been compressed back by the resistance of the substrate to expand laterally. The only direction of free expansion to accommodate the larger size is in the direction perpendicular to the plane of the substrate, where the glass-air interface opposes no resistance. This is clearly shown in, [Bradenburg 1986] and also in Section 5.4.

Translated into elastic analysis, these statements are equivalent to saying that the following longitudinal stresses σ_i have been applied to the exchanged glass [Richmond 1964]:

$$\sigma_y = \sigma_z = \sigma_0 \qquad \sigma_x = 0 \tag{5-11}$$

The change in volume resulting from these stresses is given by [Timoshenko 1951]:

$$\frac{\Delta V'}{V} = \epsilon_x + \epsilon_y + \epsilon_z \tag{5-12}$$

where the strains ϵ_i are related to the stresses by Hooke's law [Timoshenko 1951]:

$$\left.\begin{aligned} \epsilon_x &= \frac{1}{E}(\sigma_x - \nu(\sigma_y + \sigma_z)) = \frac{-2\nu\sigma_0}{E} \\ \epsilon_y &= \frac{1}{E}(\sigma_y - \nu(\sigma_x + \sigma_z)) = \frac{(1-\nu)\sigma_0}{E} \\ \epsilon_z &= \frac{1}{E}(\sigma_z - \nu(\sigma_x + \sigma_y)) = \frac{(1-\nu)\sigma_0}{E} \end{aligned}\right\} \tag{5-13}$$

This gives for the volume change (i.e. the amount of volume change that could not occur due to the resistance of the substrate):

$$\frac{\Delta V'}{V} = \frac{2\sigma_0}{E}(1-2\nu) \tag{5-14}$$

where E is Young's modulus and ν is Poisson's ratio. For soda-

lime glasses we have [Shand 1958]:

$$E = 7.2 \times 10^4 \text{ N/mm}^2$$

$$\nu = 0.21$$

In order to evaluate (5-14), an estimate of σ_0, the maximum stress at the surface of the substrate, is needed. From [Kistler 1962 and Bradenburg 1986], we can estimate σ_0 to lie between -700 and -1000 N/mm^2 (compressive stresses are negative). Of course the exact value depends on a lot of factors, like the glass composition and the temperature of the process, but we can use this range as fairly representative since their experimental conditions were reasonably similar to ours.

The highest value of the stress range (i.e. -1000N/mm^2) gives the best agreement with our Δn_s values and will be used here. This can be explained by the fact that the temperatures that we have chosen are much lower than the strain point of glass (515°C [Shand 1958], below which very little stress relaxation occurs).

First, we compute the relative volume change in terms of the molar volume (choosing $V-V_0$ = 15 cm^3/mole O^-, in (5-14)):

$$\frac{\Delta V'}{V_0} = -0.017 \qquad \Delta V' = -0.25$$

Then, the net volume change (from ionic change minus the compression) is:

$$\Delta V_{net} = \Delta V + \Delta V' = 1.054 - 0.25 = 0.804 \qquad (5\text{-}15)$$

Substituted in (5-10), the new value for ΔV yields:

$$\Delta n_{max} = 8.9 \times 10^{-3}$$

This result does not take into account the existence of a birefringence, induced by the anisotropic stress through the photoelastic effect [Morey 1938]. Light polarized along the plane of the substrate (i.e. parallel to the stress) and perpendicular to it will travel at different velocities (the former corresponds to TE waves, the latter to TM waves). Also, the maximum value of index change should occur at the minimum exchange temperature. This is because at higher temperatures the viscosity of the glass decreases and relaxation (diminution) of stress occurs. Then, $\Delta V'$ is smaller, ΔV_{net} is larger, and Δn smaller by (5-10). Both of these effects have been observed experimentally as can be seen in Table 4-2.

The birefringence can also be calculated from a stress point of view. From photoelastic theory, we have in our case [Shand 1958]:

$$\delta = \Delta n_{TE} - \Delta n_{TM} = B\sigma_0 \qquad (5-16)$$

where B is the birefringence factor of the material. For soda-lime glass [Shand 1958], $B \approx 2.4 \times 10^{-6}$ mm^2/N. This gives a δ of 2.8×10^{-3}, somewhat higher but still pretty close to the maximum measured value of $(2.1 \pm 0.6) \times 10^{-3}$ (see Table 4-2).

A comparison of the main results of this analysis with the experimental values is presented in Table 5-4.

It should be noted at this point that many stress

mesurements in glass are carried out in the opposite way as was done here. The birefringence is measured interferometrically or by some other optical means and the stress is calculated with the help of photoelastic coefficients or of the birefringence factor.

In the case of ion-exchange, this approach is to be taken with caution. First of all, most of these methods lack the sub-micron resolution needed to pinpoint the actual maximum of the stress profile (which is only one or two microns deep as a whole) and yield a value that is somewhat lower due to averaging. Secondly and perhaps more important, the material parameters used (photoelastic coefficients) are generally those of the substrate glass. This turns out to be incorrect because the photoelastic constants are fairly sensitive to glass composition [Shand 1958 and Schaefer 1953] and that the exchanged glass has a very different composition than that of the substrate: soda-lime glass can hardly be still designated as such after all the sodium is replaced by potassium. This inaccuracy is reflected in our results as a larger error in δn because we had to use the stress factor B of soda-lime glass. By contrast, the elastic properties are relatively less sensitive to composition [Shand 1958] and therefore give a better result for Δn_s.

Regarding the fact that K^+-Na^+ exchange in BK-7 glass yields waveguides with higher Δn_s than those made in soda-

lime glass [Gortych 1986a,b], even though it contains less sodium, the explanation lies probably in the blocking effect of calcium. BK-7, contrary to soda-lime, does not contain this element, which has been known to restrict the exchange of potassium for sodium [Bartholomew 1980] and therefore the size of the final index change.

Finally, the Ag^+-Na^+ process also gives rise to surface induced stresses because of the even lower temperatures used (215-250°C) and of the size mismatch (Table 5-1). Using $\sigma_0 = -200\ N/mm^2$ (from [Bradenburg 1986]), we get a stress-corrected Δn_s of 8.33×10^{-2} instead of 8.16×10^{-2} (see Table 5-4), and a stress-induced birefringence of 5×10^{-4}. Both of these corrections are very small (0.5 and 1% of the measured Δn_s respectively) and unlikely to have been observed other than by a specifically designed measurement.

TABLE 5-4

Ions	ΔV	ΔR	Δn	ΔV'	Δn(+str.)	Δn(exp)	δn	δn(exp)
K^+-Na^+	1.054	.546	.0003	-.25	.0089	.008-.009	.0024	.0014-.0021
Ag^+-Na^+	.62	1.542	.082	-.05	.083	.09	.0005	-

All ΔV and ΔR in the table are in cm^3/mole O^-.

5.4 OBSERVATION OF SURFACE COMPRESSION

The expansion of the glass resulting from ion-exchange can be observed by measuring height differences between exchanged and masked areas on a flat substrate.

To verify this, a waveguide was fabricated at a temperature of 360°C for a time of one hour with an aluminium mask covering part of the substrate. After removing the mask, a surface profiler was used to scan the height of the surface across the boundary of the exchanged area. The result is shown in Figure 5-1 and the measured height is 22 nanometers, for a waveguide which is 1300 nanometers deep. Measurements at higher temperatures yielded lower strains, again consistent with the theory of Section 5.3.

5.5 CONCLUSIONS

We have shown that the refractive index increase and birefringence resulting from potassium-sodium ion-exchange in soda-lime glass is almost exclusively due to a stress-induced surface effect. This is in total contrast with the case of silver-sodium exchange where most of the index increase is due to a volume effect and to the difference in polarizability of the ions, and where no birefringence has been reported.

Some of the implications of these results are as follows. First, the proportionality between index change and concentration of exchanged ions, which can be explained as in

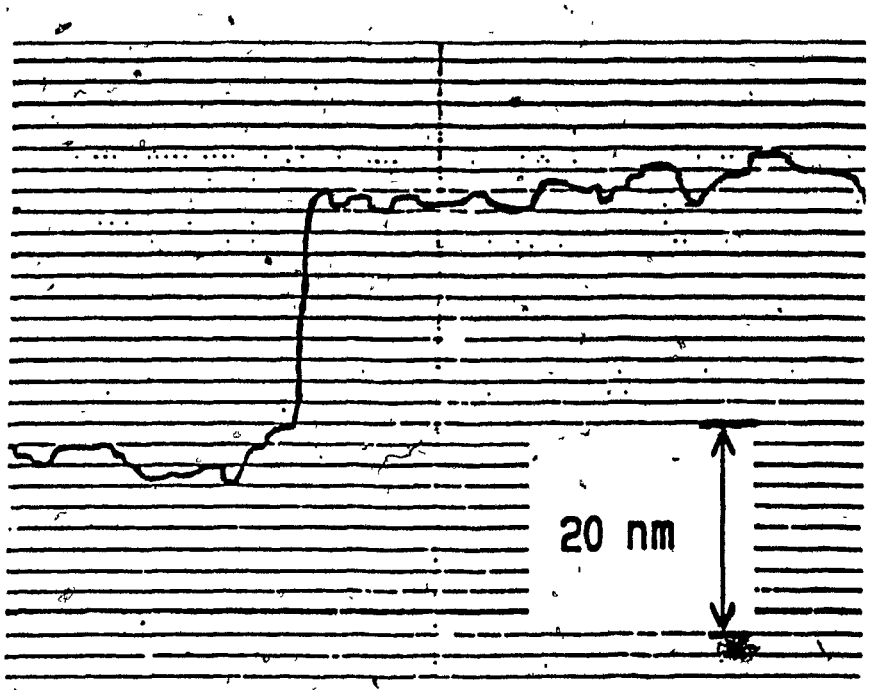

Figure 5-1. Height change due to stress-induced swelling at the boundary of ion-exchanged area.

Section 5-2, may not hold when stresses are taken into account. Near the surface the relationship is still valid because the volume correction (5-14) is proportional to σ_0, which is itself proportional to the exchanged concentration [Richmond 1964]. For deeper waveguides however, the normal stress component σ_x may no longer be neglected away from the free surface and the variation of $\Delta V'$ with depth becomes more complicated. Second, in the heat treatment of a waveguide to increase its cross-section and lower its maximum index change by allowing the diffusion to proceed without a source of exchanging ions, the effect of stress relaxation must be considered as much as the redistribution of exchanged ions. This is true of all the fabrication procedures: whenever a prediction of refractive index shape is attempted based on experimental parameters, the influence of these on the state of stress should be included in the analysis. As a final example on this topic, an attempt to bury the waveguiding layer below the surface of the substrate by back-diffusion with the original ion present in the glass (Na^+), may increase scattering loss instead of decreasing it because this process induces <u>tensile</u> stresses on the originally compressed glass, which could promote crack formation and propagation [Kistler 1962]. In view of what has been presented in this chapter, a more efficient way of burying a waveguide layer would be to subject an ordinary ion-exchanged

substrate to a very high temperature (above the softening point of soda-lime glass, 735°C [Shand 1958, Table 2-1]) for a short period of time. This would lead to total stress relaxation at the surface by allowing glass flow (thereby locally reducing the index change to zero) while deeper layers would remain unaffected because of the relatively poor thermal conductivity of glass.

CHAPTER 6. CHANNEL WAVEGUIDE MODELLING AND DESIGN

6.1 STATEMENT OF THE PROBLEM

A structure which is relatively uniform in one direction (say, the $\hat{z}$ direction to be consistent with the previous chapters), and has a limited region of refractive index higher than that of its surroundings (in the $\hat{x}$-$\hat{y}$ plane) has the property that it can be used to confine an electromagnetic wave, under the right circumstances (see for example [Marcuse 1982]). The previous chapters have demonstrated a method to fabricate such structures in glass. Here, the modes of propagation of these waveguides are derived, starting from Maxwell's equations. Using phasor notation, a time dependence of $e^{j\omega t}$ is assumed throughout since the fields are monochromatic (the dispersive effect of modulation of the optical waves is neglected because the propagation lengths are too small for frequency variations of the order of .001% (GHz vs optical frequencies) to have any effect).

In those conditions, and assuming non-magnetic materials, the source-free Maxwell's equations are written:

$$\nabla \times \mathbf{H} - j\omega\epsilon\mathbf{E} = 0 \qquad (6\text{-}1)$$

$$\nabla \times \mathbf{E} + j\omega\mu_0\mathbf{H} = 0 \qquad (6\text{-}2)$$

$$\nabla \cdot (\epsilon\mathbf{E}) = 0 \qquad (6\text{-}3)$$

$$\nabla \cdot \mathbf{H} = 0 \qquad (6\text{-}4)$$

The vector wave equation for E is derived in the usual manner

by taking the curl of (6-2) and replacing (6-3) in the result. Because of the dependence of ϵ on (x,y,z), the wave equation has one more term than is usually the case:

$$\nabla(\nabla \ln(\epsilon) \cdot \mathbf{E}) + \nabla^2\mathbf{E} + \omega^2\mu_0\epsilon\mathbf{E} = 0 \qquad (6-5)$$

The wave equation for **H** is derived similarly:

$$\nabla \ln(\epsilon) \times (\nabla \times \mathbf{H}) + \nabla^2\mathbf{H} + \omega^2\epsilon\mu_0\mathbf{H} = 0 \qquad (6-6)$$

Now, we assume that the waveguide is uniform in $\hat{z}$ and that we have propagating fields in that direction (i.e. "modes" of the waveguide). In that case, the z dependence of the fields is given by $e^{-j\beta z}$. We also replace $\omega^2\mu_0\epsilon$ by $k^2n^2(x,y)$, where k is the wavenumber in free-space ($\omega\sqrt{\epsilon_0\mu_0}$), and the wave equations become:

$$\nabla(\nabla_t \ln(\epsilon) \cdot \mathbf{E}) + \nabla_t^2\mathbf{E} + (k^2n^2(x,y) - \beta^2)\mathbf{E} = 0 \qquad (6-7)$$

$$\nabla_t \ln(\epsilon) \times (\nabla \times \mathbf{H}) + \nabla_t^2\mathbf{H} + (k^2n^2(x,y) - \beta^2)\mathbf{H} = 0 \qquad (6-8)$$

Because of the presence of the first term in (6-7) and (6-8), their solution is quite complex for general cases of $n^2(x,y)$. However, it is possible to neglect that term when the following condition is met [Marcuse 1982, p.10]*:

$$R = \frac{\Delta\epsilon}{2\pi\epsilon} \cong \frac{\Delta n}{\pi n} << 1 \qquad (6-9)$$

In our case, $R \cong .002$ and the inequality is well satisfied.

Equations (6-7) and (6-8) are written below in their new form for future reference (this is called the "scalar wave

---

*Note: This is less true for TM modes because of the large discontinuity in ϵ at the glass-air interface. For TE modes this does not pose a problem because E^y is perpendicular to the large gradient and the first term of (6-7) is zero.

approximation"):

$$\nabla_t^2 E + (k^2 n^2(x,y) - \beta^2)E = 0 \qquad (6\text{-}10)$$

$$\nabla_t^2 H + (k^2 n^2(x,y) - \beta^2)H = 0 \qquad (6\text{-}11)$$

The modes of the waveguides are obtained by solving these eigenvalue problems, with the appropriate boundary conditions, for a given field component. Once that solution is found, the other field components are calculated from Maxwell's equations.

In the case of planar waveguides, for which all derivatives with respect to y vanish (propagation along z and depth along x), the modes can be separated in two independant orthogonal groups because Maxwell's equations become partially uncoupled [Born 1980 or Landau 1969]. The only non-vanishing components for each of these groups are: TE modes (E_y,H_x,H_z) and TM modes (H_y,E_x,E_z). For the more general case of channel waveguides, such separation is not strictly possible because $\partial/\partial y \neq 0$, and the modes are "hybrid", meaning neither TE nor TM.

However, in the case of ion-exchanged waveguides fabricated by the two-step method, the index gradients in x are much larger than those in y (especially for small values of t_1), as can be seen from Figures 2-6 and 2-7. In this almost planar situation, there will be again two groups of solutions, the quasi-TE modes, where E_y, H_x, and H_z are much larger than the other three components, and the quasi-TM modes, where H_y, E_x, and E_z dominate. These 'TE' modes will be obtained by solving (6-10)

for E_y and the 'TM' modes by solving (6-11) for H_y. The two equations are exactly similar, but the boundary condition to be satisfied at the glass-air interface is not the same [Marcuse 1982], and the index anisotropy must be taken into account.

It is the solution of this set of equations for the waveguiding structures fabricated by two-step ion-exchange that will be the subject of the remainder of this chapter. As was mentioned previously, the refractive index profile n(x,y) is obtained from the normalized concentration calculated in Chapter 2 by:

$$n(x,y) = \Delta n_s \times c(x,y) \qquad (6-12)$$

with Δn_s for the TE and TM cases taken from Chapter 4, at our working temperature of 385°C.

There will be three interrelated methods of solution presented in this Chapter. To avoid confusion between them, here is a 'flow chart' to guide the reader in what follows:

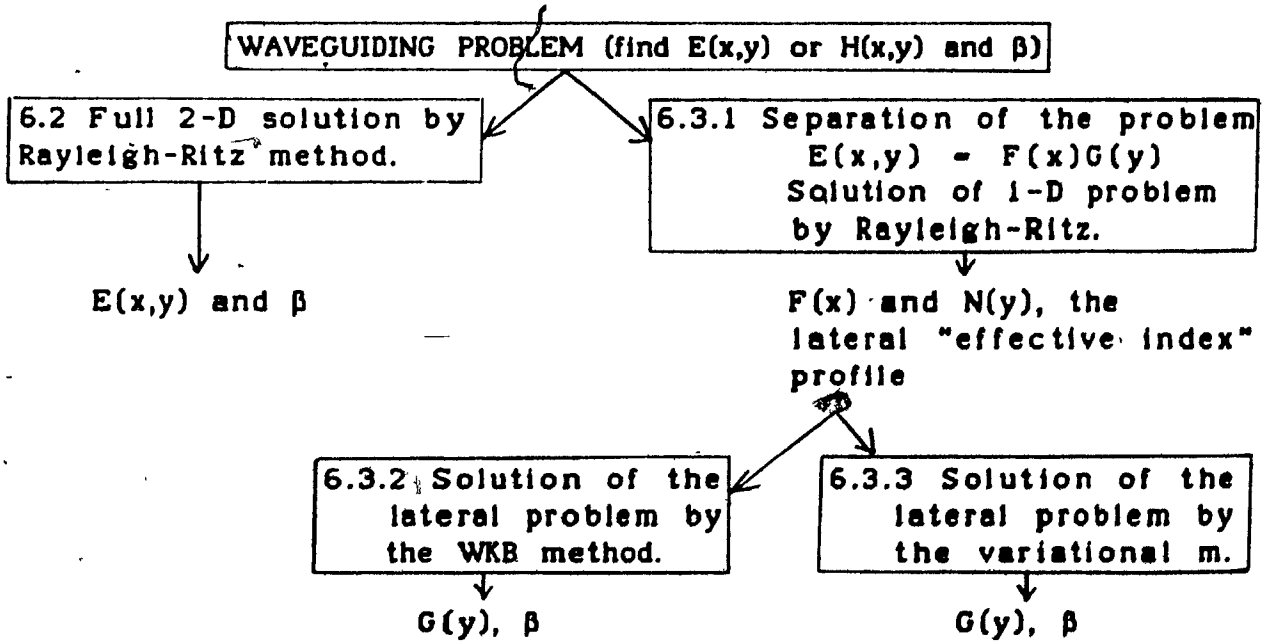

The three sets of results are discussed in Section 6.4.

6.2 FULL SCALE NUMERICAL SOLUTION OF THE WAVE EQUATION

6.2.1 Variational formulation of the eigenvalue problem

The rather complicated shape of $n(x,y)$ prevents the use of analytical methods of solution to the wave equations. On the other hand, the differential eigenvalue problem defined by (6-10) and its boundary conditions can be shown [Mathews 1970 or Marcuse 1982], to be equivalent to a variational problem.

First, let us rewrite the wave equation in truly scalar form, for the eigenfunction ψ and its associated eigenvalue β^2, to avoid constant reference to TE and TM modes (in the former case $\psi = E_y$ and in the latter case $\psi = H_y$; and the appropriate Δn_s must be used in each case).

$$\nabla^2\psi + k^2n^2(x,y)\psi = \beta^2\psi \qquad (6-13)$$

with $$\psi(\infty,\infty) = 0 \text{ and } \frac{\partial\psi}{\partial\hat{n}}(\infty,\infty) = 0 \qquad (6-14)$$

where $\hat{n}$ is an outward normal to the boundary of the domain in the x-y plane. Condition (6-14) ensures that there is no power flow in direction $\hat{n}$, for modes propagating along the $\hat{z}$ axis.

The variational problem to which (6-13) and (6-14) is equivalent can be stated as follows [Adams 1981]:

Defining the functional $B[\psi]$ by:

$$B[\psi] = \frac{\iint_{-\infty}^{\infty} dxdy\ [-(\nabla\psi)^2 + k^2n^2\psi^2]}{\iint_{-\infty}^{\infty} dxdy\ \psi^2} \qquad (6-15)$$

Then, the eigenmodes ψ_n and associated eigenvalues β_n^2 are such that:

$$\delta B\Big|_{\psi=\psi_n} = 0 \qquad \text{and } \beta_n^2 = B[\psi_n] \tag{6-16}$$

meaning that the extrema of the functional occur when ψ is equal to an eigenmode, and that the values of the functional at those points correspond to the eigenvalues. In the particular case of equation (6-13), the extrema to be found are the maxima of B. This can be seen by rewriting it as:

(in all of the following, $\int\int_{-\infty}^{\infty} dxdy$ is replaced by $\int dA$ to simplify the notation)

$$\int dA(B - k^2n^2)\psi^2 = -\int dA(\nabla\psi)^2 \tag{6-17}$$

$$\int dA(B - k^2n^2)\psi^2 < 0 \tag{6-18}$$

$$B < \frac{\int dA\ k^2n^2\psi^2}{\int dA\ \psi^2} \tag{6-19}$$

Since B is bounded from above, it has a maximum value, β_0^2, which corresponds to the mode of the waveguide with the largest propagation constant, i.e. the fundamental mode ψ_0.

$$\beta_0^2 = \max_{\psi} B[\psi] = B[\psi_0] \tag{6-20}$$

The other modes (corresponding to smaller local maxima of B), are found by using the property that the solutions ψ_n of the problem form an orthogonal set in the following sense:

$$\int dA\ \psi_r\psi_s = 0 \qquad \text{for } r \neq s \tag{6-21}$$

Then, the maximum value of $B[\psi]$, restricted to the space of the functions orthogonal to ψ_0, will yield the next mode of the waveguide:

$$\beta_1^2 = \max_{\psi\perp\psi_0} B[\psi] = B[\psi_1] \tag{6-22}$$

and so on for the rest of the modes:

$$\beta_p^2 = \max_{\psi \perp (\psi_0, \psi_1, \ldots, \psi_{p-1})} B[\psi] = B[\psi_p] \qquad (6\text{-}23)$$

since ψ_p must be orthogonal to all the modes with higher values of β^2.

It is worth noting at this point that the problems (6-20), (6-22), (6-23) are exactly equivalent to (6-13), provided that (6-14) is satisfied in all cases. Hence, finding the absolute maxima of the functional B is just as difficult as solving (6-13). However, the variational formulation of the problem allows approximate solutions to be found far more easily than the differential equation formulation. Also, the value of β^2 is "stationary", meaning that it is relatively insensitive to small changes in ψ and that even an approximation of ψ can yield a pretty good result for β^2 [Mathews 1970]. Such an approximate solution is described next.

6.2.2 The Rayleigh-Ritz method

Since the exact eigenfunction ψ_0 yields the absolute maximum of B, any approximate function for ψ_0 will result in a smaller value. Therefore, a strategy for finding ψ_0 consists of trying a succession of functions in (6-20) in a manner such that the value of B increases, meaning that the trial functions approximate ψ_0 better and better. This strategy is at the heart of the Rayleigh-Ritz procedure [Matsuhara 1973, Taylor 1976, Adams 1981].

The solutions of (6-15)-(6-16) belong to a space of

functions with the following characteristics. They are continuous, and so are their derivatives (at least up to second order), over the whole x-y plane. They are integrable, meaning that for any pair of functions belonging to that space:

$$\int dA\ \phi(x,y)\theta(x,y) \leq M = \text{a non-infinite number} \qquad (6\text{-}24)$$

We can find a complete set of basis functions for the function space in the sense that any of its functions can be written as a combination of basis functions:

$$\psi(x,y) = \sum_{i=0}^{\infty} a_i\phi_i(x,y) \qquad (6\text{-}25)$$

The basis functions chosen should be orthonormal:

$$\int dA\ \phi_i\phi_j = \delta_{ij} \qquad (6\text{-}26)$$

The last property facilitates calculations enormously.

Note that the basis functions must form an infinite set to be able to satisfy (6-25) for any function of the space that we have defined. This is of course not very practical. By truncating the series (6-25) to a finite number (say, N) of terms, the function ψ is only approximated. As N gets larger, the approximation improves. This is the idea behind the Rayleigh-Ritz process. The trial function ψ^N used to approximate ψ is obtained by truncating (6-25) to N terms:

$$\tilde{\psi_0}^N = \sum_{i=0}^{N-1} a_i\phi_i(x,y) \qquad (6\text{-}27)$$

Then, for each value of N, the "best" trial function is found by calculating the set of coefficients a_i which maximizes B. This is done by solving the following set of equations:

$$\frac{\partial B}{\partial a_i} = 0 \qquad i = 0,1,2,..N-1 \qquad (6\text{-}28)$$

for the a_i's and B (β^2). As soon as B has converged to an acceptable precision, the process is stopped.

If the basis is well chosen among the many that can be used for the function space which has been defined, the successive trial functions resulting from an increasing N will yield a value of B converging rapidly to its maximum [Meunier 1983].

The only problem that remains is the method by which (6-28) is solved. First, replacing (6-27) in (6-20) leads to:

$$B = \frac{\int dA \left[-(\nabla(a_i\phi_i)\cdot\nabla(a_j\phi_j)) + k^2n^2\, a_i\phi_i a_j\phi_j \right]}{a_i a_j\, \delta_{ij}} \qquad (6\text{-}29)$$

where the repeated indices imply summation on these indices:

$$a_k b_k \Rightarrow \sum_k a_k b_k$$

and where orthonormality (6-26) has been used in the denominator. Now, using (6-29) in (6-28):

$$\frac{\int dA \left[-a_j\nabla\phi_i\cdot\nabla\phi_j + k^2n^2\, a_j\phi_i\phi_j \right]}{a_i a_j\, \delta_{ij}} - \frac{a_j\delta_{ij}}{a_i a_j\delta_{ij}} B = 0 \quad (i=0,1,2,..,N-1) \qquad (6\text{-}30)$$

or:

$$\left(\int dA \left[-\nabla\phi_i\cdot\nabla\phi_j + k^2n^2\phi_i\phi_j \right] - B\delta_{ij} \right) a_j = 0 \quad (i=0,1,..,N-1) \qquad (6\text{-}31)$$

which is a matrix eigenvalue problem with eigenvalues $B = \beta^2$ and eigenvectors $a = \{ a_0, a_1, a_2, \ldots, a_{N-1} \}$, for the matrix M, of which the (i,j)th element is defined by the first two terms in the parenthesis of (6-31). With the help of the identity matrix I, (6-31) can be written as:

$$(M - \beta^2 I)a = 0 \qquad (6\text{-}32)$$

In order to introduce a notation used later in the Chapter,

where the x and y dependence of $\phi_i(x,y)$ is explicitly specified by separate subscripts p and q, (6-25) is written:

$$\psi(x,y) = \sum_{i=0}^{\infty} \sum_{j=0}^{\infty} a_{ij}\phi_{ij}(x,y) \qquad (6-33)$$

and (6-31) becomes:

$$\left(\int dA\ [-\nabla\phi_{ij}\cdot\nabla\phi_{kl} + k^2n^2\phi_{ij}\phi_{kl}] - B\delta_{ik}\delta_{jl}\right) a_{kl} = 0 \qquad (6-34)$$

with $(i = 0,1,..,N_x - 1; j = 0,1,..,N_y - 1)$.

It is important to remember that a given pair of indices (i,j) or (k,l) refers to a single basis function of x and y. Therefore, the set of coefficients a_{kl} specifies unambiguously the solution of the problem.

The eigenvector of M corresponding to the largest eigenvalue approximates the fundamental mode. Since the eigenvectors of a matrix are orthogonal to each other, the second eigenvector corresponds to the second mode, and so on for all the eigenvectors. However, the accuracy of the approximation decreases with the increasing mode order for a given N because the size of the available basis decreases. This phenomenon is due to the fact that the search for the second mode occurs in the function space that is spanned by the basis but orthogonal to the first eigenfunction. Therefore, there is one less degree of freedom to adjust to maximize the trial function, which limits its eventual accuracy [Gould 1966]. Higher-order modes have to be orthogonal to all the previously found eigenvectors, and since the total base is limited to N dimensions, the

available degrees of freedom available to them become severely limited. For this reason, this method will only be used for the first two modes of the waveguides in this work.

It turns out that because the index profile is symmetric with respect to y, the eigenmodes will be either even or odd in y [Yariv 1975]. Therefore the problem can be split in two by considering separately superpositions of even basis functions or odd basis functions. This is because a superposition of both odd and even functions has no definite parity (i.e. is neither odd nor even) and can not be a solution. Using even functions will yield the fundamental mode (mode 0) with the largest eigenvalue, while odd functions will superpose to give the lowest order odd mode (i.e. mode 1, with the second largest eigenvalue).

6.2.3 Implementation of the Rayleigh-Ritz method

The first step is the determination of the set of basis functions. Since the waveguides made by two-step ion-exchange have a high aspect ratio (width/depth), it is more convenient to have basis functions made up of products of functions in x and in y. Also, the basis functions have to be scaled to fit the dimensions of the problem and centered somewhere in the core of the waveguides. Therefore we will use basis functions of the form:

$$\phi_{pq}(x,y) = f_p\left(\frac{x-x_0}{w_x}\right) g_q\left(\frac{y}{w_y}\right) \qquad (6\text{-}35)$$

Note that the origin of y axis is at the center of the channel,

therefore no offset in y is needed. Furthermore, the functions g_q must be even or odd.

Another desirable feature of a basis, is that its functions should be the exact solutions (modes) of a problem that resembles the one at hand [Meunier 1983]. Although these conditions are not necessary in principle, they contribute to accelerate the convergence of the Rayleigh-Ritz process.

A particularly useful basis with all of the above characteristics, is composed of products of Hermite-Gaussian functions [Marcuse 1982], also called parabolic cylinder functions [Jahnke 1945]. They are solutions of the following equation:

$$\frac{\partial^2 h_n}{\partial x^2} + \left((n+\tfrac{1}{2}) - \frac{x^2}{4}\right)h_n = 0 \qquad (6\text{-}36)$$

which can be transformed to become a one-dimensional scalar wave equation for a parabolic index profile [Marcuse 1982], a reasonably close problem to ours. These functions are defined by:

$$h_n(x) = \frac{e^{-\frac{x^2}{4}}}{\sqrt{n!}\sqrt{2\pi}} H_n(x) \qquad (6\text{-}37)$$

where $H_n(x)$ is the Hermite polynomial of order n:

$$H_n(x) = e^{\frac{x^2}{2}}\left(-\frac{\partial}{\partial x}\right)^n e^{-\frac{x^2}{2}} \qquad (6\text{-}38)$$

and they obey:

$$\int_{-\infty}^{\infty} dx\; h_p(x)h_q(x) = \delta_{pq} \qquad (6\text{-}39)$$

This basis has been used in many instances for the analysis

of various types of 1-D and 2-D waveguiding problems by the Rayleigh-Ritz method in the past [Matsuhara 1973, Taylor 1976, Meunier 1983]. Finally, the basis functions are:

$$\phi_{pq}(x,y) = \frac{h_p(\frac{x-x_0}{w_x})h_q(\frac{y}{w_y})}{\sqrt{w_x}\ \sqrt{w_y}} \qquad (6-40)$$

where the denominator has been added to preserve (6-39) with the scaled variables. Note also that two indices are kept to identify a single basis function in order to highlight its features in both x and y (p and q are the number of nodes in each direction).

Before we begin the calculation of the matrix elements, we have to specify how the additional parameters (x_0, w_x and w_y) are chosen. We cannot simply add equations of the type:

$$\frac{\partial B}{\partial x_0} = 0 \qquad (6-41)$$

to the set defined by (6-31) because they would not be linear in the a_i's and would not fit in the matrix eigenvalue problem. On the other hand, it is not necessary that equations such as (6-41) be satisfied exactly because of the stationarity of B near the exact value of ψ. Therefore, following [Matsuhara 1973] and [Taylor 1976], the values of x_0, w_x, and w_y are determined separately by maximizing M_{0000}, the first diagonal element of the matrix **M**. The reason for doing so is that in the simplest form of the Rayleigh-Ritz method, only one basis function is used (ϕ_{00}) to set an estimate of β^2; and since the estimate improves by maximizing B (equal to M_{0000}

for N=1, see (6-32)), the values of x_0, w_x, and w_y which do so are the best ones for that one-dimensional problem. Strictly speaking, enlarging the basis requires recalculating those parameters. However, if Φ_{00} is not too far from the fundamental mode field ψ_0, the parameters found are close to their exact values and the linear combination (6-27) gives an excellent approximation to β^2_0 in spite of the small inaccuracy in ψ_0. Figure 6-1 illustrates schematically how the best value of β^2_0 is approached.

The matrix elements are calculated as follows. The first term of (6-34) is expanded:

$$\int dA\ (-\nabla\phi_{ij}\cdot\nabla\phi_{ki}) = \int dA\ (\phi_{ij}\nabla^2\phi_{kl} - \nabla\cdot(\phi_{ij}\nabla\phi_{kl})) \qquad (6-42)$$

$$= \int dA\ \phi_{ij}\nabla^2\phi_{kl} - \oint(\phi_{ij}\nabla\phi_{kl})\cdot\hat{n}\ dl \qquad (6-43)$$

The second term of the RHS of (6-43) is obtained from the divergence theorem (noting that the integrand has no z component), and is equal to zero since the integration path is located at infinity, where ϕ_{ij} and $\nabla\phi_{kl}$ are zero. Also, expanding the Laplacian (with the definitions $u=\frac{x-x_0}{w_x}$ and $v=\frac{y}{w_y}$):

$$\int dA\ \phi_{ij}\nabla^2\phi_{kl} = \int\frac{dA}{w_x w_y}(h_i(u)h_j(v)\frac{\partial^2}{\partial x^2}h_k(u)h_l(v) + h_i(u)h_j(v)\frac{\partial^2}{\partial y^2}h_k(u)h_l(v)) \qquad (6-44)$$

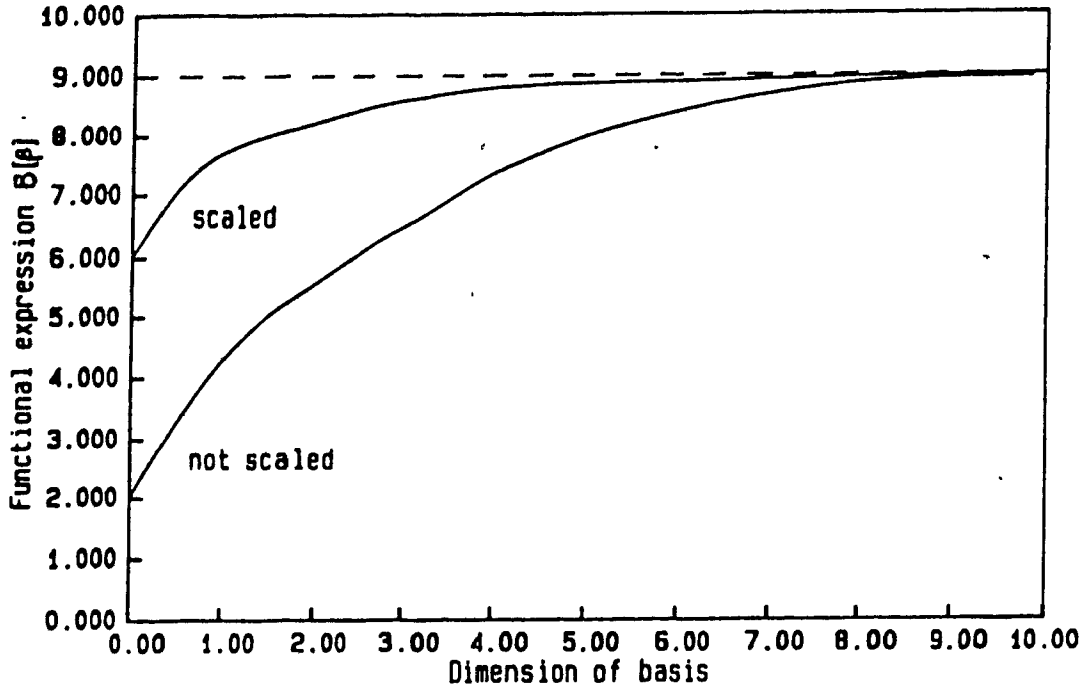

Figure 6-1. Effect of optimizing M_{0000}, by scaling and recentering the basis functions, on the convergence of the Rayleigh-Ritz process (simulated).

$$- \int\int du dv (h_j(v)h_l(v)\ h_i(u)\frac{\partial^2}{\partial x^2}h_k(u) + h_i(u)h_k(u)\ h_j(v)\frac{\partial^2}{\partial y^2}h_l(v))$$

$$= \int du\ \frac{\delta_{jl}}{w_x^2}\ h_i(u)\frac{\partial^2}{\partial u^2}h_k(u) + \int dv\ \frac{\delta_{ik}}{w_y^2}\ h_j(v)\frac{\partial^2}{\partial v^2}h_l(v) \qquad (6-45)$$

where (6-39) has been used to get the delta functions(δ_{nm}). Both terms on the RHS of (6-45) contain the same type of integral:

$$\int du\ h_m(u)\frac{\partial^2}{\partial u^2}h_n(u) = \int du\ h_m(u)(\frac{u^2}{4} - n - \frac{1}{2})h_n(u) \qquad (6-46)$$

with the help of (6-36). Continuing, we get:

$$(6-46) = (-n - \tfrac{1}{2})\delta_{mn} + \tfrac{1}{4}\int du\ h_m(u)u^2h_n(u) \qquad (6-47)$$

$$= (-n - \tfrac{1}{2})\delta_{mn} + \tfrac{1}{4}\int du\ h_m(u)(\sqrt{(n+1)(n+2)}h_{n+2}(u) + \ldots$$

$$\ldots + \sqrt{n(n-1)}h_{n-2}(u) + {}^{0}(2n+1)h_n(u)) \qquad (6-48)$$

with the help of recursion relations for the Hermite-Gaussian functions [Jahnke 1945]. Using orthonormality:

$$(6-48) = \tfrac{1}{4}\left(\sqrt{(n+1)(n+2)}\delta_{m(n+2)} + \sqrt{n(n-1)}\delta_{m(n-2)} - (2n+1)\delta_{nm}\right) \qquad (6-49)$$

So that finally:

$$M_{ijkl} = \frac{\delta_{jl}}{4w_x^2}(\sqrt{(i+1)(i+2)}\delta_{(i+2)k} + \sqrt{i(i-1)}\delta_{(i-2)k} - (2i+1)\delta_{ik}) + \ldots$$

$$\ldots + \frac{\delta_{ik}}{4w_y^2}(\sqrt{(j+1)(j+2)}\delta_{(j+2)l} + \sqrt{j(j-1)}\delta_{(j-2)l} - (2j+1)\delta_{jl}) + \ldots$$

$$\ldots + k^2\int\frac{dA}{w_x w_y}\ n^2(x,y)\ h_i\left(\frac{x-x_0}{w_x}\right)h_k\left(\frac{x-x_0}{w_x}\right)h_j\left(\frac{y}{w_y}\right)h_l\left(\frac{y}{w_y}\right) \qquad (6-50)$$

and the problem is reduced to solving the last integral.

Note that $M_{ijkl} = M_{klij}$ in (6-50) which is easy to see in the last term, but also in the first two in the cases where they are not identically zero because of the delta functions. Therefore the matrix is symmetric and we do not need to calculate all its elements. A further simplification arises again because of the symmetry of $n^2(x,y)$ with y in the integral. Since even and odd basis functions are treated separately, their products in (6-50) are always even and we can replace:

$$\int_{-\infty}^{\infty} dy \quad \text{by} \quad 2\int_{0}^{\infty} dy$$

again reducing the numerical computation time in half.

The final simplification of the problem comes from the fact that in a large part of the integration domain the function $n^2(x,y)$ is equal to 1 (for all the region $x<0$). Then, we can replace:

$$\frac{2k^2}{w_x w_y}\int_0^{\infty}dy\int_{-\infty}^{\infty}dx\; h_i\left(\frac{x-x_0}{w_x}\right)h_j\left(\frac{y}{w_y}\right)h_k\left(\frac{x-x_0}{w_x}\right)h_l\left(\frac{y}{w_y}\right)\; n^2(x,y) \qquad (6-51)$$

by:

$$\frac{2k^2}{w_x w_y}\int_0^{\infty}dy\int_{-\infty}^{\infty}dx\; h_i h_j h_k h_l\; (n^2(x,y) - 1) + \frac{2k^2}{w_x w_y}\int_0^{\infty}dy\int_{-\infty}^{\infty}dx\; h_i h_j h_k h_l \qquad (6-52)$$

$$= \frac{2k^2}{w_x w_y}\int_0^{\infty}dy\int_0^{\infty}dx\; h_i h_j h_k h_l\; (n^2(x,y) - 1) + k^2\,\delta_{ik}\delta_{jl} \qquad (6-53)$$

where the x integral domain is reduced in half since $n^2 - 1 = 0$ when $x < 0$.

The integration is done numerically with a Simpson's Rule algorithm [Conte 1980]. To calculate the "function"

$n^2(x,y)$ at points not located on the grid on which it is defined, linear interpolation is used because of the smoothness of the profile (except at all points lying between the grid points x(8) and x(9) where a cubic spline interpolation is needed, see Figure 6-2). The 2-D integral is separated into a succession of 1-D problems as follows. First, the integral along y is solved at all 10 grid points in x, and stored in array YINT. Then, the integral along x is performed:

$$\frac{2k^2}{w_x w_y}\int_0^\infty dx\ h_l\left(\frac{x-x_0}{w_x}\right)h_k\left(\frac{x-x_0}{w_x}\right)\ \int_0^\infty h_j\left(\frac{y}{w_y}\right)h_l\left(\frac{y}{w_y}\right)(n^2(x,y)\ -\ 1)\,dy$$

$$-\frac{2k^2}{w_x w_y}\int_0^\infty dx\ h_l h_k\ \mathrm{YINT}(x) \qquad (6-54)$$

The integration domain extends over the first 10 grid points in x and the first 15 points in y, corresponding to x = 0 to 9μm and y = 0 to 35μm. The Simpson's Rule algorithm divides these into 40 subintervals for integration (the number of subintervals was chosen after trials with various numbers showed that convergence was attained to one part in 10^5.

After all its elements have been calculated, the matrix eigenvalue problem must be solved. Since we are principally concerned with single-mode channel waveguides, only two propagation constants are needed: that of the fundamental mode and that of the second mode, in order to determine its cut-off point, i.e. the limit of the single-mode range. Mode 0

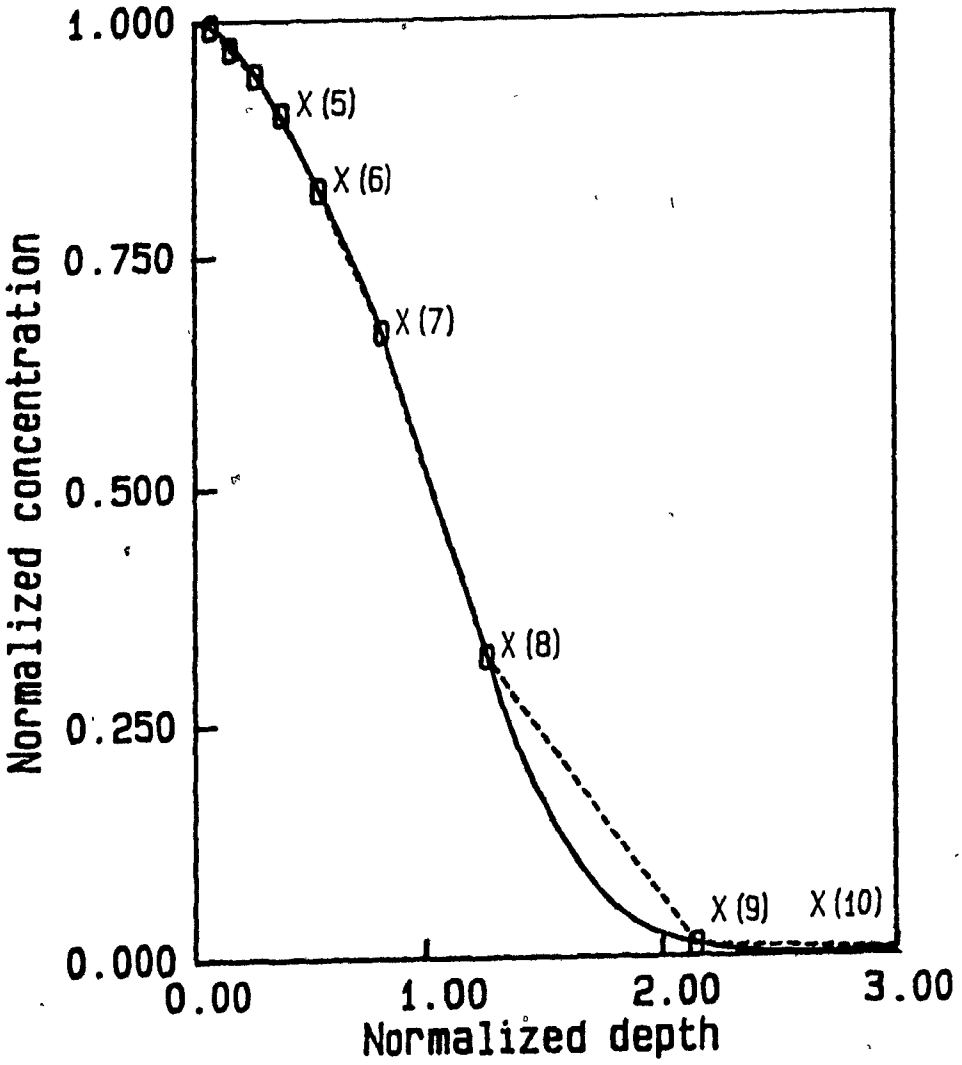

Figure 6-2. Justification for using a linear interpolation between the discrete values of n(x), except between elements (8) and (9), where a cubic spline interpolant is used.

corresponds to the largest eigenvalue in the even mode problem while mode 1 is obtained from the fundamental odd mode problem (which is treated separately). Since only the largest eigenvalue is needed in each case, this is a simpler problem than the one of finding all the eigenvalues of a given matrix and it is solved efficiently by the method of inverse iteration (a variant of the power method), which yields only the largest eigenvalue and its associated eigenvector (the FORTRAN source program for that method was taken from [Conte 1980] without modification).

Before presenting the results of these numerical calculations, the number of basis functions to be used must be determined. In order to do that, a test run is made with a given problem (here specified by t_1 = 6', t_0 = 54', T = 38.5°C, D = 10μm, TE mode) for different numbers of basis functions in x and y. The scalings and offset for that case are: w_x = 0.518, w_y = 3.9, and x_0 = 1.55 , all in μm. They are found by trial and error using the program to calculate M_{0000} interactively until its maximum value is found.

At first, a single function was used in y (h_0), and the number of functions in x (N_x) was varied. Figure 6-3 shows the value of the propagation constant β/k that results. From this graph, it is estimated that an accuracy better than 2×10^{-5} is achieved with N_x = 21. It takes that many functions because the depth profile of refractive index is highly asymmetrical

with a large discontinuity at x = 0. Returning to the lateral direction (along y, and remembering to use only even basis functions), no change in β (within 1 part in 10^5) was found for N_y as high as 5 (with N_x = 14) or N_y = 3 (with N_x = 21). Therefore, only one basis function is sufficient to describe the fundamental mode laterally, and that function is a Gaussian (the lowest order Hermite-Gaussian). It is because of the smoothness, symmetry, and weak guidance of the lateral index profile that the Gaussian function approximate so well the fundamental mode, as in other cases of weakly guiding single-mode waveguides [Marcuse 1982]. Note that the N_x = 14, N_y = 5 case involves the calculation of 2485 matrix elements and the solution of a symmetric 70×70 matrix eigenvalue problem.

To end this section, a list of the scalings and offsets is presented in Table 6-1. All the waveguides have a mask width of 10 μm and the total exchange time ($t_1 + t_0$) is kept at 1 hour, at a temperature of 385°C (refer to chapters 2 and 3 for other details of geometry or fabrication).

The procedure just outlined is rather lengthy and involved, and it is preferable to have simpler ways to characterize channel optical waveguides in optical circuit design situations. Such methods are described in the following sections. Their results will be presented along with those of the Rayleigh-Ritz method at the end of the chapter for comparison purposes.

TABLE 6-1

SCALINGS AND OFFSETS FOR THE 2-D RAYLEIGH-RITZ METHOD

TE MODES

t_1	t_0	w_x	x_0	w_y
planar	guides			
0'	30'	.550	1.64	-
0'	43'	.527	1.57	-
0'	48'	.524	1.565	-
0'	51'	.522	1.565	-
0'	54'	.521	1.56	-
0'	58'	.518	1.56	-
0'	60'	.518	1.56	-
two-step	guides	even/odd	even/odd	even/odd
02'	58'	.518/ c.o	1.56/ c.o	7.6/c.o
06'	54'	.518/ c.o	1.55/ c.o	3.9/c.o
09'	51'	.518/.526	1.57/1.58	3.4/4.7
12'	48'	.520/.527	1.55/1.58	3.0/3.4
15'	43'	.523/.526	1.58/1.58	2.7/2.8
30'	30'	.526/.530	1.59/1.59	2.3/2.2
channel	guides	even/odd	even/odd	even/odd
60'	00'	.529/.533	1.59/1.60	2.0/1.8

TM MODES

two-step	guides	even/odd	even/odd	even/odd
02'	58'	.518/ c.o	1.56/ c.o	
06'	54'	.518/ c.o	1.55/ c.o	3.7/c.o
09'	51'	.518/.526	1.57/1.58	3.2/3.7
12'	48'	.520/.527	1.55/1.58	2.9/3.0
15'	43'	.523/.526	1.58/1.58	2.6/2.5
30'	30'	.526/.530	1.59/1.59	2.2/2.1

-All quantities are in μm (except the times, in minutes).

-The values of w_x and x_0 for the TM modes were taken to be the same as those for the TE modes since the fact that we are using 21 functions in x corrects for small changes in these parameters.

-"even" and "odd" refer to the parity of the modes in the y direction.

-"c.o" refers to a mode below cut-off.

-Scalings and offsets are given for the second mode at t_1 = 9' even though it is below cut-off because this was not known beforehand

6.3 SEMI-ANALYTICAL METHODS

6.3.1 Separation of the problem

A great simplification in the solution of the waveguiding problem (eqn. (6-13)) would result if the method of separation of variables could be used. Unfortunately, this is not the case because the index profile $n^2(x,y)$ cannot be put in the form $n_x^2(x) + n_y^2(y)$ [Danko 1985]. However, we have seen in the previous section that a very good approximation to the eigenmodes is obtained by a superposition of basis functions in which a single function in y is used. In that case, and only in that case, the solution can be separated into its x and y dependences:

$$\psi_0(x,y) = \frac{h_0\left(\frac{y}{w_y}\right)}{w_y} \sum_{n=0}^{20} \frac{h_n\left(\frac{x-x_0}{w_x}\right)}{w_x} \qquad (6-55)$$

$$= G(y)F(x) \qquad (6-56)$$

The fact that this approximate form gives useful results comes from the fact that the guidance is much stronger in the depth direction than in the lateral direction; this also suggests that it is worth trying a method of partial separation of variables, called "effective index method" [Knox 1970] to solve the problem. Its results will be compared with those of the previous section to check on their accuracy. The method is described below.

First, equation (6-13) is rewritten here for convenience:

$$\frac{\partial^2\psi}{\partial x^2} + \frac{\partial^2\psi}{\partial y^2} + (k^2n^2(x,y) - \beta^2)\psi = 0 \qquad (6-57)$$

Then, we rewrite ψ as:

$$\psi(x,y) = F(x,y)G(y) \qquad (6-58)$$

which transforms (6-57) into:

$$G\frac{\partial^2F}{\partial x^2} + G\frac{\partial^2F}{\partial y^2} + F\frac{\partial^2G}{\partial y^2} + 2\frac{\partial F}{\partial y}\frac{\partial G}{\partial y} + (k^2n^2(x,y) - \beta^2)FG = 0 \qquad (6-59)$$

A new function, $N(y)$, is introduced and defined by:

$$\frac{\partial^2G}{\partial y^2} + (k^2N^2(y) - \beta^2)G = 0 \qquad (6-60)$$

and substituted in (6-59):

$$G\frac{\partial^2F}{\partial x^2} + G\frac{\partial^2F}{\partial y^2} + 2\frac{\partial F}{\partial y}\frac{\partial G}{\partial y} + (k^2n^2(x,y) - N^2(y))FG = 0 \qquad (6-61)$$

Note that until now no approximations have been made, (6-61) is exactly equivalent to (6-57), just written differently. The approximation consists of neglecting the derivatives of F with respect to y in (6-61), meaning that we assume that most of the y dependence of ψ is taken up by G with whatever that is left included in F so that (6-58) can still be satisfied. The appropriateness of that assumption will be verified later, after F(x,y) has been calculated. Using that approximation, (6-61) reduces to:

$$\frac{\partial^2F}{\partial x^2} + k^2(n^2(x,y) - N^2(y))F = 0 \qquad (6-62)$$

which is a one-dimensional problem in x, with y as a parameter; meaning that this problem can be solved at a given position y because $n(x,y)$ is known there, and yielding a local value of

N(y) and F(x,y). After the local effective index N(y) is found for all the values of y, it is substituted in (6-60) to yield G(y) and β. It must be noted that the waveguides analyzed here are particularly well suited for the effective index method since N(y) is unambiguously defined at all lateral points because of the shallower planar guide that surrounds the channel (for "ordinary" channel waveguides, there is no guidance away from the channel and N(y) is taken to be equal to the substrate index there, a somewhat unrealistic assumption).

Since n(x,y) represents a graded-index profile, N(y) is a continuous function of y and we should solve (6-62) at an infinite number of points to describe it completely for use in (6-60). This is of course impossible and instead we will derive an analytical model for N(y) (as in [Kirby 1976], in a different context), valid for a practical range of values of t_1. This model allows for the solution of waveguiding structures defined by any combination of aperture widths in y and for any set of fabrication conditions (times, temperature, ion species, substrate) that can be used in two-step ion-exchange, as long as the second exchange time is such that a depth mode can be supported outside of the main channels.

The depth characteristics (F(x,y) and N(y)) of the model need to be derived only once so it is worthwhile to use an exact numerical method, even if fairly lengthy, to solve (6-62). The

same Rayleigh-Ritz method that was described previously was used, but modified to work in one dimension only (i.e. replacing $h_0(y)$ by 1 and not integrating in y). The value of N(y) is calculated in that manner (again with $N_x = 21$) for all the values of y on which n(x,y) is defined. Then, the individual results are fitted (by a least-squares procedure [Conte 1980]) with the following function:

$$N(y) = N(\infty) + \left(\frac{N(0)-N(\infty)}{2}\right)\left(\mathrm{erf}\left(\frac{y+D/2}{H}\right) - \mathrm{erf}\left(\frac{y-D/2}{H}\right)\right) \qquad (6-63)$$

where: -H is the fitting parameter,

-N(0) the effective index of a planar guide exchanged for one hour ($t_1 + t_0$), i.e. N(y=0),

-N(∞) the effective index of a planar guide exchanged for time t_0, i.e. N(y) away from the edge of the aperture in the mask,

-D the width of the aperture in the mask,

-erf is the error function [Jahnke 1945]

This process has been repeated for six different values of t_1, keeping $t_1 + t_0$ = 1 hour, and for both TE and TM modes. A few examples of the results of the fit are shown on Figure 6-4. The choice of that particular fitting function, and the excellent agreement that it provides with the data, come from the fact that it represents the exact solution of a very close problem. This problem is the classical (Fickian) diffusion (with constant diffusion coefficients) in one dimension (y) with a

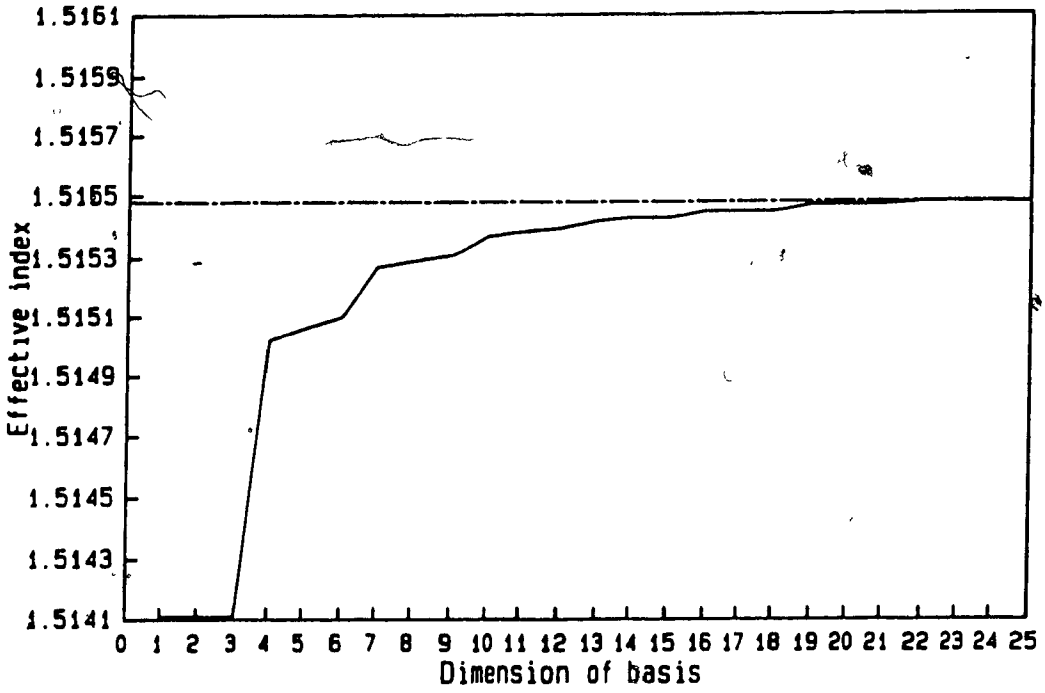

Figure 6-3. Observed convergence of the effective index with increasing basis dimension.

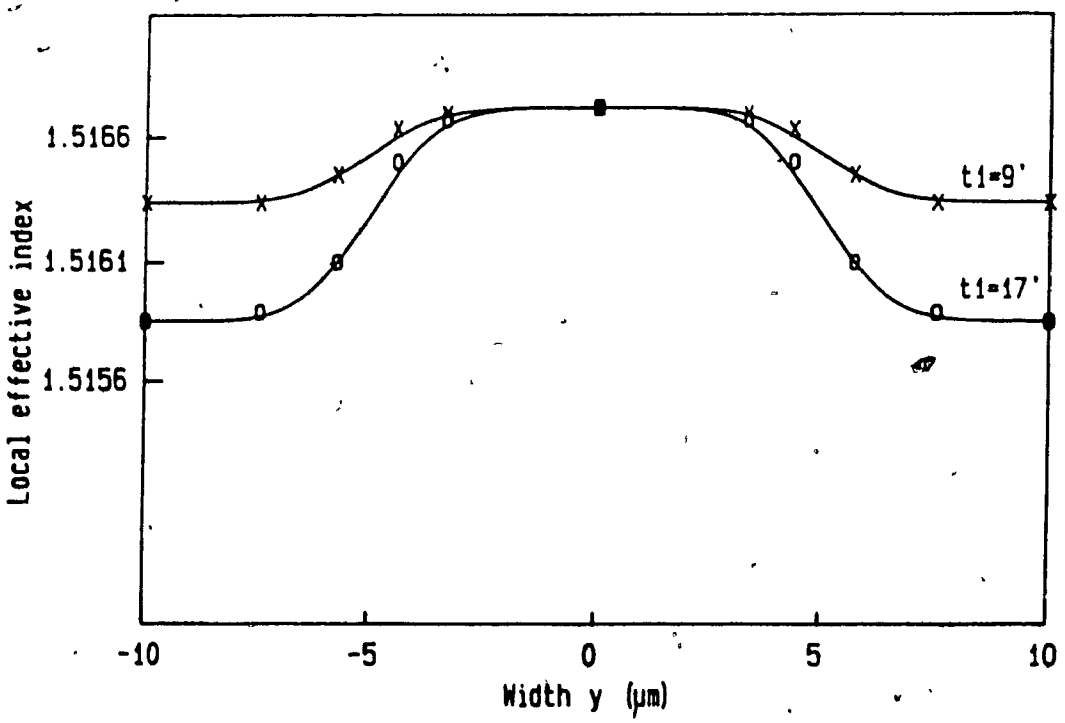

Figure 6-4. Discrete values of local effective index (x and o), along with fitting function (contnuous line), for two values of t_1.

finite source of diffusant, initially limited in space (to a size equal to the mask aperture) [Crank 1975]. By analogy with that problem, the fitting parameter H (determined here statistically by minimizing the difference between (6-63) and the individual points) should be nearly equal to the following formula, which is related to the lateral diffusion length:

$$H = \sqrt{D_y t} \qquad (6\text{-}64)$$

where D_y is an effective lateral diffusion coefficient and t the time of diffusion. In the case discussed here, since glass is an isotropic substance, D_y must be equal to the depth diffusion coefficient D_e found in chapter 4. As for t, it is taken to be equal to t_0 because during t_1 the lateral diffusion is inhibited near x=0 by the presence of the metallic mask (see Chapter 2). This becomes a poorer estimate for large values of t_1 because then the new ions have reached greater depths where side diffusion can occur. A comparison of the values of H obtained by fitting the individual results of (6-62) and by equation (6-64) is presented in Table 6-2. The agreement is very good and the solution of (6-60) obtained by the substitution of (6-63) with either value of H gives the same result for β/k_0 (within 1×10^{-5}).

Therefore, the combination of (6-63) and (6-64) represents a model for the lateral effective index profile of two-step ion-exchanged waveguides that depends exclusively on data derived from planar waveguide measurements (i.e. N(0), N(∞), and D_e).

TABLE 6-2

LATERAL DIFFUSION PARAMETER 'H'

t_i	H(TE)		H(TM)	
	Fit	Eqn.(6-60)	Fit	Eqn.(6-60)
06'	1.80	1.87	1.86	1.85
09'	1.80	1.82	1.69	1.80
12'	1.79	1.77	1.74	1.75
17'	1.72	1.67	1.73	1.65
30'	1.54	1.40	1.52	1.38

$D_e(TE) = 10.8 \times 10^{-16}$ m^2/s

$D_e(TM) = 10.6 \times 10^{-16}$ m^2/s

All values of H in μm.

This means that it can be applied to all the types of ion-exchange for which such characterizations are available (see [Findakly 1985] or [Chartier 1983] for reviews on planar ion-exchange papers, and [Gortych 1986] or [Lagu 1986] for more recent work). After the description of methods of solution of (6-60) in the following sections, the full design of optical circuits involving channel waveguides will prove to be especially simple.

Also, it is now the time to examine our neglect of the y dependence of F(x,y) in (6-62). Far from the edges of the channel the waveguides are essentially planar and the steps leading to equation (6-62) should become "locally" exact. Assuming further that the variation of F(x,y) across the region where n(x,y) changes with y (i.e. between the two planar regions) is gradual and smooth, a qualitative estimate of the size of $\partial F/\partial y$ can be obtained by comparing F(x,0) with F(x,70) in the fairly extreme case of $t_1 - t_0 = 30'$. This is shown on Figure 6-5. We see that $\partial F/\partial y$ is indeed very small, and should be even less for smaller values of t_1. This can be explained by the fact that in the channel, the depth mode is well-confined in a relatively deep layer while in the "cladding" the guide is shallower but the mode is extending more into the substrate because it is closer to cut-off. The net result is that F(x,y) is fairly independent of y and that the

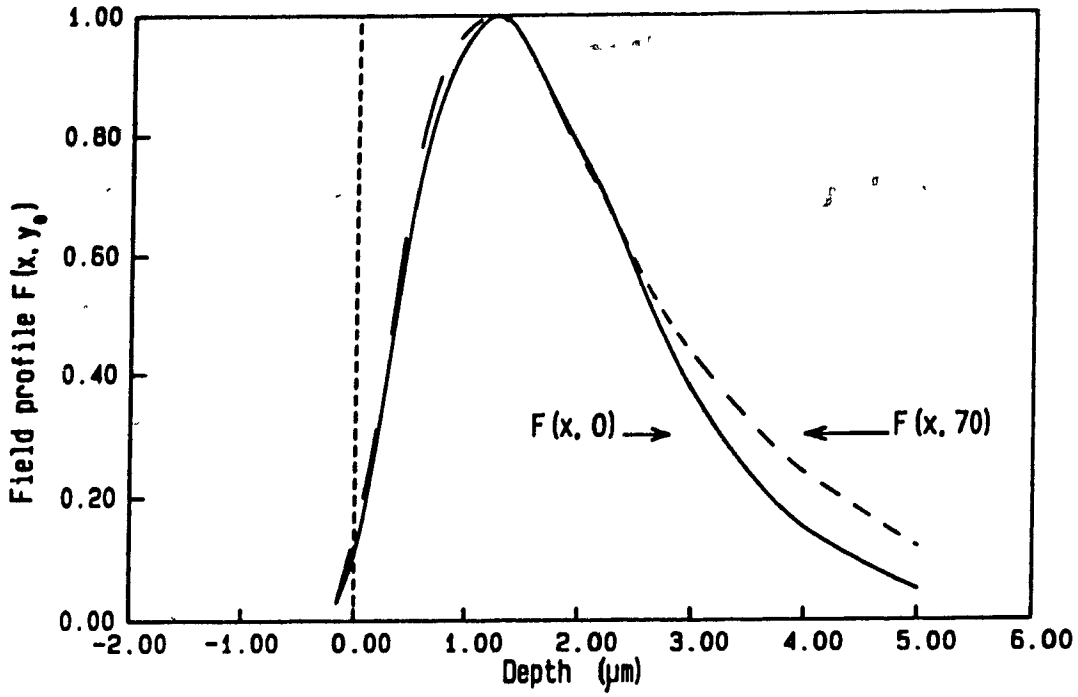

Figure 6-5. Depth dependence of the field profile at the center (y=0) and in the planar section (y=70 μm) of a two-step channel (t_i = 30 minutes, T=385°C).

effective index method becomes almost approximation-free!

6.3.2 The WKB method

Having an analytical profile function for N(y) to put into the 1-D boundary problem (6-60) helps in using the various methods of solution available for such problems. In the previous section, we could afford to use a rather long and complicated method to solve (6-62) because this had to be done only a few times, enough to characterize the model for N(y) from fabrication parameters. On the other hand, (6-60) has to be solved each time a new waveguide is planned or designed. Therefore, a quick solution method is desirable in this case. One such method is provided by the so-called WKB (or quasi-classical) method approximation (see [Landau 1965], [Mathews 1970], [Schiff 1968] for instance). For the case of a symmetric continuous profile N(y), the dispersion relation becomes [Kogelnik 1979]:

$$\int_0^{y_t} \sqrt{k^2N^2(y) - \beta_m^2}\, dy = \left(m+\tfrac{1}{2}\right)\frac{\pi}{2} \qquad (m=0,1,2,\ldots) \qquad (6-65)$$

which is root-searched for β_m, the propagation constant of the m^{th} mode. The turning point y_t of a mode is defined by:

$$N(y_t) = \beta_m/k \qquad (6-66)$$

The WKB method relies on asymptotic representations of the solutions of the wave equation to establish formula (6-65). Near the turning points, these asymptotic expressions "blow up" and

require another form of approximation to the solutions [Landau 1965]. When the zero of $k^2N^2-\beta^2$ at y_t is of first order, an approximate solution valid across the turning point can be derived [Rapp 1971 or Schiff 1968]. The solutions of (6-60) in the various regions of interest are given by the following formulas (where the numerical factors in front of each expression ensure the continuity of the function for the whole y axis). The definitions are given for $y > 0$, since we know that the modes are either symmetric or anti-symmetric relative to y (see [Schiff 1968], eqns. (28-16), (28-14) and the associated discussion):

$$G(y) = \frac{2\sqrt{2}\cos(\pi/6)}{\sqrt{\pi}\sqrt{k^2N^2(y)-\beta^2}}\cos\left(\xi_b - \frac{\pi}{4}\right) \qquad (y \ll y_t) \qquad (6\text{-}67)$$

$$G(y) = \frac{2^{\frac{1}{3}}3^{\frac{2}{3}}\xi_b^{\frac{1}{6}}}{(k^2N^2-\beta^2)^{\frac{1}{4}}}\,Ai\left(-\left(\frac{3\xi_b}{2}\right)^{\frac{2}{3}}\right) \quad \text{with } \xi_b = \int_y^{y_t}\sqrt{k^2N^2-\beta^2}\,dy \quad (y \le y_t) \quad (6\text{-}68)$$

$$G(y) = \frac{2^{\frac{1}{3}}3^{\frac{2}{3}}\xi_a^{\frac{1}{6}}}{(\beta^2-k^2N^2)^{\frac{1}{4}}}\,Ai\left(\left(\frac{3\xi_a}{2}\right)^{\frac{2}{3}}\right) \quad \text{with } \xi_a = \int_{y_t}^{y}\sqrt{|k^2N^2-\beta^2|}\,dy \quad (y \ge y_t) \quad (6\text{-}69)$$

$$G(y) = \frac{\sqrt{2}\cos(\pi/6)}{\sqrt{\pi}\sqrt{\beta^2-k^2N^2}}\exp(-\xi_a) \qquad (y \gg y_t) \qquad (6\text{-}70)$$

Note that $\xi_b = -\xi_a$ when $y \le y_t$.

The equations (6-68) and (6-69) are obtained from a local, linearized N(y), and are asymptotically equivalent to (6-67) and (6-70). The function Ai(z) is the Airy function [Abromovitz 1965], a linear combination of Bessel functions of order

$\pm 1/3$.

In spite of the complexity of these expressions, they represent a particularly simple way to solve (6-60), and they are exact solutions both near and far from y_t. The only region where they may be less accurate is in the intermediate range where the Airy functions transform into their asymptotic representations, if that region is too far away from the turning point for the linear approximation to N(y) to be still valid. On the other hand, the propagation constants obtained from the dispersion relation (6-65) are known to be inaccurate for low order modes [Landau 1965].

This situation is interesting in the sense that the other semi-analytic method used in this work (as described in the next section) has the complementary characteristic, i.e. a very accurate propagation constant with a relatively approximate mode function for G(y).

6.3.3 The single function variational method (SFV)

The other semi-analytical method of solution for (6-60) is a variational method [Sharma 1980], similar to the one presented in section 6.2. Here, we make use of the fact that the Rayleigh-Ritz procedure has indicated that the Gaussian function approximates very well the lateral variation of the fundamental mode (and also that the Hermite-Gaussian of order 1 approximates well the second mode). Therefore, we use again the variational

formula for β^2 given by (6-15), transformed slightly to apply in y only:

$$\beta^2 = \max_{[G]} \frac{\int_{-\infty}^{\infty} dy \left[k^2N^2(y)G^2(y) - \left(\frac{\partial G}{\partial y}\right)^2\right]}{\int_{-\infty}^{\infty} dy\ G^2(y)} \qquad (6-71)$$

But this time, instead of a series of functions, we use a single function for the two first modes, a Gaussian for the fundamental:

$$G_0(y) = e^{-\sigma_0 y^2} \qquad (6-72)$$

and the Hermite-Gaussian of order 1 for the second mode:

$$G_1(y) = \sqrt{\sigma_1}\, y e^{-\sigma_1 y^2} \qquad (6-73)$$

This way, the maximization of the functional (6-71) is reduced to finding the value of σ_i (i=0,1) which satisfies:

$$\frac{\partial \beta^2}{\partial \sigma_i} = 0 \qquad (6-74)$$

Once σ_i is found, it is replaced in (6-71) to yield β_i, the propagation constant of the i^{th} mode. Again, we emphasize that with a variational approach, the propagation constant can be very accurate even for an approximate mode function. Defining:

$$P = \int_{-\infty}^{\infty} dy\, G^2 \qquad \text{and} \qquad G' = \frac{\partial G}{\partial \sigma} \qquad (6-75)$$

equation (6-74) can be written:

$$\left(\int_{-\infty}^{\infty} dy\ k^2N^2GG' - \frac{\partial G}{\partial y}\frac{\partial}{\partial \sigma}\left(\frac{\partial G}{\partial y}\right)\right) - \left(\int_{-\infty}^{\infty} dy\ k^2N^2G^2 - \left(\frac{\partial G}{\partial y}\right)^2\right)\left(\frac{\int_{-\infty}^{\infty} dy\ GG'}{P}\right) = 0 \qquad (6-76)$$

The solution of (6-76) for σ is very easy to find with a computer. In fact, if N(y) was a little bit simpler (the error

functions are difficult to integrate), (6-76) could probably be solved analytically.

This completes the description of the semi-analytical methods that were used to find the waveguiding characteristics of two-step ion-exchanged channels.

6.4 DISPERSION CURVES AND MODES OF TWO-STEP CHANNEL WAVEGUIDES

The dispersion curves usually show the propagation constant of the modes in terms of the physical parameters of a guide, regrouped into what is called a normalized frequency [Kogelnik 1979]. The usefulness of that representation lies in the fact that the curves can be read directly for any value of wavelength or size of the waveguides. In this study of two-step waveguides, the depth of the channel is kept fixed, corresponding to a constant value of the local effective index N(0) and of the depth dependance of the modes F(x,0). The depth of the surrounding planar guide is varied, corresponding to changes in its effective index, N(∞), which can be considered as the "cladding" index of the equivalent 1-D waveguide in y. This also results in a variation of the lateral dependence of the mode, i.e. G(y).

Therefore, the results of the analysis will be presented using the following conventions, which all relate to the lateral waveguiding properties. The normalized propagation constant b is:

$$b = \frac{\left(\frac{\beta}{k}\right)^2 - N^2(\infty)}{N^2(0) - N^2(\infty)} \qquad (6-77)$$

and the normalized frequency:

$$V = kD\sqrt{N^2(0) - N^2(\infty)} \qquad (6-78)$$

We see that b varies from 0 to 1 for guided modes since β must lie between $kN(\infty)$ and $kN(0)$.

In order to compare the results of the three aforementioned methods, a common set of base data must be used. This poses no problem for the two semi-analytical methods since it suffices to use the same function N(y) in both (i.e. the same N(0), N(∞), H, and D). However, a further comparison with the 2-D Rayleigh-Ritz method reveals a problem of consistency in the treatment of the depth mode solution. In the Rayleigh-Ritz method, the exact profile resulting from given parameters Δn_s and D_e is used and the propagation constant determined very accurately. However, these parameters were found by using the Gaussian approximation for n(x) and solving the WKB dispersion relation (also an approximation) of section 4.2 to reproduce as closely as possible the measured effective indices. This model is based on two approximations, but they balance each other out in the sense that the pair of parameters Δn_s and D_e that it yields for given fabrication conditions lead directly to the measured effective indices of the resulting waveguide. Using the same pair of parameters in a different method for specifying the profile (even if in principle more accurate, as in the case of

the Rayleigh-Ritz method applied to the results of the ion-exchange diffusion equation) and extracting the effective indices from it , has to yield different answers. In fact, the effective indices obtained from the 1-D Rayleigh-Ritz of section 6.3.1 are systematically 1×10^{-4} higher than the results of chapter 4, for the same waveguide, and the same effect occurs implicitly in the 2-D Rayleigh-Ritz calculations of section 6.2.

Therefore, in order to be able to compare the results of this last method with those of the semi-analytical approaches (Table 6-3)), we must use in them the same values of effective indices that it uses, i.e. those that can be calculated from the 1-D Rayleigh-Ritz method (they are listed in the Table). Of course, it can be argued that the exact numerical solution for n(x) and the 1-D Rayleigh-Ritz procedure should have been used in the characterization, but that would have made it an almost intractable problem (because it would have required solving the 1-D diffusion equation of ion-exchange numerically and the full 1-D Rayleigh-Ritz problem at each step of a 2-D root search for Δn_s and D_e), with very little profit. In fact, the Gaussian-WKB approach continues to be helpful here through the ease with which we can get almost exact effective indices from fabrication parameters to input in the channel waveguide model.

TABLE 6-3

SUMMARY OF RESULTS FOR PROPAGATION CONSTANTS OF CHANNEL WAVEGUIDES

TE MODES

t_1	$N^{RR}(\infty)$	β/k (WKB)	β/k (SFV)	β/k (RR)
00'	1.51558	-	-	-
06'	1.51535	1.51547	1.51547	1.51547
09'	1.51521	1.51545	1.51545	1.51545
12'	1.51507	1.51544	1.51542	1.51542
17'	1.51482	1.51542 1.51491	1.51540 1.51495	1.51540 1.51497
30'	1.51402	1.51541 1.51471	1.51535 1.51474	1.51534 1.51475

TM MODES

00'	1.51676	-	-	-
06'	1.51648	1.51664	1.51664	1.51665
09'	1.51633	1.51662	1.51662	1.51662
12'	1.51616	1.51661 1.51618	1.51659 1.51621	1.51659 1.51623
17'	1.51585	1.51659 1.51604	1.51656 1.51608	1.51656 1.51609
30'	1.51485	1.51658 1.51583 1.51498	1.51652 1.51585	1.51650 1.51585

The values of H that were used are those calculated from (6-64). When two or more values are listed for a given t_1 they correspond to successive modes of increasing order.

From the results of Table 6-3, it is obvious that the single function variational method is sufficient to describe the waveguiding characteristics of the two-step ion-exchange channels. Using that method, and, this time, the measured set of effective indices, it is possible to find the full dispersion curves of the waveguides, presented graphically as b-V diagrams (Figures 6-6 and 6-7). The single-mode range extends from V = 0 to 3.8 (corresponding to $t_1 \cong 0$ to 10', at T=385°C, t_1+t_0 = 1 hour and D=10 μm). For other temperatures and times, the propagation constants are obtained directly from the graphs by finding the appropriate normalized frequency V.

As far as the mode solutions $\psi(x,y)$ are concerned, we can examine separately the behaviour of F(x,0) and G(y). The depth dependence of the modes, F(x,y), which we have shown to be almost independent of y was presented on Figure 6-5 and remains the same for any value of t_1 (submitted to the same restrictions of constant total time and temperature). The lateral dependence of the modes (G(y)) is shown on Figure 6-8 for the three methods and for two well separated values of t_1 (actually, the results of the two variational methods are equivalent and their curves overlap, since a single function in y was eventually used in the Rayleigh-Ritz case).

Here, it is the WKB solution that sets the standard against which the others are to be judged. We see that indeed the Gaussian function approximates the lateral behaviour of the mode

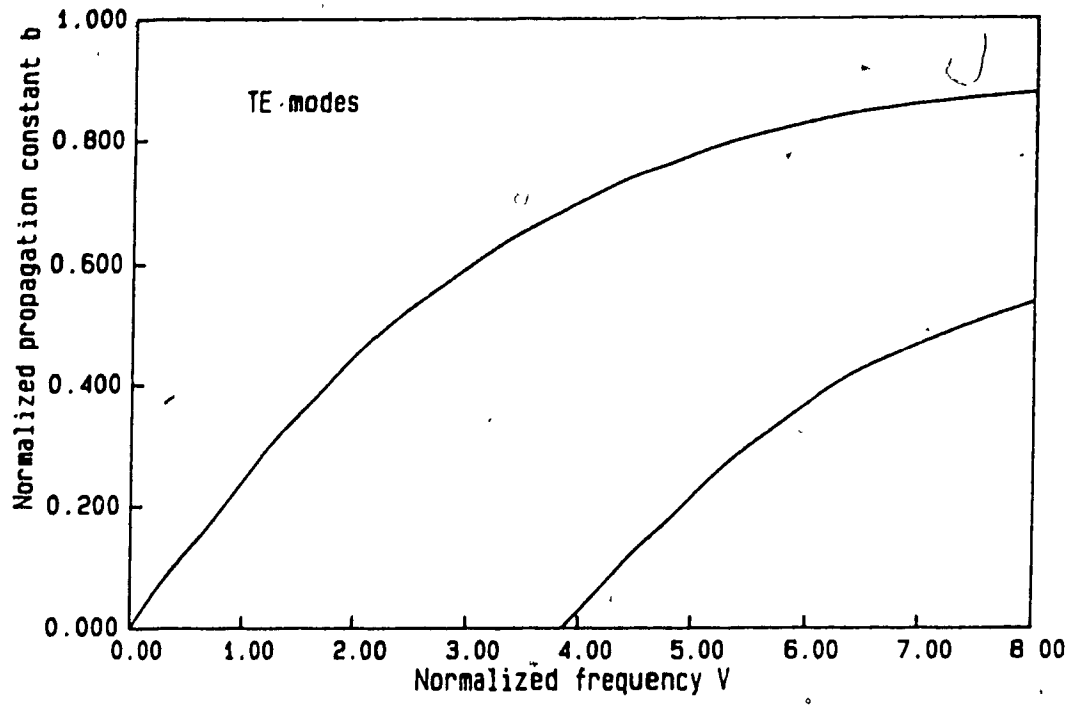

Figure 6-6. Normalized dispersion curves for channel guides made by two-step ion-exchange. D=10 μm, T=385°C and the total time (1 hour) are fixed, and t_1 is allowed to vary between 0 and 30'. TE modes.

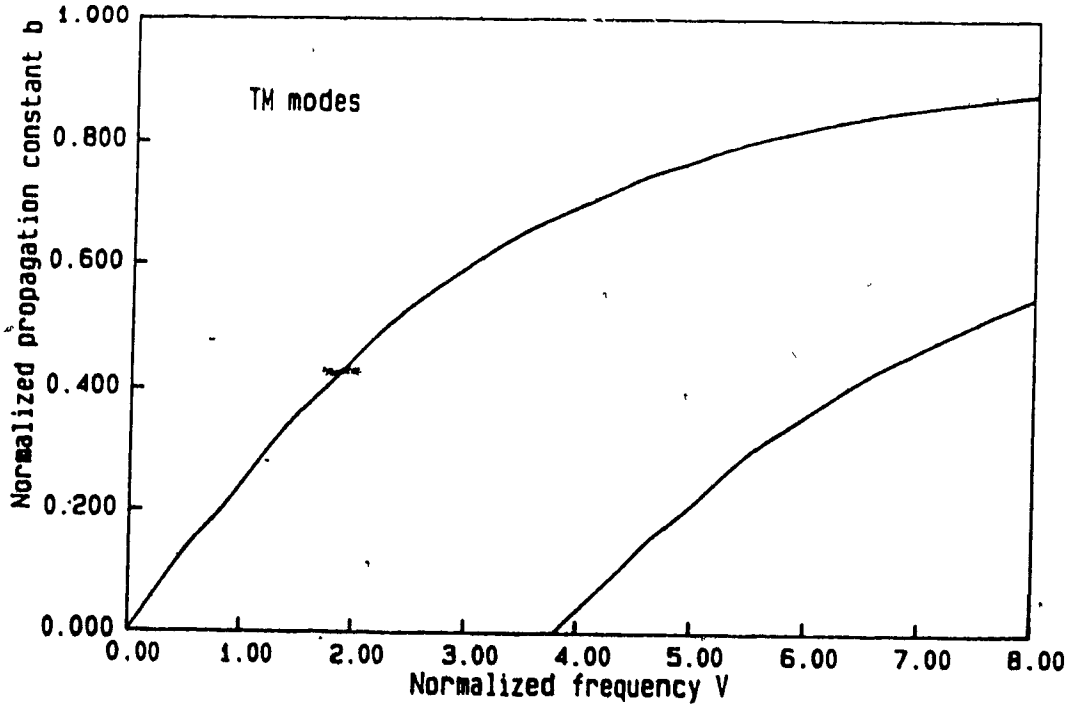

Figure 6-7. Normalized dispersion curves for channel guides made by two-step ion-exchange. D=10 μm, T=385°C and the total time (1 hour) are fixed, and t_1 is allowed to vary between 0 and 30'. TM modes.

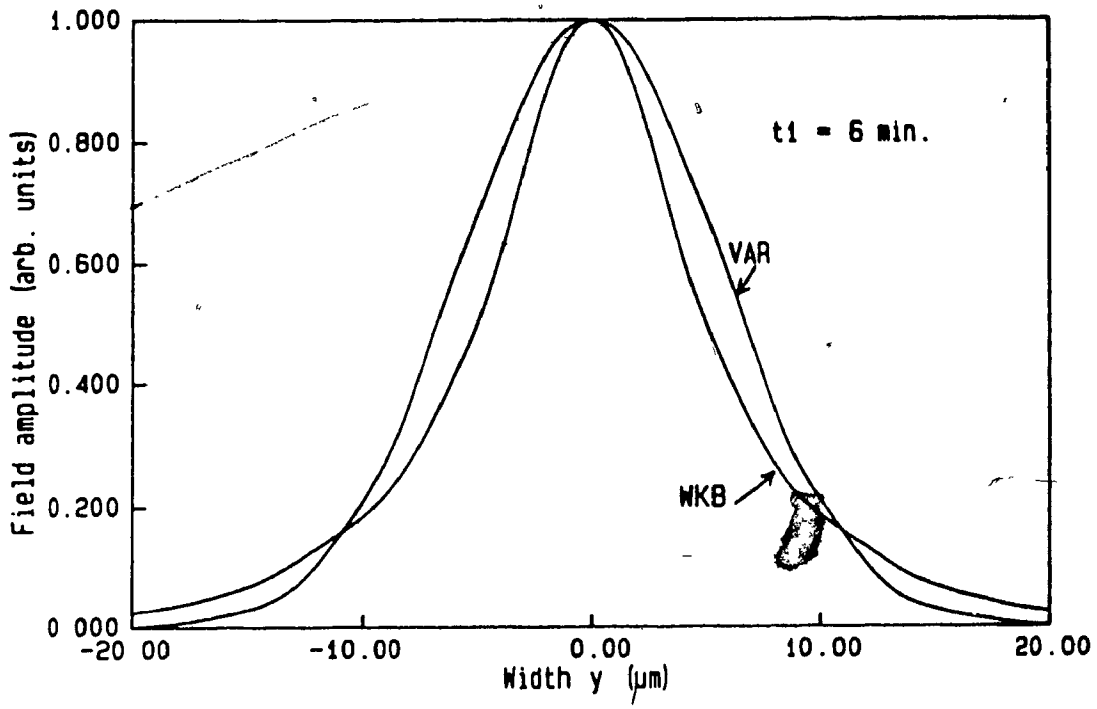

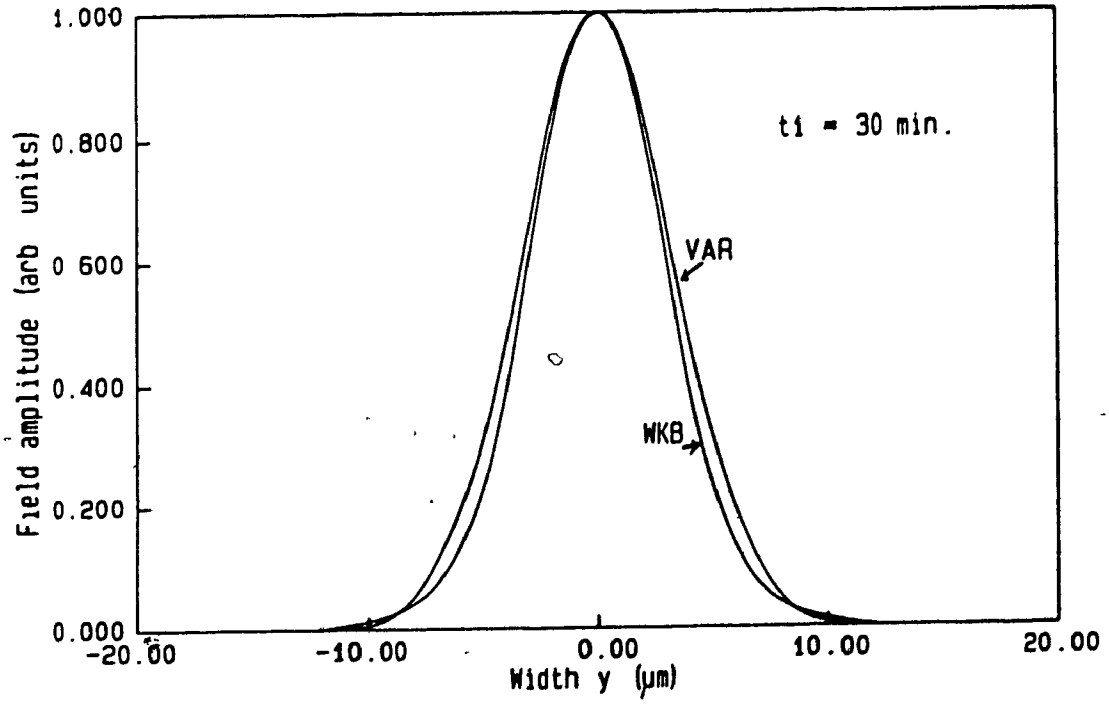

Figure 6-8. Field plots for channel guides. Lateral dependence. Comparison of the WKB and variational results.
a) Fundamental TE mode, t_1=6'
b) Fundamental TE mode, t_1=30'

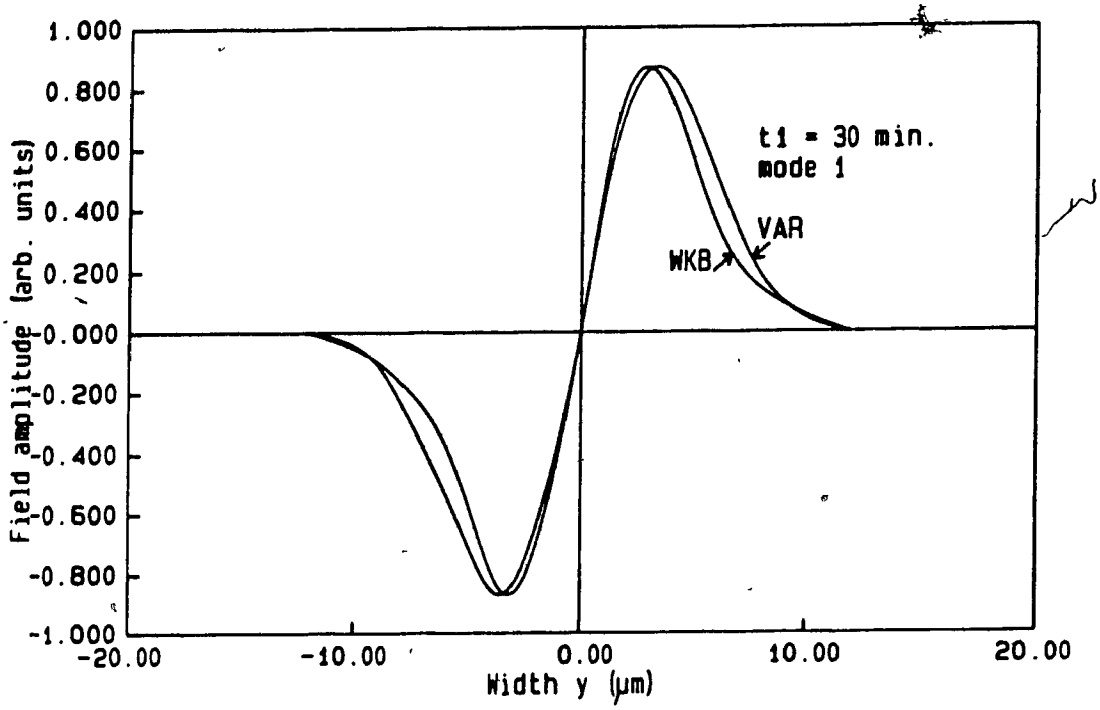

Figure 6-8. Field plots for channel guides. Lateral dependence. Comparison of the WKB and variational results.

c) Second TE mode, t_1=30'

very well and that in view of its extreme simplicity of calculation, compared with the complex formulas for the WKB solutions, it should be used to represent G(y) whenever high accuracy is not required.

The parameters that define the shape of G(y) for both semi-analytical methods are presented in Table 6-4 for reference. These were calculated with the measured effective indices.

6.5 FINAL REMARKS

To conclude this rather long chapter it may be useful to recall what we intended to do at the start and what has been accomplished. Starting from the 2-D refractive index profile that was defined from the results of chapters 2 and 4, the waveguiding characteristics of channel waveguides fabricated by two-step ion-exchange were sought after. In particular, through the reduction of the dimensionality of the problem by the use of the effective index method (which we showed to be especially appropriate in our case), a simple model of the equivalent lateral guide was derived and shown to be very accurate by comparing it with an exact numerical method (which was also described fairly extensively).

In summary, the method of characterization is as follows:

-From the results of a planar waveguide characterization, obtain the values of D_e, and of the effective indices as a function of the temperature and duration of the ion-exchange.

TABLE 6-4

SUMMARY OF RESULTS FOR LATERAL MODE PROFILE CHARACTERISTICS

	TE MODES				TM MODES			
t_1	N(∞)	β/k(WKB)	y_t	σ	N(∞)	β/k(WKB)	y_t	σ
04'	1.51531	1.51538	5.30	.0114	1.51625	1.51634	5.17	.0125
05'	1.51527	1.51537	5.06	.0136	1.51620	1.51633	4.92	.0152
06'	1.51523	1.51536	4.87	.0158	1.51614	1.51632	4.70	.0181
09'	1.51509	1.51535	4.48	.0218	1.51598	1.51630	4.35	.0242
12'	1.51495	1.51533	4.25	.0264	1.51582	1.51629	4.13	.0289
				.0108		1.51585	7.22	.0162
17'	1.51468	1.51532	3.99	.0332	1.51547	1.51627	3.88	.0367
		1.51480	6.27	.0237		1.51570	5.88	.0289
30'	1.51384	1.51531	3.76	.0463	1.51442	1.51526	3.67	.0504
		1.51459	5.10	.0439		1.51550	4.92	.0494
						1.51461	6.32	

$N^{TE}(0) = 1.51548$ $N^{TM}(0) = 1.51644$

The effective indices and propagation constants for the WKB solutions are included because they are needed explicitly in the field profiles. The values of H can be found in Table 6-2 under the column (eq. (6-64)).

When two or more values are listed for a given t_1 they correspond to successive modes of increasing order.

For example, at $t_1 = 17'$, the first value of σ corresponds to σ_0 and the second one to σ_1.

-Calculate the profile function N(y) and substitute it in the single-function variational formula of section 6.3.3 to get the propagation constant and lateral profile shape of the modes by a simple root-search procedure.

As the following chapters demonstrate, the method just outlined can be used in the design of more complex structures made up of many two-step channels patterned on a substrate to perform some optical signal processing function.

CHAPTER 7. DIRECTIONAL COUPLER DESIGN

7.1 INTRODUCTION TO THE PROBLEM

The goal of the fabrication of optical waveguides on planar substrates is to achieve some sort of signal processing function, or field transformation. For passive devices, such as those that can be made in glass, typical examples include power splitters [Findakly 1982], [Cullen 1984], directional couplers [Walker 1983], [Yip 1984], ring resonators [Walker 1983a], [Honda 1984], tapered junctions [Campbell 1979]], etc... All of these can be fabricated advantageously by using the two-step ion-exchange method, which provides a better control of performance than single-step methods through the fine tuning of the propagation constants and mode fields that it provides.

The method of solution of waveguide problems presented in the previous chapter can be extended to such structures provided that some conditions are met. The individual channels composing the circuits should be wide enough and separated enough to avoid overlap of the error functions that describe the effective index transitions on each side of the channels.

To test both the accuracy of the model developed in Chapter 6 and the control of device performance provided by the two-step method, it was decided that we would design, fabricate, and measure a single-mode directional coupler.

An optical directional coupler (abbreviated as DC in the

following) consists of two waveguides brought into sufficiently close proximity to allow the transfer of light power between the two by tunneling (i.e. coupling through the evanescent fields that propagate outside the cores of the waveguides). A particularly convenient form of DC to design and fabricate consists of two parallel identical waveguides. The analysis of this type of DC is simplified considerably in comparison with more complex structures and allows detailed quantitative predictions to be made. As long as the coupling between the branches remains weak, a total transfer of power from one branch to the other is possible [Suematsu 1977]. Of course, in a practical design, the parallel section must be preceded and followed by transition sections to facilitate input and output coupling to the device (because the width of the single-mode channels and their spacing are of the order of 10 μm).

The analysis of the DC is split up into two parts. First, the parallel section, and then the input/output transitions.

7.2 OVERVIEW OF THE METHODS OF SOLUTION

Using as before the effective index method to reduce the problem to one dimension, a typical lateral effective index profile for a parallel DC is (Figure 7-1):

$$N^{DC}(y) = N^{C}(y-W/2) + N^{C}(y+W/2) - N(\infty) \qquad (7-1)$$

where $N^{C}(y)$ is the single channel index profile (6-63).

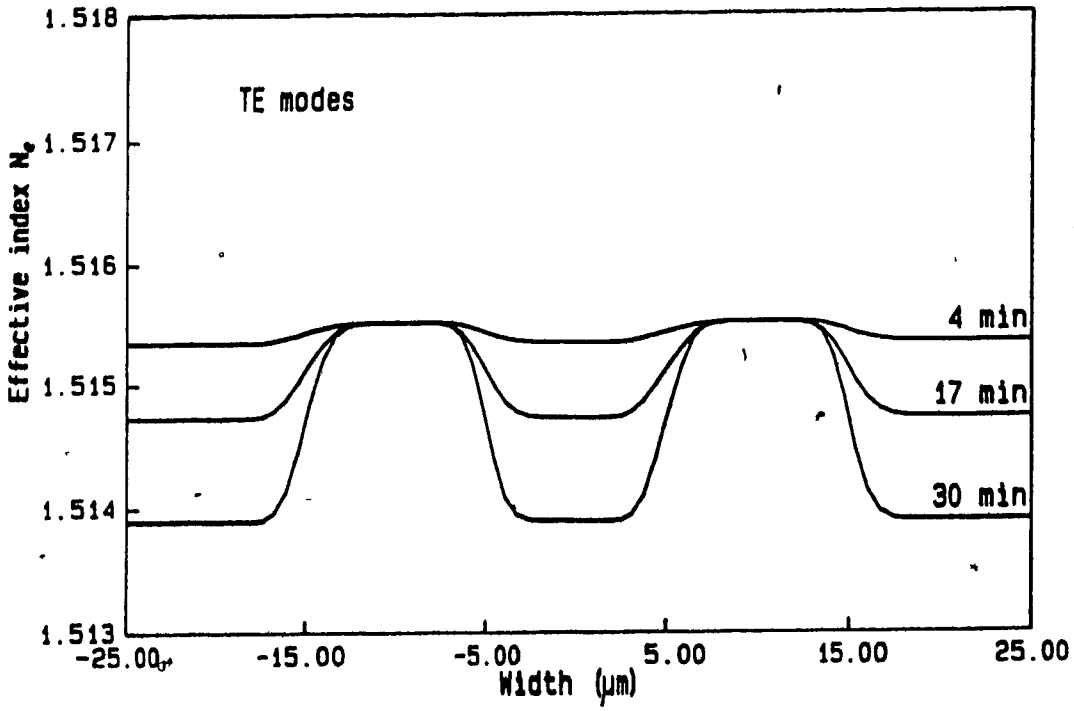

Figure 7-1. Directional coupler effective index profile for W=20 μm, and various values of t_1.

The channels, defined by two-step ion-exchange through 10 μm wide masks have a center-to-center spacing W and effective index difference ΔN. Having fixed the width D at 10 μm, the amount of coupling between the guides is determined solely by W and ΔN, becoming smaller as either or both increase.

The step-index equivalent of this one-dimensional problem has been the subject of many studies [Marcuse 1982], [Yariv 1973], [Kogelnik 1979] based on the earlier problem of coupled transmission lines [Miller 1954]. In these so-called "coupled-mode" approaches, the field of the DC is taken to be a superposition of the modes of the individual guides, calculated as if they were isolated from each other. The presence of the other guide then acts as a perturbation whose effect is to "tap" part of the propagating mode power. This is most easily seen for identical guides. The evanescent field that extends outside the core of one guide into the core of the other one becomes a source term (i.e. variable electric and magnetic field) of just the right temporal and spatial frequency to excite a mode of that waveguide (Figure 7-2). The inverse transfer is exactly equivalent and the exchange of power is described by a "coupling coefficient" calculated from an overlap integral between the two modes involved. Recent changes have been made to the theory to improve the treatment of radiation modes and power conservation [Streifer 1987], [Haus 1987], [Marcatili 1986], [Chuang 1987]. However, this method is still limited to cases of weak coupling

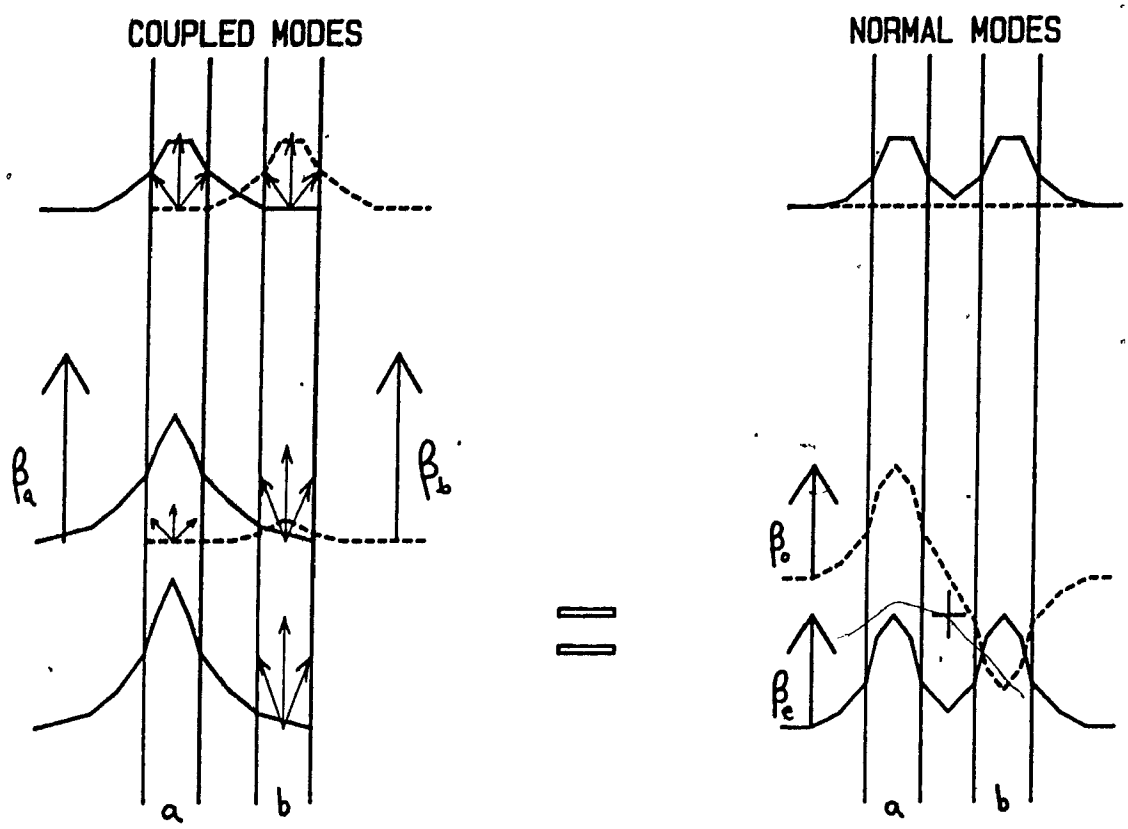

Figure 7-2. Schematic view of power transfer between parallel channels. On the left, the arrows indicate the induced polarization from the evanescent field of the adjacent channel. On the right, the interference between the odd (dashed line) and even (cont. line) modes is seen to correspond to power redistribution between the channels.

because of the use of the modes of the isolated waveguides in the calculation. In the limit of large separation, the method becomes exact but useless, since the guides are then decoupled. Partly because of this limitation, and partly because it is difficult to keep track of the approximations that are involved, another approach was taken here, the "normal modes" method ([Suematsu 1977], [Suhara 1979], [Donnely 1983], [Ctyroky 1984b] and many others).

In this case, we make use of the fact that the structure is confined in the y and uniform in the axial direction z. Therefore, it can support modes characterized by a constant functional shape G(y) and a z dependence of the form $e^{-j\beta z}$ (for time harmonic fields with $e^{j\omega t}$). Other than the approximation made to arrive at the scalar wave equation, and those of the effective index method (which were both also present in the coupled-mode approaches), this is an exact mathematical problem. The exact modes of the DC can be obtained in principle, numerically if necessary. Again, since N(y) is symmetric, the modes are either symmetric or anti-symmetric. To have a device with unequivocal transfer characteristics, the two channels must be individually single-moded; this means that the DC supports only two modes, the fundamental symmetric mode (which looks somewhat like a superposition of two channel modes) and the first anti-symmetric mode (that resembles a

superposition of a channel mode with the negative of the other channel mode).

From that point of view, the transfer of power from one guide to the other results from the interference between the two DC modes (heretofore referred to as the "even" and the "odd" modes). Specifically, the transfer characteristics can be calculated from a knowledge of the difference in their propagation constants $\Delta\beta$ and of the initial condition (i.e. the relative amplitudes of the two modes at the start of the parallel section). See Figure 7-2 for schematic view of power transfer due to mode interference. A detailed discussion of the relation between the coupled-modes and normal modes approaches can be found in [Marom 1984].

Various methods of solution for the normal modes of graded-index DC's have been used in the past. Some approximate results were obtained by using an approximate lateral profile N(y) for which analytical solutions of the wave equation were possible [Mueller 1985]. However, apart from the fact that their profile would not fit the special case of two-step ion-exchange, the agreement with experimental results (good for channel guides) was relatively poor for the transfer characteristics of directional couplers. Exact numerical methods can be used [Feit 1983], [Yeh 1979], [Ctyroky 1984b], but the computational cost is high for the resolution needed (apart from the difficult

implementation of the methods if the numerical programs are not already available). The WKB method is applicable to the parallel waveguides case [Suhara 1979] but requires more computations than the single channel case because asymptotic solutions decaying exponentially to $y = \pm\infty$ must be "connected" across 4 turning points. This makes the derivation of the dispersion relation fairly difficult but once it is done, the propagation constants are still obtained by a simple root-search procedure (see section 7.3.1). It also yields accurate field solutions. Its main drawback is that its accuracy decreases for strong coupling (as the coupled-modes methods) because the turning points become too close together for the asymptotic representations used in the connection formulas to be valid.

The simplest method, as in the previous chapter, is to use the single function variational method [Sharma 1980]. As we will see in section 7.3.2, it works even for small waveguide separations (i.e. strong coupling) even though the trial functions begin to be less accurate. This is due again to the stationarity of the variational formula, which tolerates slight deviations in the mode function and yet yields the right propagation constants.

The last two methods are described in more details in the next sections, and their results compared. In order to illustrate the limitations of the coupled-mode approaches, the results of one of these methods will also be presented. It is

described in [Landau 1965] as a worked out problem.

7.3 NORMAL MODE SOLUTIONS

7.3.1 The WKB method

Following [Suhara 1979], we can write down the field solutions in all the regions of interest of the coupler (refer to Figure 7-3), concentrating on $y \geq 0$ because of symmetry. For large values of y, the field must decay exponentially in the following manner to satisfy the lateral wave equation (6-60):

$$G(y) = \frac{A}{|f|^{1/4}}\sqrt{\frac{3}{2\pi}}\, e^{-\xi_a} \qquad (y >> y_{t_o}) \tag{7-2}$$

$$\xi_a = \int_{y_{t_o}}^{y} |f|^{1/2}\, dy \tag{7-3}$$

$$f = (k^2N^2(y) - \beta^2) \tag{7-4}$$

The outer turning point is defined by $kN(y_{t_o}) = \beta$, for y greater than W/2. Near that turning point, a solution can be obtained by using a linear approximation for N(y) and requiring that the solution behaves asymptotically like (7-2). This solution is:

$$G(y) = \frac{A\sqrt{\xi_a}}{|f|^{1/4}}\,\frac{3Ai(z)}{\sqrt{z}} \qquad (y \geq y_{t_o}) \tag{7-5}$$

$$z = \left(\frac{3\xi_a}{2}\right)^{\frac{2}{3}} \tag{7-6}$$

where the following relation between the Bessel functions of order 1/3 and the Airy function has been used [Abramowitz 1965]:

$$\frac{Ai(z)}{\sqrt{z}} = \frac{1}{3}\,(I_{-1/3}(\xi_a) - I_{1/3}(\xi_a)) \tag{7-7}$$

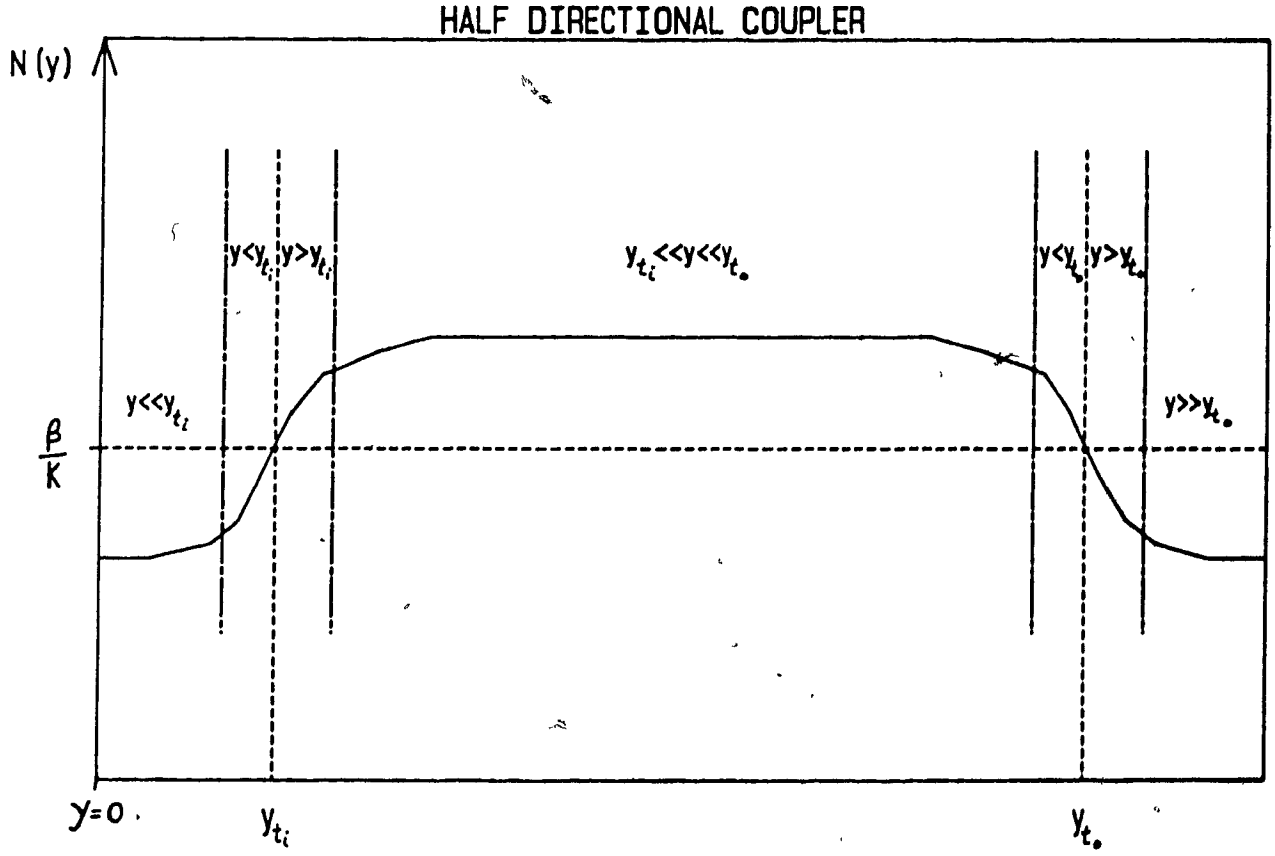

Figure 7-3. Approximate regions of applicability of the various WKB expressions for the field of the DC.

On the other side of the turning point, continuity requires:

$$G(y) = \frac{A\sqrt{\xi_b}}{f^{1/4}} \frac{3Ai(-z)}{\sqrt{z}} \qquad (y \le y_{t_0}) \tag{7-8}$$

$$z = \left(\frac{3\xi_b}{2}\right)^{\frac{2}{3}} \tag{7-9}$$

with ξ_b defined as in (6-68), relative to y_{t_0}. This solution behaves asymptotically as:

$$G(y) = \frac{A}{f^{1/4}} \sqrt{\frac{6}{\pi}} \cos(\xi_b - \frac{\pi}{4}) \qquad (y_{t_1} << y << y_{t_0}) \tag{7-10}$$

For the solutions surrounding the other turning point, a complication arises from the fact that the boundary condition is not as straightforward due to the presence of the other channel. The boundary conditions to be satisfied come from symmetry arguments as:

$$\left.\frac{\partial G(y)}{\partial y}\right|_{y=0} = 0 \text{ for symmetric modes} \tag{7-11}$$

and $$G(y=0) = 0 \text{ for anti-symmetric modes} \tag{7-12}$$

The most general solution for a linearized N(y) near y_{t_1} is [Schiff 1968]:

$$G(y) = \frac{\sqrt{\xi_c}}{f^{1/4}} (CJ_{1/3}(\xi_c) + DJ_{-1/3}(\xi_c)) \qquad (y \ge y_{t_1}) \tag{7-13}$$

$$\xi_c = \int_{y_{t_1}}^{y} \sqrt{f}\, dy \tag{7-14}$$

$$G(y) = \frac{\sqrt{\xi_d}}{|f|^{1/4}} (EI_{1/3}(\xi_d) + FI_{-1/3}(\xi_d)) \qquad (y \le y_{t_1}) \tag{7-15}$$

$$\xi_d = \int_{y}^{y_{t_1}} |f|^{1/2}\, dy \tag{7-16}$$

Taking the limit of both (7-13) and (7-15) as $y \to y_{t_1}$ (with $\xi_c,\ \xi_d \to 0$) we get necessarily:

$$E = -C \qquad \text{and} \qquad F = D \tag{7-17}$$

which means that (7-15) becomes:

$$G(y) = \frac{\sqrt{\xi_d}}{|f|^{1/4}} \left(-CI_{1/3}(\xi_d) + DI_{-1/3}(\xi_d)\right) \qquad (y \le y_{t_1}) \tag{7-18}$$

Using (7-18), we get from (7-12):

$$\frac{C}{D} = \frac{I_{-1/3}(\xi_d(0))}{I_{1/3}(\xi_d(0))} \quad \text{for the anti-symmetric mode,} \tag{7-19}$$

and from (7-11), along with the fact that $\frac{df}{dy} = 0$ at $y = 0$:

$$|f|^{1/4}\frac{dG}{dy}\Big|_{y=0} = \frac{-C}{2\sqrt{\xi_d}} I_{1/3}(\xi_d)\frac{d\xi_d}{dy} - C\sqrt{\xi_d}\frac{dI_{1/3}(\xi_d)}{dy} + \ldots$$

$$\ldots + \frac{D}{2\sqrt{\xi_d}} I_{-1/3}(\xi_d)\frac{d\xi_d}{dy} + D\sqrt{\xi_d}\frac{dI_{-1/3}(\xi_d)}{dy} \tag{7-20}$$

where:

$$\frac{dI_{\pm 1/3}(\xi_d)}{dy} = \frac{dI_{\pm 1/3}(\xi_d)}{d\xi_d}\frac{d\xi_d}{dy} = I'_{\pm 1/3}\frac{d\xi_d}{dy} \tag{7-21}$$

so that for the symmetric mode:

$$\frac{C}{D} = \frac{I_{-1/3}(\xi_d(0)) + \xi_d(0)(I_{2/3}(\xi_d(0)) + I_{-4/3}(\xi_d(0)))}{I_{1/3}(\xi_d(0)) + \xi_d(0)(I_{4/3}(\xi_d(0)) + I_{-2/3}(\xi_d(0)))} \tag{7-22}$$

where we have used a recurrence relation to get rid of the derivatives [Dwight 1961]:

$$2I'_n = I_{n-1} + I_{n+1} \tag{7-23}$$

We still have to connect (7-13) to (7-10) for continuity of G(y). Taking the limit of (7-13) for large ξ_c we get [Dwight 1961]:

$$G(y) = \frac{\sqrt{\xi_c}}{f^{1/4}}\left(C\sqrt{\frac{2}{\pi\xi_c}}\cos(\xi_c - \frac{5\pi}{12}) + D\sqrt{\frac{2}{\pi\xi_c}}\cos(\xi_c - \frac{\pi}{12})\right) \qquad (7\text{-}24)$$

And we note that in the region between the turning points:

$$\xi_b = \int_{y}^{y_{t_0}} \sqrt{f}\, dy = \int_{y_{t_1}}^{y_{t_0}} \sqrt{f}\, dy - \xi_c \qquad (7\text{-}25)$$

Therefore, the equality between (7-10) and (7-24) becomes:

$$\sqrt{3}A\cos\left(\int_{y_{t_1}}^{y_{t_0}} \sqrt{f}\, dy - \xi_c - \frac{\pi}{4}\right) = C\cos(\xi_c - \frac{5\pi}{12}) + D\cos(\xi_c - \frac{\pi}{12}) \qquad (7\text{-}26)$$

which must be valid for any value of ξ_c between 0 and $\int_{y_{t_1}}^{y_{t_0}} \sqrt{f}\, dy$ (i.e. y between y_{t_1} and y_{t_0}).

We use this property to find the dispersion relation and the value of C (or D, which is related to C by (7-19) or (7-22) in terms of the arbitrary amplitude A. First, we define:

$$\theta = \int_{y_{t_1}}^{y_{t_0}} \sqrt{f}\, dy - \frac{\pi}{4} \qquad (7\text{-}27)$$

and we use $\xi_c = 0$:

$$\sqrt{3}A\cos(\theta) = C\frac{\sqrt{3}-1}{2\sqrt{2}} + D\frac{\sqrt{3}+1}{2\sqrt{2}} \qquad (7\text{-}28)$$

Now with $\xi_c = \pi/2$:

$$\sqrt{3}A\sin(\theta) = C\frac{\sqrt{3}+1}{2\sqrt{2}} + D\frac{\sqrt{3}-1}{2\sqrt{2}} \qquad (7\text{-}29)$$

and by taking the ratio of these two results:

$$\tan(\theta) = \frac{(\sqrt{3}+1)C + (\sqrt{3}-1)D}{(\sqrt{3}-1)C + (\sqrt{3}+1)D} \qquad (7\text{-}30)$$

from which we can get (by isolating (C-D) and (C+D) and using trigonometric identities):

$$\frac{C - D}{\sqrt{3}(C + D)} = \tan(\theta - \frac{\pi}{4}) \qquad (7\text{-}31)$$

or:

$$\int_{y_{t_1}}^{y_{t_0}} \sqrt{f}\, dy + \tan^{-1}\left(\frac{1 - C/D}{\sqrt{3}(1 + C/D)}\right) = (n + \tfrac{1}{2})\pi \quad (n = 0,1,2,3,\ldots) \qquad (7\text{-}32)$$

which is a transcendental equation in only one unknown, β, i.e. the dispersion relation for the modes of the DC.

Finally, taking $\xi_c = \pi/4$:

$$\sqrt{3}A \cos(\theta - \frac{\pi}{4}) = \frac{(C + D)\sqrt{3}}{2} \qquad (7\text{-}33)$$

$$A = \frac{C + D}{2} \sec(\theta - \frac{\pi}{4}) \qquad (7\text{-}34)$$

$$A = \pm\frac{C + D}{2}\sqrt{1 + \tan^2(\theta - \frac{\pi}{4})} \qquad (7\text{-}35)$$

in which we replace (7-31):

$$A = \pm\sqrt{\frac{C^2 + D^2 + CD}{3}} \qquad (7\text{-}36)$$

To choose the sign of the radical in (7-36), we note that in replacing the secant in going from (7-34) to (7-35), the sign of the radical depends on the quadrant in which the argument is located [Dwight 1961]. Defining A to be positive for the fundamental mode (n=0), its sign will be negative for all the odd modes (n=1,3,5,...).

This completes the derivation of the WKB solution for the normal modes of the full DC problem. The propagation constants are obtained from (7-32), and the fields from (7-2), (7-5),

(7-8), (7-10), (7-13), and (7-18). Examples of normal modes are given in Figure 7-4. Before the discussion of power transfer in terms of the normal modes representation, we will describe the variational approach to find the normal modes.

7.3.2 The variational method

This method is based on the work of [Sharma 1980], and is strictly an extension of the single channel solution of section 6.3.3. The method consists of using a single trial function with a shape that can reasonably be expected to look like an eigenmode of the DC.

The trial function to be used in this case is a superposition of Gaussian functions centered in the middle of each channel. The width of the Gaussians is determined by the variational parameter used to maximize the functional (6-71). For the profile of Figure 7-1, the trial function is:

$$G_{e/o}(y) = e^{-\sigma_{e/o}(y - W/2)^2} + s * e^{-\sigma_{e/o}(y + W/2)^2} \qquad (7-37)$$

where: s = +1 for the even mode (subscript e)

s = -1 for the odd mode (subscript o)

It must be stressed that (7-37) is not a superposition of modes of the individual channels. The width factor σ is different, and depends on W, as well as on D and ΔN. To find σ and β, we proceed again to solve:

$$\frac{\partial \beta^2}{\partial \sigma} = 0 \qquad (7-38)$$

which is exactly the same as (6-76), except that in this case,

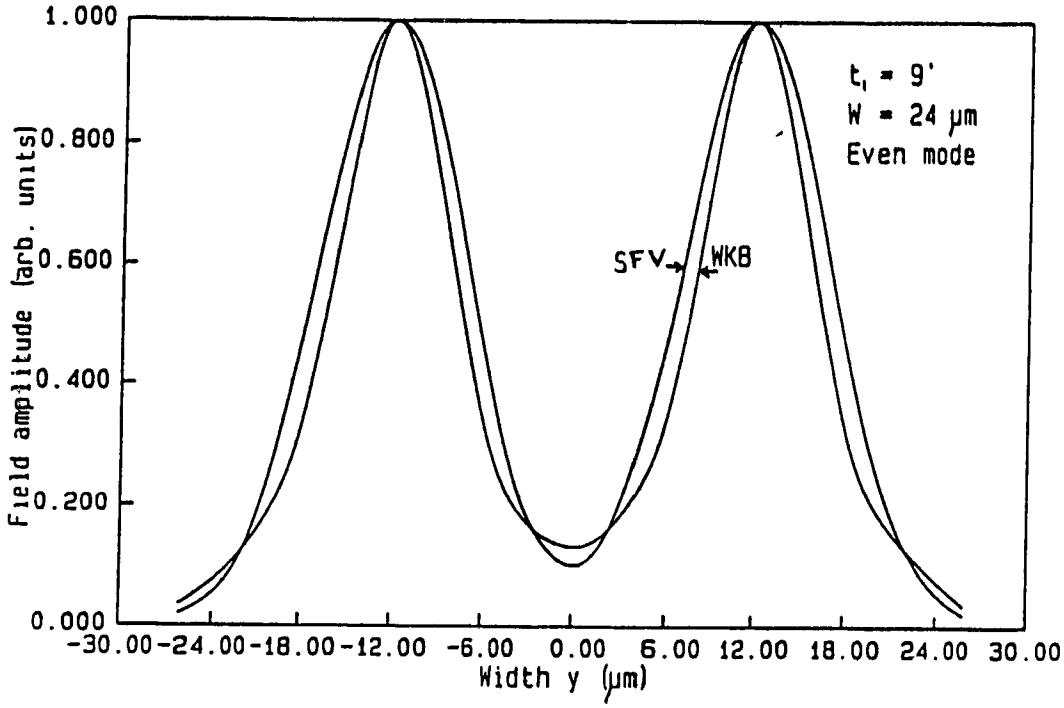

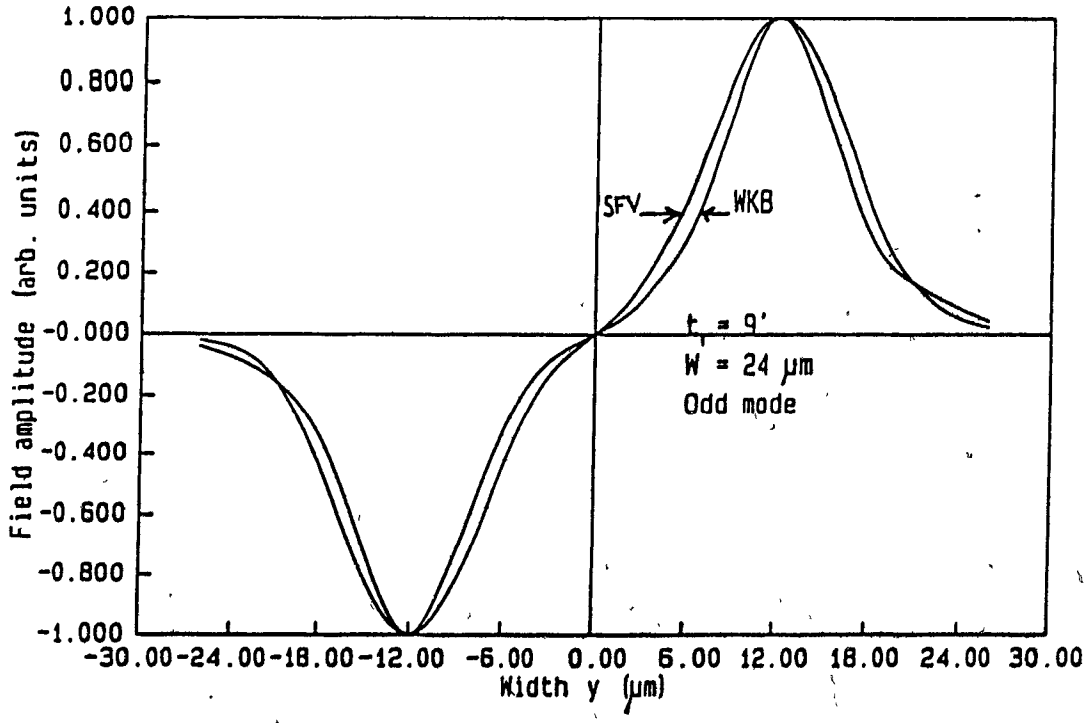

Figure 7-4a. Field plots for the DC. Lateral dependence. Comparison between the WKB and variational results.

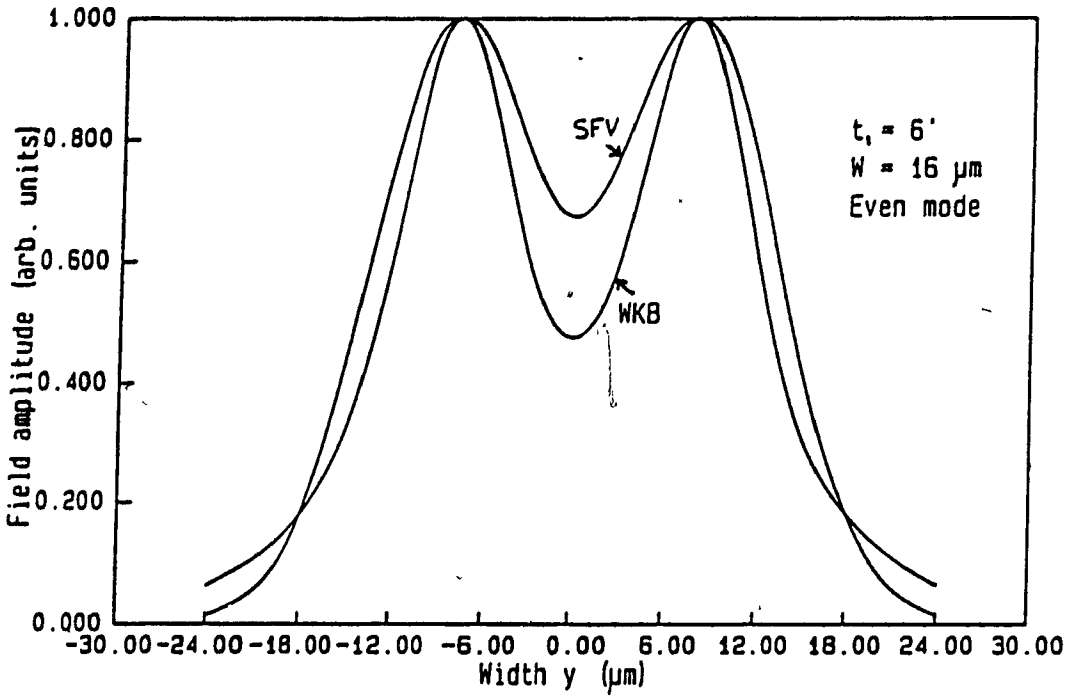

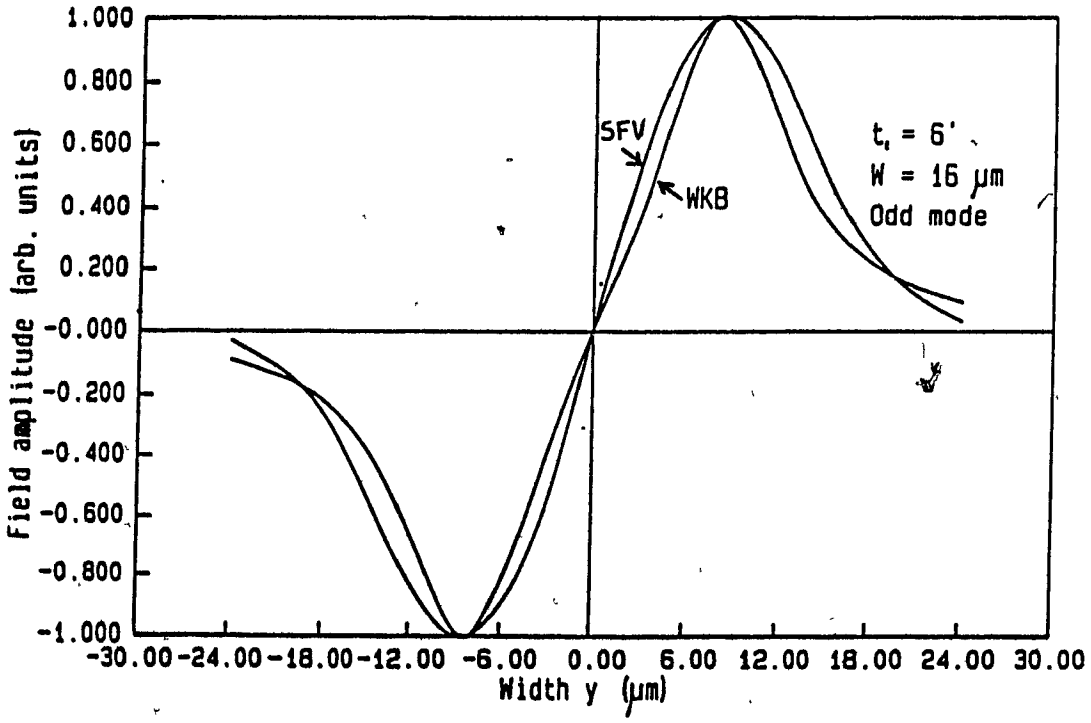

Figure 7-4b. Field plots for the DC. Lateral dependence. Comparison between the WKB and variational results.

the expressions for G(y) and its various derivatives are slightly more complicated. Examples of normal modes calculated by this method are shown in Figure 7-4.

7.3.3 Results of the normal mode methods

As we have seen in section 7.2, the parameters of importance are the difference in propagation constant $\Delta\beta$ and the relative amplitudes of the modes at the start of the parallel section. The discussion of the latter point must be delayed until section 7.4, where different input-output conditions are considered. For now, we can present graphical results for $\Delta\beta$ vs W and ΔN. These will be useful as design tools in later sections and in Chapter 8, for the fabrication of a working prototype.

In addition to the results of the two previous sections, a few points obtained with the coupled-mode analysis of [Landau 1965] are plotted for comparison. The method uses a superposition of individual channel modes obtained by the WKB approximation. Three sets of results are presented in Figure 7-5 (for t_1=9'), while additional data are plotted for the variational method only in Figure 7-6. As can be seen in the first figure, the curves for both the coupled-mode and WKB methods begin to flatten for strong coupling, indicating that their range of validity has been exceeded. The last data points, at W=24 μm, are not very accurate because $\Delta\beta/k$ becomes of the

same order of magnitude as the accuracy with which β/k is calculated (0.00001). Also, as W tends towards D, the propagation constants of the even and odd modes should tend towards those of the single channel of width 2D. Using the SFV of section 6.3.3, the two propagation constants were calculated and yielded $\Delta\beta(t_1=9')/k = 1.5 \times 10^{-4}$. This point is plotted at W = 10 μm in Figure 7-5 and is a direct extrapolation of the remaining SFV data. We may also note that for large separation or ΔN, both β_e and β_o tends towards the propagation constant of a single guide in isolation. For instance, for TM modes at $t_1=9'$ and W=24 μm β_e and β_o are equal to 1.516292 and 1.516290 respectively, while for an isolated channel, $\beta=1.51629$.

For the field solutions, Figure 7-4 indicates very good agreement between the WKB and variational methods.

This confirms the conclusion of Chapter 6 that the single function variational method is a very useful and accurate way of describing the waveguiding properties of these channels. A summary of the results for directional couplers is presented in Table 7-1.

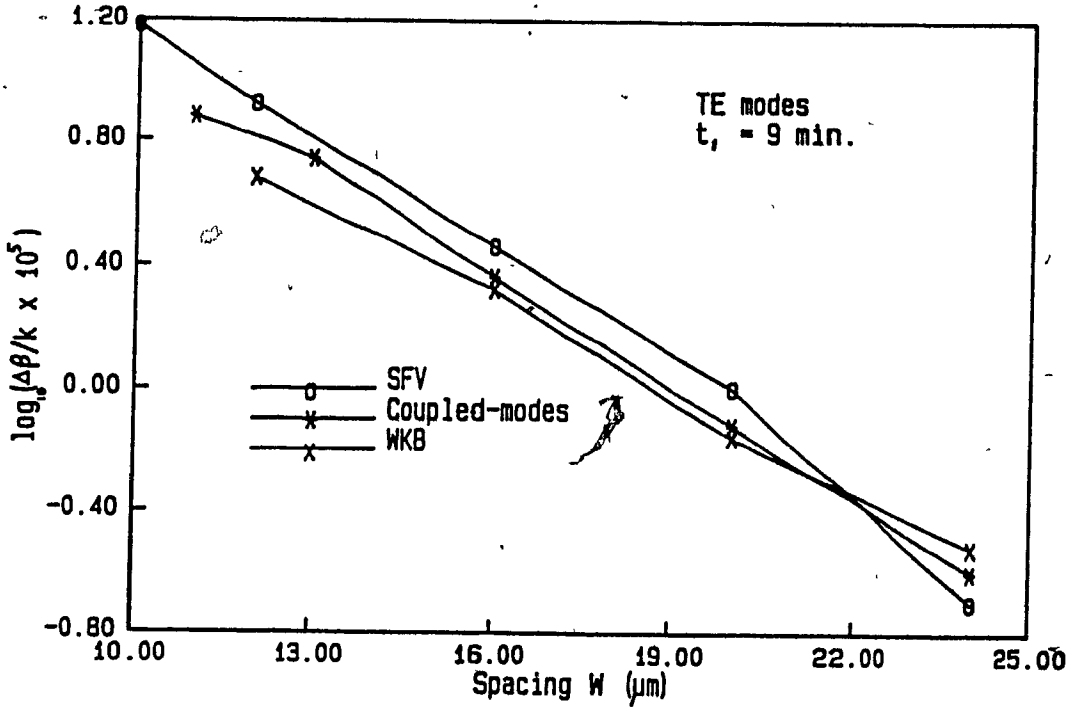

Figure 7-5. Base 10 logarithm of $\Delta\beta$ versus spacing W for the three methods used. Straight lines join the discrete results for clarity.

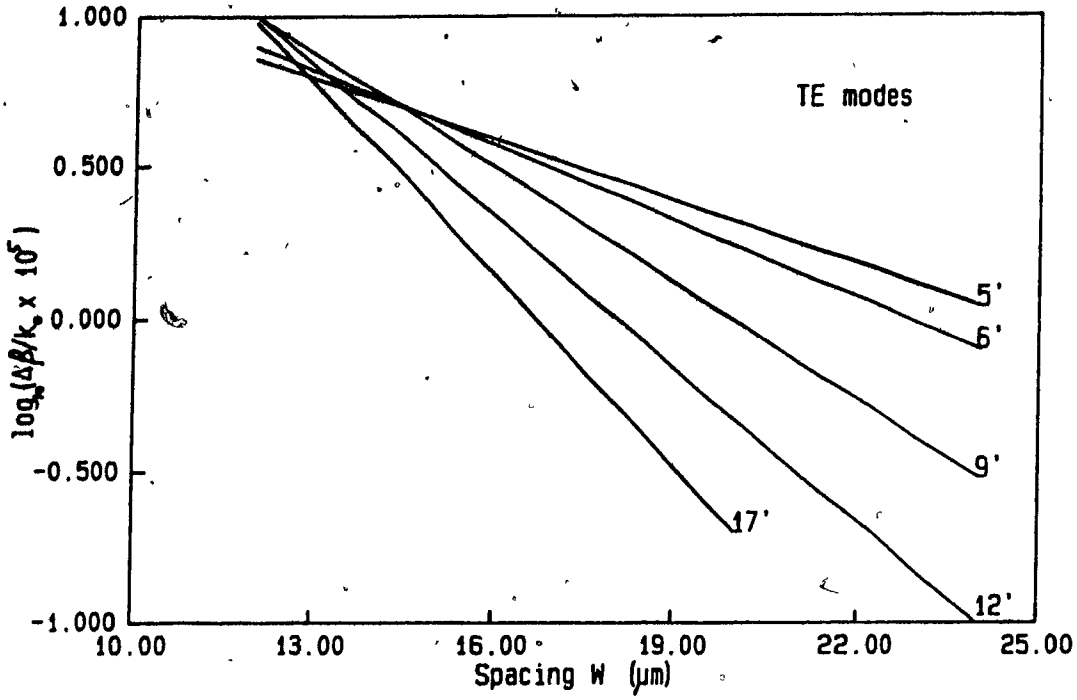

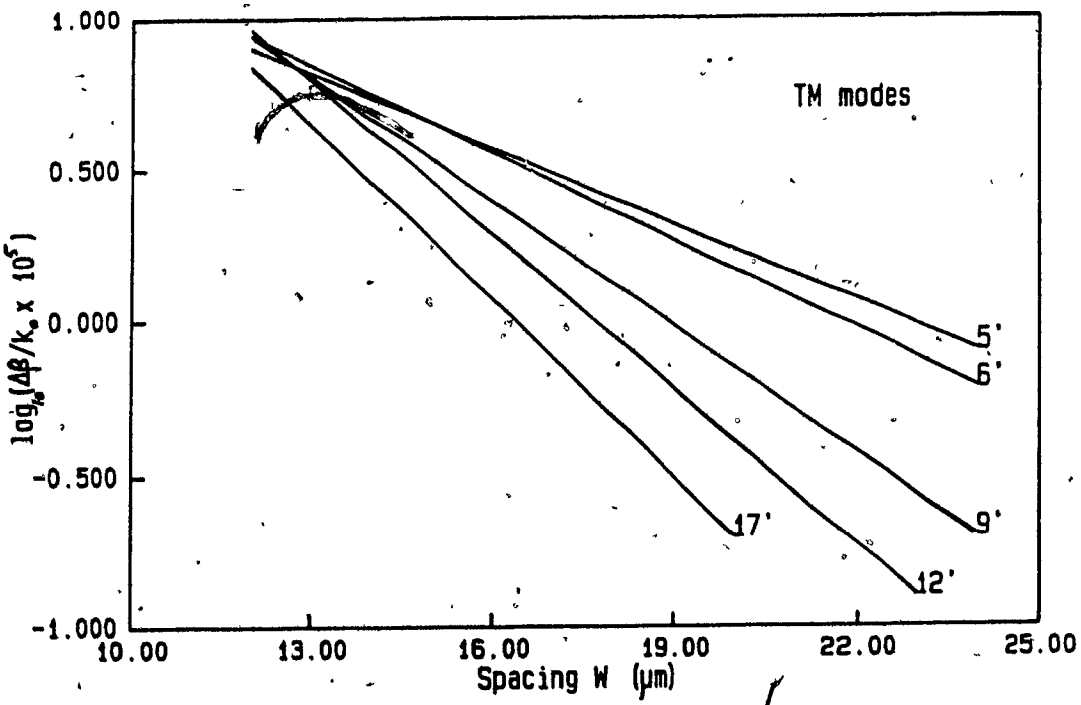

Figure 7-6. Best straight line fits for the exponential relation between Δβ and W.

7.4 INPUT-OUTPUT PROBLEM AND POWER TRANSFER CHARACTERISTICS

7.4.1 Introduction

For single-mode individual channels, the DC can support only two modes at the most, i.e. the even and odd modes shown in Figure 7-4. The odd mode may even be cut-off if W and/or ΔN are too small. Therefore, whatever incident field is input to the DC, it can only launch these two modes, plus non-guided scattering in the form of radiation modes. Assuming that these are minimized, the power transfer between the channels is totally determined by the relative amplitudes of the two propagating modes at the start, and by their relative phase at the end. But before we are able to quantify "power transfer", we must determine what that term means.

For strongly coupled guides, even if they are identical, the power is never totally in one guide or the other (or more precisely, there is no superposition of modes of the DC that yields zero power in one of the branches) [Suematsu 1977]. At any point along the DC, a good measure of how much power actually propagates in one branch is given by the projection of the field of the DC on the single-mode of that channel by means of an overlap integral.

The idea of input-output transition sections is to have totally uncoupled guides in which to launch and receive power. Two distinct cases are possible. First, an abrupt transition between a region with only one waveguide and a region with two

waveguides. This is preferred at the input (to ensure launching from one branch only). However, it is not a good design for the output because any power left in the terminated branch would scatter in the same general direction as the remaining branch and induce noise in it. A second type of transistion is a smooth and gradual increase in the separation W, until the two guides become totally decoupled (Figure 7-7). Such transition should be adiabatic, meaning that the total power is conserved as guided modes. In principle, it can be used without problems as input or output. The two types of transitions are analyzed below.

7.4.2 Abrupt transition

When used at input, the problem to be solved is to determine how the incident mode of the single waveguide excites the normal modes of the DC (and how much ends up lost in radiation modes also). Neglecting the backward reflection due to the slight mismatch of wave impedances, this is simply the problem of the projection of a given function onto a basis of functions (in the same sense as in section 6.2.2), using a scalar product defined by:

$$\langle f|g\rangle = \int_{-\infty}^{\infty} f(y)g(y)\,dy \qquad (7-39)$$

The modes of the DC (plus the radiation modes) form an orthogonal basis and we can express the field of an incident channel as:

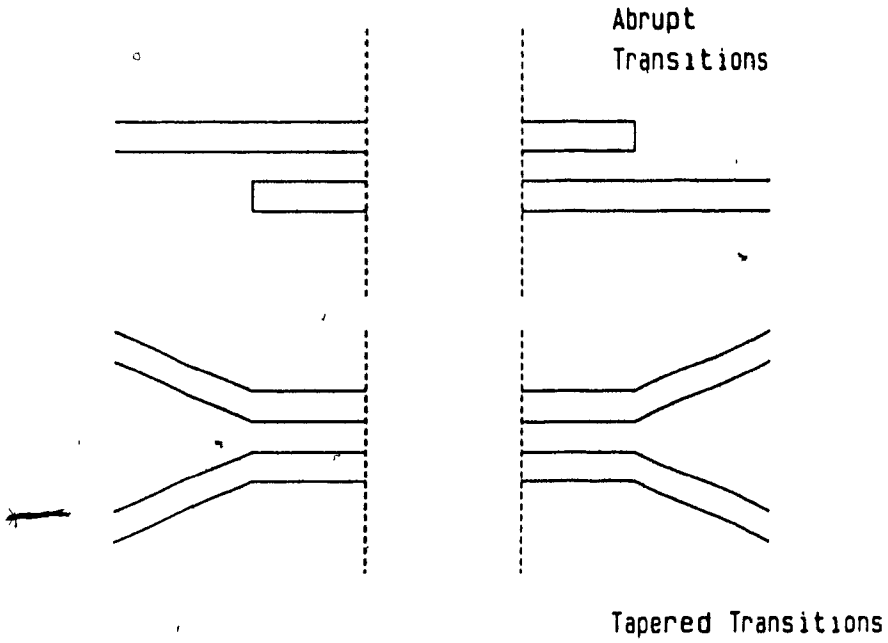

Figure 7-7. Schematic view of the two types of transitions between the parallel DC and the individual channel guides.

$$\hat{G}_c(y) = A_e\hat{G}_e(y) + A_o\hat{G}_o(y) + F_r \qquad (7-40)$$

using normalized modes:

$$\hat{G}_i(y) = \frac{G_i(y)}{\sqrt{\langle G_i|G_i\rangle}} \qquad (7-41)$$

where F_r is the total radiation field excited because $\hat{G}_c$ does not necessarily match exactly a superposition of $\hat{G}_e$ and $\hat{G}_o$, the even and odd modes of the DC, with amplitudes A_e and A_o (the amplitude transfer functions, relative to unit input power). These are obtained by taking the scalar product of $\hat{G}_e$ and $\hat{G}_o$ with (7-40):

$$A_e = \langle\hat{G}_e|\hat{G}_c\rangle \qquad (7-42)$$

$$A_o = \langle\hat{G}_o|\hat{G}_c\rangle \qquad (7-43)$$

And the radiated power $|F_r|^2$ by:

$$|F_r|^2 = P_r = 1 - (A_e^2 + A_o^2) \qquad (7-44)$$

Using the variational method, we use expression (6-72) (centered at W/2) for $G_c(y)$ (and replace σ by σ_c), and expression (7-37) for G_e and G_o and get:

$$A_e = \frac{(\sigma_e\sigma_c)^{1/4}}{\sqrt{\sigma_e+\sigma_c}} \frac{\left(1 + e^{\frac{-\sigma_e\sigma_c W^2}{\sigma_c + \sigma_c}}\right)}{\sqrt{1 + e^{\frac{-\sigma_e W^2}{2}}}} \qquad (7-45)$$

$$A_o = \frac{(\sigma_o\sigma_c)^{1/4}}{\sqrt{\sigma_o+\sigma_c}} \frac{\left(1 - e^{\frac{-\sigma_o\sigma_c W^2}{\sigma_c + \sigma_c}}\right)}{\sqrt{1 - e^{\frac{-\sigma_o W^2}{2}}}} \qquad (7-46)$$

Results for various cases of interest are presented in Table 7-2. We see that both A_e and A_o converge towards $1/\sqrt{2}$

as W or ΔN increases, meaning that the incoming normalized mode splits equally into the two modes of the DC with no scattered power P_r. The only entry of the table for which P_r is measurable (=4%) is at t_1 equal 5' for the TM modes. The fact that P_r increases for strong coupling means that no superposition of DC modes can represent a mode of a channel, i.e. the guided power is never restricted to only one guide, and of course, total transfer is not possible.

The inverse problem (i.e. output from the 2-guide parallel section to a single guide by abrupt termination of one guide, can also be addressed with equations (7-45) and (7-46). In that case, A_e and A_o are to be interpreted as transfer functions between the normalized modes of the DC and the channel remaining for output. The total output power is calculated by projecting the field of the DC onto the field of the output channel:

$$P_{out} = (a_e A_e + a_o(-A_o))^2 \qquad (7-47)$$

where a_e and a_o are the arbitrary amplitudes (magnitude and phase) of the normal modes at the junction plane (where one waveguide abruptly ends). Note that $-A_o$ is used because it is assumed that the output channel is not the same as the input channel, and the sign of A_o depends on which channel is used for the overlap integral (replacing $\hat{G}_o(y)$ by $-\hat{G}_o(-y)$).

Also, we note that for anything but a 100% transfer coupler this design is not very good because of the forward scattering of the power remaining in the interrupted branch.

7.4.3 Gradual transition

Inasmuch as the transition is smooth enough for scattering losses to be neglected, this is a much simpler problem. However, because the structure is not uniform in the z direction, strictly speaking, there can be no modes as such (with a constant propagation β and modal shape G(y)). We assume instead that the modes exist locally, with slowly varying properties.

At input, we launch power into one branch, at a point where the spacing is so large that there is no coupling with the other branch. Then, as we have seen in the previous sections, the single channel mode can be thought of as an exact superposition of the even and odd modes of the DC (with equal amplitudes). The channels get closer together as they approach the parallel section, but for a sufficiently smooth transition, we can assume that the power carried by each mode is constant (as for a uniform waveguide).

The change in spacing has one important effect, however, a gradual variation of the propagation constant of the normal modes. Assuming unit power in the incident channel, we get for all the regions where coupling occurs:

$$\hat{G}(y,z) = \frac{1}{\sqrt{2}}\,\hat{G}_e(y,z)\; e^{-j\int_0^z \beta_e(z')\,dz'} + \frac{1}{\sqrt{2}}\,\hat{G}_o(y,z)\; e^{-j\int_0^z \beta_o(z')\,dz'} \qquad (7\text{-}48)$$

where z is measured from the start of the coupling region, where the two modes are equal in amplitude and phase. The integrals

represent the accumulated phase increase for each mode in going from 0 to z with a varying propagation constant $\beta(z)$. Variants of this method for the treatment of non-parallel waveguides have been used by various authors in the past: [Matsuhara 1975], [Findakly 1978], [Anderson 1979].

The validity of the approach comes from the adiabaticity of the transition, i.e. the fact that the power carried by each mode in conserved. Obviously, this is only correct for small axial non-uniformities (small angles between the axes of the channels) so that modes can be identified at all. Intuitively therefore, we must have:

$$\left|\frac{\partial \hat{G}(y,z)}{\partial z}\right| , \left|\frac{\partial \beta}{\partial z}\right| << |\beta| \qquad (7-49)$$

When the coupled-mode approach is used for the same problem of non-parallel waveguides, conceptual difficulties arise from the non-parallelism of the wave-fronts of the modes to be coupled (see [McHenry 1984] and references therein for a full discussion on this topic).

Now, when an output section is made up of such a gradual increase in spacing, equation (7-48) still applies, but in general, the amplitudes of the modes need not be equal, depending on the input condition. Instead, we get (assuming input amplitudes A_e and A_o):

$$G(y,z) = A_e\hat{G}_e(y,z)\, e^{-j\int_0^z \beta_e(z')\,dz'} + A_o\hat{G}_o(y,z)\, e^{-j\int_0^z \beta_o(z')\,dz'} \qquad (7-50)$$

When the spacing becomes so large that coupling no longer occurs, the normal modes can be expressed as a superposition of channel modes in the following manner:

$$\hat{G}_e(y) = \frac{1}{\sqrt{2}}\hat{G}_a(y) + \frac{1}{\sqrt{2}}\hat{G}_b(y) \qquad (7\text{-}51a)$$

$$\hat{G}_o(y) = \frac{1}{\sqrt{2}}\hat{G}_a(y) - \frac{1}{\sqrt{2}}\hat{G}_b(y) \qquad (7\text{-}51b)$$

or:

$$\hat{G}_a(y) = \frac{1}{\sqrt{2}}(\hat{G}_e+\hat{G}_o) \text{ and } \hat{G}_b(y) = \frac{1}{\sqrt{2}}(\hat{G}_e-\hat{G}_o) \qquad (7\text{-}52)$$

and the power ending up in each channel is obtained by the projection of G(y,z-end) onto either $\hat{G}_a$ or $\hat{G}_b$:

$$P_a = |\langle\hat{G}_a|G(y)\rangle|^2 = \frac{A_e^2}{2}\left|1 + \frac{A_o}{A_e}e^{j\int_0^z\Delta\beta(z')\,dz'}\right|^2$$

$$= \frac{A_e^2}{2}\left(1 + \left(\frac{A_o}{A_e}\right)^2 + 2\left(\frac{A_o}{A_e}\right)\cos\left(\int_0^z \Delta\beta(z')\,dz'\right)\right) \qquad (7\text{-}53)$$

$$P_b = |\langle\hat{G}_b|G(y)\rangle|^2 = \frac{A_e^2}{2}\left|1 - \frac{A_o}{A_e}e^{j\int_0^z\Delta\beta(z')\,dz'}\right|^2$$

$$= \frac{A_e^2}{2}\left(1 + \left(\frac{A_o}{A_e}\right)^2 - 2\left(\frac{A_o}{A_e}\right)\cos\left(\int_0^z \Delta\beta(z')\,dz'\right)\right) \qquad (7\text{-}54)$$

with $\Delta\beta = \beta_e - \beta_o$.

We see from (7-53) and (7-54) that only in the special case of equal normal mode amplitudes, $A_o/A_e = 1$, is total transfer possible (i.e. P_a or $P_b = 0$). Note that when a gradual converging section is used as input, this condition is automatically satisfied (see (7-48)).

To conclude this analysis, we must establish how the difference in propagation constants $\Delta\beta$ depends on the spacing W.

If we can find a relationship for $\Delta\beta(W)$, then, in a given DC design for which we specify an input or output section with variable spacing W(z), we will be able to solve the integrals in (7-53) and (7-54), and predict the power transfer characteristics. Fortunately, the functional relationship between $\Delta\beta$ and W is easily apparent from Figure 7-5. A straight line provides a very good fit to the linear-log graph of $\Delta\beta(W)$ and we get:

$$\frac{\Delta\beta(W)}{k} = A\, e^{-mW} \qquad (7\text{-}55)$$

The relevant parameters, taken from the results of section 7.3.2, are listed in Table 7-3, and the straight line fits are shown in Figure 7-6 for various cases of interest. For other exchange times, A and m can be found easily from two appropriate $\Delta\beta$ values (themselves calculated with (7-1), (7-37), and (7-38)).

7.5 SUMMARY OF FULL DIRECTIONAL COUPLER DESIGN CALCULATION

For a given input condition, generally a single channel excitation, the power ending up into each of the output branches is given by (7-53) and (7-54). Within these, the relative amplitudes of the normal modes are either equal (for the case of input from a gradual tapered section) or calculated from (7-45) and (7-46) for input from a sudden transition from one to two channels. And, finally, the total phase difference is obtained by specifying the shape of the DC, W(z), along its full length,

and replacing it in (7-55), to get $\Delta\beta(z)$ which is integrated over the whole length of the coupler. Note that in the parallel section, $W(z)$ = constant, so is $\Delta\beta$, and the phase integrals reduce to $\Delta\beta(W_0)L$, where L is the length of the parallel section and W_0 its spacing.

Two examples of "real" designs are given in the next chapter, along with experimental results.

TABLE 7-1a

SUMMARY OF RESULTS FOR DIRECTIONAL COUPLERS

TE MODES

t_1 min	W μm	σ_e μm^{-2}	σ_o μm^{-2}	β_e/k	β_o/k	$\Delta\beta/k \times 10^5$
4	12	.0138	.0089	1.515425	1.515350	7.5
	16	.0135	.0091	1.515408	1.515369	3.9
	20	.0121	.0103	1.515400	1.515378	2.2
	24	.0109	.0131	1.515396	1.515384	1.2
5	12	.0157	.0108	1.515417	1.515337	8.0
	16	.0152	.0113	1.515397	1.515358	3.9
	20	.0138	.0146	1.515388	1.515368	2.0
	24	.0128	.0154	1.515383	1.515375	0.8
6	12	.0172	.0126	1.515409	1.515327	8.2
	16	.0168	.0136	1.515386	1.515349	3.7
	20	.0154	.0173	1.515377	1.515360	1.7
	24	.0146	.0172	1.515372	1.515366	0.6
9	12	.0216	.0181	1.515386	1.515302	8.4
	16	.0217	.0221	1.515356	1.515327	2.9
	20	.0207	.0233	1.515347	1.515337	1.0
	24	.0209	.0225	1.515343	1.515341	0.2
12	12	.0251	.0230	1.515366	1.515284	8.2
	16	.0258	.0275	1.515332	1.515310	2.2
	20	.0253	.0274	1.515324	1.515319	0.5
	24	.0259	.0267	1.515322	1.515321	0.1
17	12	.0307	.0313	1.515334	1.515262	7.2
	16	.0324	.0343	1.515300	1.515286	1.4
	20	.0326	.0337	1.515294	1.515292	0.2
	24	.0331	.0333	1.515293	1.515293	0.0

TABLE 7-1b

SUMMARY OF RESULTS FOR DIRECTIONAL COUPLERS

TM MODES

t_1 min	W μm	σ_e μm^{-2}	σ_o μm^{-2}	β_e/k	β_o/k	$\Delta\beta/k \times 10^5$
4	12	.0148	.0099	1.516381	1.516304	7.7
	16	.0144	.0102	1.516363	1.516323	4.0
	20	.0130	.0127	1.516354	1.516333	2.1
	24	.0118	.0143	1.516350	1.516339	1.1
5	12	.0169	.0122	1.516371	1.516290	8.1
	16	.0164	.0130	1.516349	1.516311	3.8
	20	.0150	.0168	1.516340	1.516322	1.8
	24	.0142	.0168	1.516335	1.516328	0.7
6	12	.0189	.0146	1.516361	1.516277	8.4
	16	.0186	.0167	1.516334	1.516299	3.5
	20	.0174	.0198	1.516325	1.516311	1.4
	24	.0169	.0192	1.516320	1.516316	0.4
9	12	.0234	.0206	1.516336	1.516252	8.4
	16	.0238	.0251	1.516304	1.516278	2.6
	20	.0231	.0255	1.516295	1.516288	0.7
	24	.0236	.0247	1.516292	1.516290	0.2
12	12	.0270	.0259	1.516314	1.516235	7.9
	16	.0282	.0301	1.516279	1.516260	1.9
	20	.0280	.0297	1.516272	1.516268	0.4
	24	.0286	.0291	1.516270	1.516270	0.0
17	12	.0337	.0354	1.516276	1.516210	6.6
	16	.0359	.0375	1.516243	1.516233	1.0
	20	.0362	.0370	1.516239	1.516237	0.2
	24	.0365	.0367	1.516238	1.516238	0.0

TABLE 7-2

AMPLITUDE RATIOS FOR SUDDEN TRANSITIONS BETWEEN A SINGLE WAVEGUIDE AND A PARALLEL DIRECTIONAL COUPLER

t_1	W	TE A_e	TE A_o	TE R	TM A_e	TM A_o	TM R
4	12	.85	.53	.62	.84	.54	.65
	16	.78	.62	.79	.78	.63	.81
	20	.74	.67	.90	.74	.68	.92
	24	.72	.69	.96	.72	.70	.97
5	12	.83	.56	.67	.82	.54	.66
	16	.77	.64	.83	.76	.65	.86
	20	.73	.68	.93	.72	.69	.96
	24	.71	.70	.99	.71	.70	.99
6	12	.81	.58	.72	.80	.60	.75
	16	.75	.66	.88	.74	.67	.91
	20	.72	.69	.96	.72	.70	.97
	24	.71	.70	.99	.71	.71	1.0
9	12	.78	.63	.81	.77	.64	.83
	16	.73	.69	.95	.72	.69	.96
	20	.71	.70	.99	.71	.70	.99
	24	.71	.71	1.0	.71	.71	1.0
12	12	.76	.65	.86	.75	.66	.88
	16	.72	.70	.97	.72	.70	.97
	20	.71	.71	1.0	.71	.71	1.0
	24	.71	.71	1.0	.71	.71	1.0
17	12	.74	.67	.91	.73	.68	.93
	16	.71	.70	.99	.71	.70	.99
	20	.71	.71	1.0	.71	.71	1.0
	24	.71	.71	1.0	.71	.71	1.0

The ratio R is defined as A_o / A_e

TABLE 7-3

FITTING PARAMETERS FOR $\frac{\Delta\beta}{k}$ VS W

	TE		TM	
t_1 (min)	$A\times10^4$	m (μm^{-1})	$A\times10^4$	m (μm^{-1})
4	3.85	.14	5.26	.16
5	4.92	.16	7.81	.18
6	2.78	.18	13.9	.23
8	36.1	.30	40.8	.33
12	99.6	.38	95.8	.42
17	346.	.49	190.	.47

CHAPTER 8. EXPERIMENTAL VERIFICATION OF THE DIRECTIONAL COUPLER PROPERTIES

8.1 INTRODUCTION

In this chapter, two directional coupler designs are presented, in order to verify some of the claims made in previous chapters. The main points to consider are: the accuracy of the model for N(y) and of the method of solution to the waveguiding problem in predicting device performance; and the adjustability of the device properties provided by the two-step ion-exchange fabrication process.

It is the basic phenomenon of directional coupling in these novel structures that will be examined, not the functionality of the device from a system point of view. Therefore, parameters of technological importance, such as insertion loss or throughput loss, will not be considered here. This will be needed at a further stage in the development of practical devices, after optimization of some of the waveguiding properties (as will be discussed in the conclusion). Accordingly, in the choice of these optical circuits, many design decisions will be made while keeping in mind the fact that the main concern is only to test quantitatively the two points mentioned in the first paragraph. In particular, the circuits should be easy to fabricate and measure, with good reproducibility, in our laboratory facilities.

8.2 ACTUAL DESIGNS

As was done for all channel waveguides studied until now, the width D_x is fixed at 10 μm. This is fairly large for a single mode guide at a wavelength of 0.6328 μm, and it facilitates input/output coupling to the guides. It also relaxes the constraints in the fabrication of the aluminium masks by photolithography. Usually, single-mode waveguides made by conventional methods in glass or other materials have much smaller dimensions (2-3 μm). Compatibility with single-mode fibers is also improved since they have typical radii of around 5 μm.

The total exchange time $(t_1 + t_0)$ is kept at 1 hour, but t_1 is allowed to vary.

For the spacing of the channels in the parallel section, three things have to be considered: 1) If total power transfer is desired (at least as a possibility) at a value of t_1 where the guides are single-moded, then the coupling must not be too strong (W not too small); 2) the linewidths realizable with our photolithographic set-up are no smaller than about 2-3 μm; 3) the longest dimension that can be accommodated by the equipment is about 50 mm. Therefore, W cannot be too large either if we want the possibility of total transfer occurring at least once in that length.

A good compromise turns out to be W = 16 μm. At that spacing, total transfer is possible for t_1 = 6' and 9' in a

length of the order of 10 mm, and the minimum pattern size appearing in the mask is 6 μm (the separation between the two open channels in the mask).

The final design decisions concern the input/output sections.

For one design, a fully symmetrical 4-port device is chosen (and referred to as the 4P device in the following) with stepped sections of linearly increasing (or decreasing) spacing (Figure 8-1).

Because the channels are very weakly guiding in the single-mode regime ($\Delta N \cong 2 \times 10^{-4}$), such discrete bends may contribute to in-plane scattering. To investigate that problem, another device is included on the same mask, and will therefore be fabricated simultaneously on the same substrate. That device is made up of one completely straight waveguide adjacent to another guide, parallel to it for a length L, and then branching out as in the first case (Figure 8-1). This circuit is a three-port device (3P), a configuration which is sufficient for many applications of directional couplers (see [Cochrane 1986], for instance). Scattering is more or less eliminated from the input branch, which is a big improvement over the 4P device because, in the latter case, the scattered power generated in the input section could be recoupled into the guides at the bends of the output branches. On the other hand,

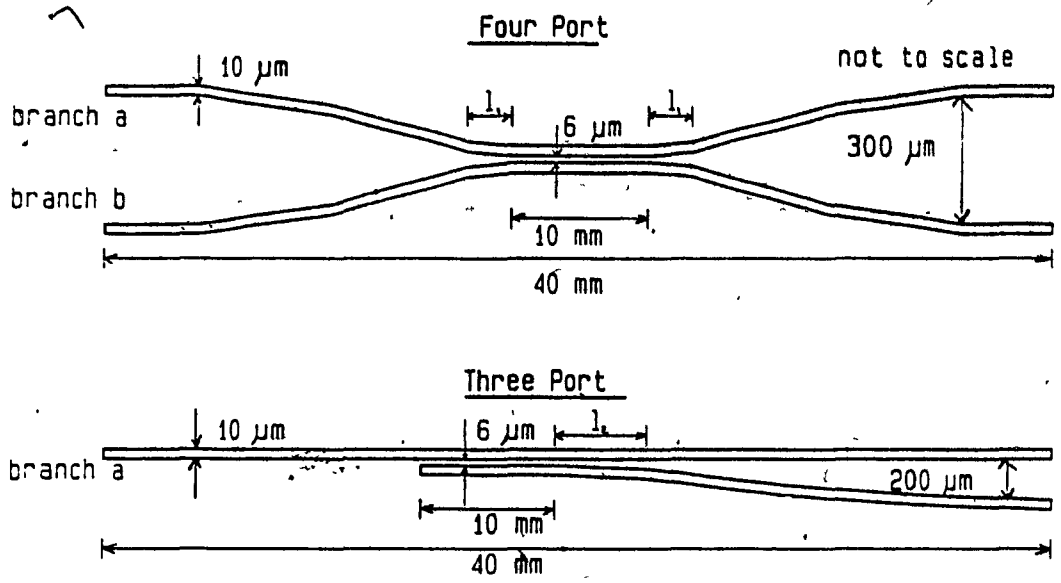

Figure 8-1. Design of the two fabricated directional couplers.

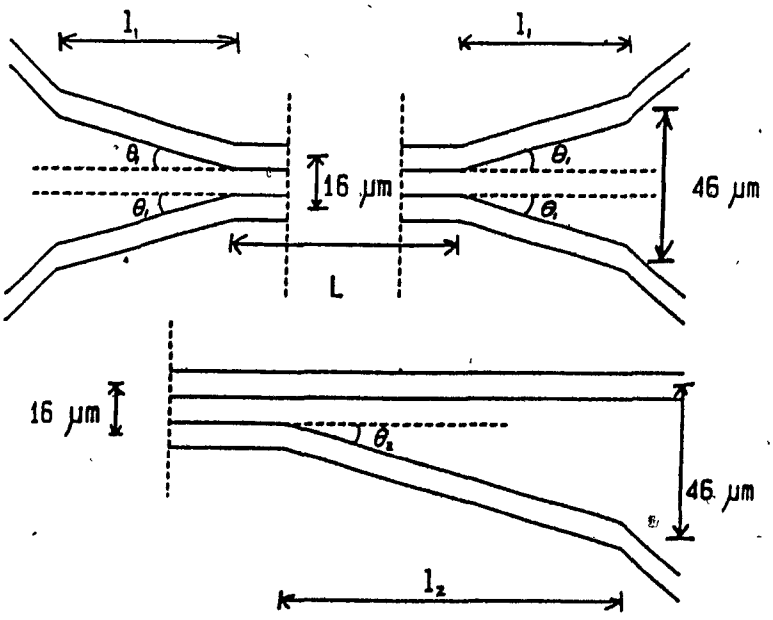

Figure 8-2. Design details for the transition sections.

scattering generated near the end of the directional couplers stands less chance of being recoupled into the guides to spoil the comparison between the power transfer measurements and predicted values (based on negligible scattering).

8.3 CALCULATED TRANSFER CHARACTERISTICS

For both devices, the parallel section length L is fixed at 10 mm. Also, for both cases, the first branching section is used to separate the two waveguides beyond the point where there is no more coupling. A spacing of 46 μm is more than sufficient for that purpose. Finally, individual bends in the waveguides are kept smaller than 0.5° to minimize scattering losses.

The details of the initial transition sections are shown in Figure 8-2. For the 4P device, the spacing varies from W = 16 to 46 μm in a distance l_1 so that $\theta_1 < 0.5°$. We have,

$$\tan\theta_1 = \frac{(46 - 16)}{2l_1} \Rightarrow l_1^{min} = \frac{15}{\tan\theta_1^{max}} \ \mu m \qquad (8-1)$$

or $l_1 > 1.72$ mm on both sides of the parallel section. Let us take $l_1 = 1.75$ mm for a "round" number (this yields an actual branching angle of 0.49°).

For the 3P device, only one branch is bent. Therefore, to reach the same final separation, we need:

$$\tan\theta_2 = \frac{(46 - 16)}{l_2} \Rightarrow l_2^{min} = \frac{30}{\tan\theta_2^{max}} \ \mu m \qquad (8-2)$$

or $l_2^{min} = 2\, l_1^{min}$. We take:

$$l_2 = 2l_1 = 3.5 \text{ mm} \qquad (8-3)$$

The complete design of both devices is shown in Figure 8-1. All the individual bends are smaller than 0.5° and the channel separations at input and output are at least 200 μm for ease of launching power in the individual channels and measuring their outputs.

For the 4P device, we need to consider the coupling for three regions: the parallel section, and the first divergent sections on each side of it. In that case, A_0/A_e = 1 and the only parameter needed is the total phase change.

For the parallel section, we have:

$$\Delta\phi_1 = \Delta\beta(W-16)*L \tag{8-4}$$

and, in the input section, we have:

$$W(z) = 46 - 2z\tan(\theta_1)\ \mu m \tag{8-5}$$

$$\Delta\phi_0 = \int_0^{l_1} kA\ e^{-mW(z)}\ dz \tag{8-6}$$

$$= kAe^{-46m}\int_0^{l_1} e^{2mz\tan\theta_1}\ dz = \frac{kA\ e^{-16m}}{2m\tan\theta_1} = \frac{\Delta\beta(16)}{2m\tan\theta_1} \tag{8-7}$$

Similarly, at output:

$$W(z) = 16 + 2z\tan\theta_1\ \mu m \tag{8-8}$$

$$\Delta\phi_2 = \int_0^{l_1} kA\ e^{-mW(z)}\ dz \tag{8-9}$$

$$= kAe^{-16m}\int_0^{l_1} e^{-2mz\tan\theta_1}\ dz = \frac{\Delta\beta(16)}{2m\tan\theta_1} \tag{8-10}$$

and the total phase change is:

$$\Delta\phi = \Delta\beta(16)\left(L + \frac{1}{m\tan\theta_1}\right) \tag{8-11}$$

When the design values (L_1 10 mm and $\tan\theta_1 = 30\ \mu m/2l_1$) are replaced in (8-11), we get:

$$\Delta\phi = \Delta\beta(16)\left(10 + \frac{2(1.75)}{30m}\right) \qquad (8\text{-}12)$$

with m expressed in μm^{-1}, and $\Delta\beta$ taken from Table 7-2 and expressed in rad/mm.

For the 3P device, we have again in the parallel section:

$$\Delta\phi_1 = \Delta\beta(16)L \qquad (8\text{-}13)$$

and in the output section:

$$W(z) = 16 + z\tan\theta_2 \qquad (8\text{-}15)$$

$$\Delta\phi_2 = \int_0^{l_2} kA\ e^{-mW(z)}\,dz \qquad (8\text{-}16)$$

$$= \Delta\beta(16)\int_0^{l_2} e^{-mz\tan\theta_2}\,dz \qquad (8\text{-}17)$$

$$= \frac{\Delta\beta(16)}{m\tan\theta_2} = \frac{\Delta\beta(16)l_2}{30m} = \frac{2\Delta\beta(16)l_1}{30m} \qquad (8\text{-}18)$$

so that the total phase change is:

$$\Delta\phi = \Delta\beta(16)\left(10 + \frac{2(1.75)}{30m}\right) \qquad (8\text{-}19)$$

i.e. exactly the same as for the 4P device. However, in this case, $A_o/A_e \neq 1$ and depends on t_1 (for W = 16 μm). Again, m must be in μm^{-1} and $\Delta\beta$ in rad/mm.

Using equations (8-19) and (8-12) in (7-53) and (7-54) allows the calculation of the power transfer characteristics of the directional couplers. For the 3P device, the amplitude ratio must also be calculated from (7-45) and (7-46).

If we define the power transfer by:

$$\eta = \frac{P_b}{P_a + P_b} \qquad (8\text{-}19)$$

for input from branch "a", and the amplitude ratio by:

$$R = \frac{A_o}{A_s} \qquad (8\text{-}20)$$

we get the following formula for η:

$$\eta = \frac{1}{2} - \left(\frac{R}{1 + R^2}\right)\cos\Delta\phi \qquad (8\text{-}21)$$

As an example, η is plotted on Figure 8-3 against the length of the center section L, for two values of t_1 in the single-mode regime.

We see that for a given mask (i.e. fixed L), a wide range of transfer values can be obtained by varying t_1. This interesting property allows for the fine tuning of the performance obtained with a mask, without having to replace it. Minor fabrication or design inaccuracies can therefore be compensated easily with this two-step method.

In Figure 8-4, another type of relation is plotted, namely the transfer η against t_1 for the two designs that were specified in this chapter. The two curves overlap over the whole range shown. Actually, the difference becomes of the order of 1% at t_1 = .5', at which value the ratio of amplitudes R is 0.86 for TM and 0.83 for TE.

The portion of the curve that extends past t_1 = 10 minutes has a restricted meaning. All the calculations were carried out assuming single-mode channels, which is no longer the case in that time range. Therefore, the transfer is dependant on the amount of power carried by each of the possible modes, and other values than those shown are possible by changing the input conditions.

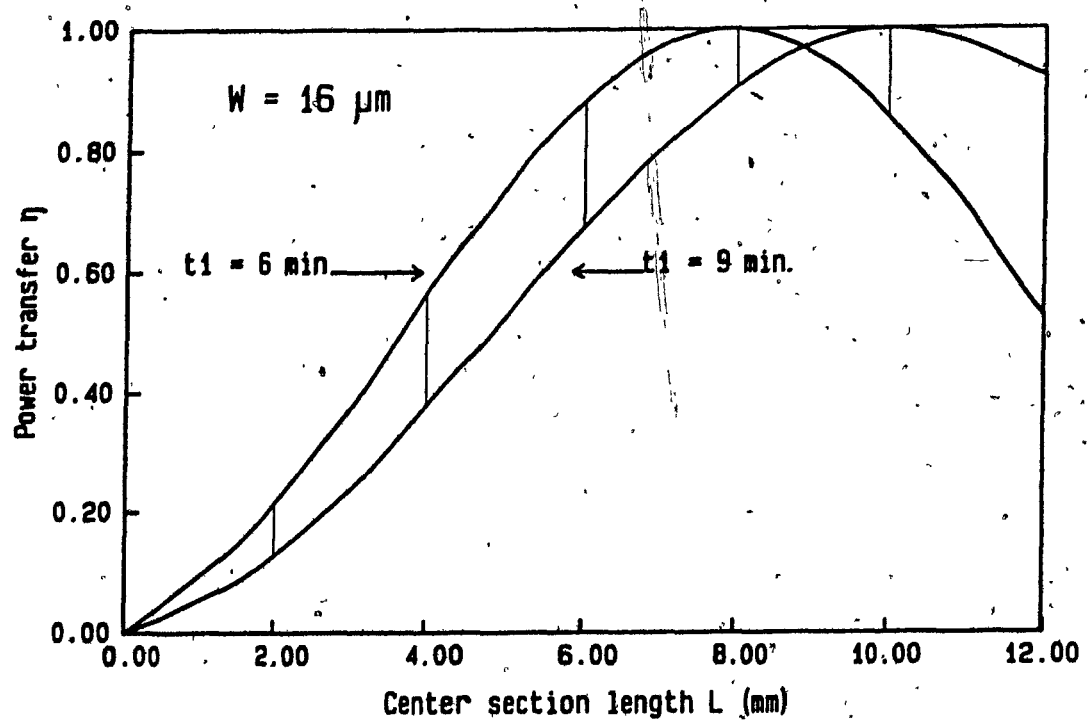

Figure 8-3. Theoretical power transfer from the input branch to the output branch as a function of the center (parallel) section length, for two values of t_1 (valid for both designs). TE.

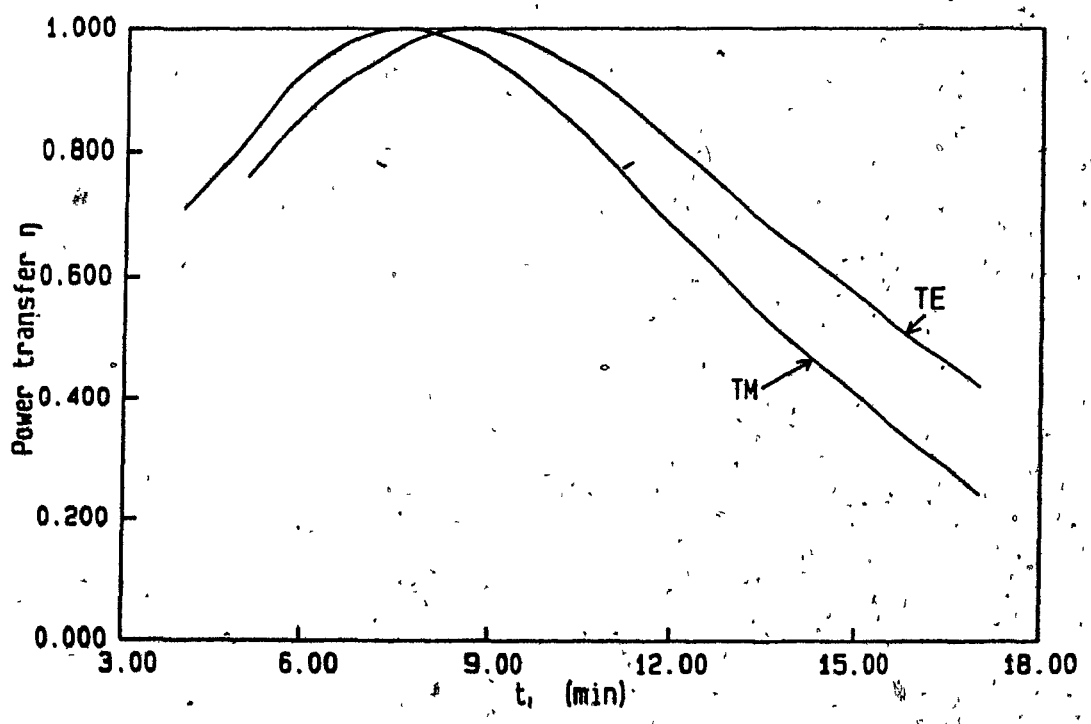

Figure 8-4. Theoretical power transfer versus t_1 for the chosen designs (valid for both 3P and 4P).

8.4 EXPERIMENTAL RESULTS

The directional couplers were fabricated and measured with the methods outlined in Chapter 3. On each substrate and for each polarization, three sets of power measurements can be made (each set consisting in a scan of the power across the two output branches of a device): one set for the 3P device, and two sets for the 4P device because of the two possible input branches. For each polarization, the three transfer (η) measurements are expected to yield identical results (as long as $t_1 \geq 5$ ').

We can make allowances for scattering in the following fashion. For the 4P device, both input branches have the same shape and should have the same fraction of scattered power H_1. Therefore, for an input power P, the power reaching the coupling section is $(1-H_1)P = P_a(0)$. At the end of the coupling section, a fraction η has been transferred to branch "b", $P_b(end) = \eta P_a(0) = \eta(1-H_1)P$, and $(1-\eta)(1-H_1)P$ remains in branch "a". At the output, the power in the branches become (accounting for a fraction H_0 being scattered):

$$P_b(out) = (1-H_0)\eta(1-H_1)P \qquad P_a(out) = (1-H_0)(1-\eta)(1-H_1)P \qquad (8-22)$$

Then η is obtained directly from a measurement of the following ratio:

$$\frac{P_b}{P_a+P_b} = \frac{\eta}{(1-\eta)+\eta} = \eta \qquad (8-23)$$

The measured value is independent of H_1 and H_0.

For the 3P device, there is no loss in the input branch, and at the end of the coupling section we have: $P_a(end) = (1-\eta)P$ and $P_b(end) = \eta P$. At the output, P_a has not changed but P_b has reduced to $P_b(out) = (1-H_o)\eta P$ because of the bends. Therefore:

$$\frac{P_b}{P_a + P_b} = \frac{(1-H_o)\eta P}{(1-H_o)\eta P + (1-\eta)P} = \frac{(1-H_o)\eta}{(1-\eta H_o)} < \eta \qquad (8\text{-}24)$$

and the measured transfer efficiency should be somewhat lower than the calculated ones, especially at smaller values of t_1 (larger H_o).

The scattering that occurs at the various discontinuities of the devices should be restricted mainly to the plane of the waveguides. This is because the confinement is much weaker in that direction ($\Delta N \cong 2\text{-}10 \times 10^{-4}$) than in the depth direction ($\Delta n \cong 1\%$). Therefore, most of the scattering will be observable on the output profile traces as peaks of power outside of the channel regions, e.g. Figure 8-5.

Significant results for η are shown in Tables 8-1 and 8-2 and in Figures 8-5 and 8-6.

8.5 DISCUSSION OF THE RESULTS

Several points must be addressed regarding these results. First of all, the transfer value for the 4P device is not symmetrical and does not correlate well with predicted values. As we have just shown, this cannot be explained by scattering

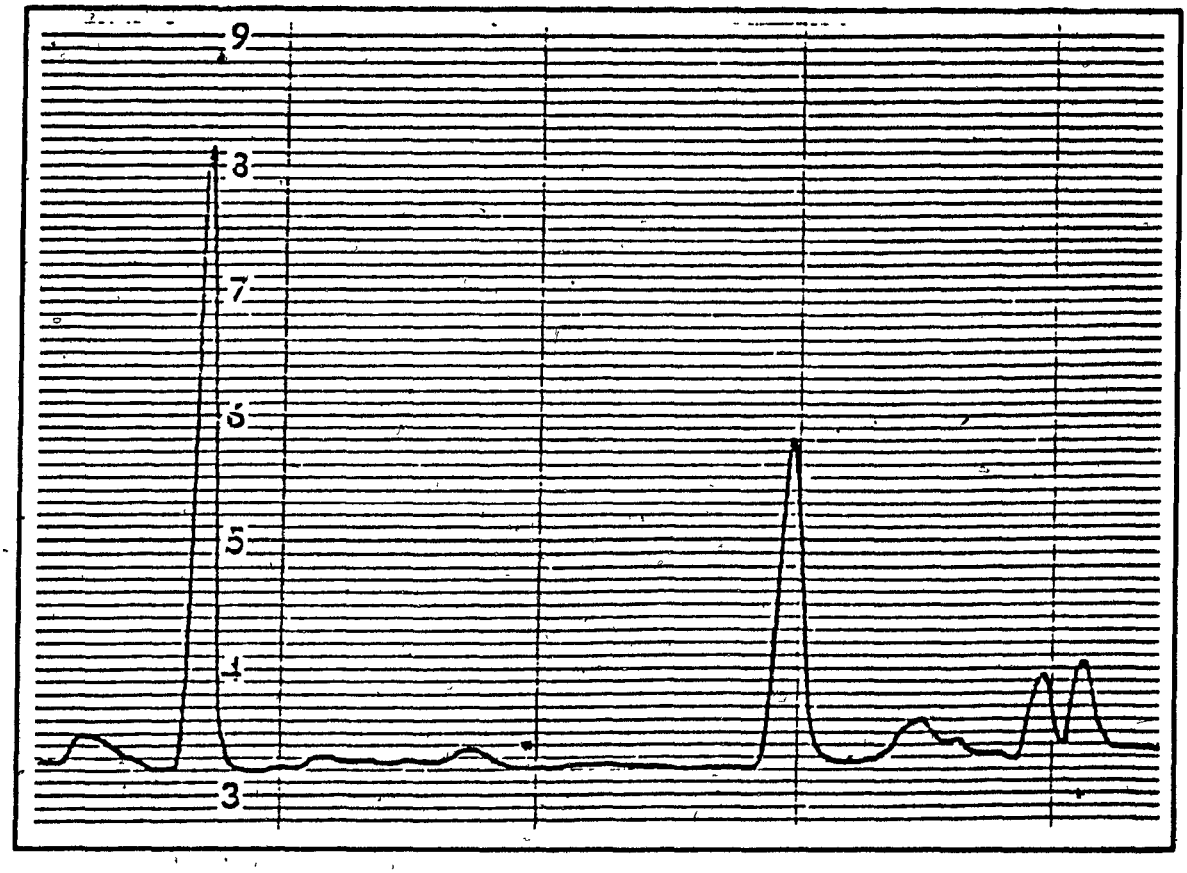

t1 = 7.5 min. η = 67 %

Figure 8-5. Typical lateral power distribution for a 4P device, TM polarization.

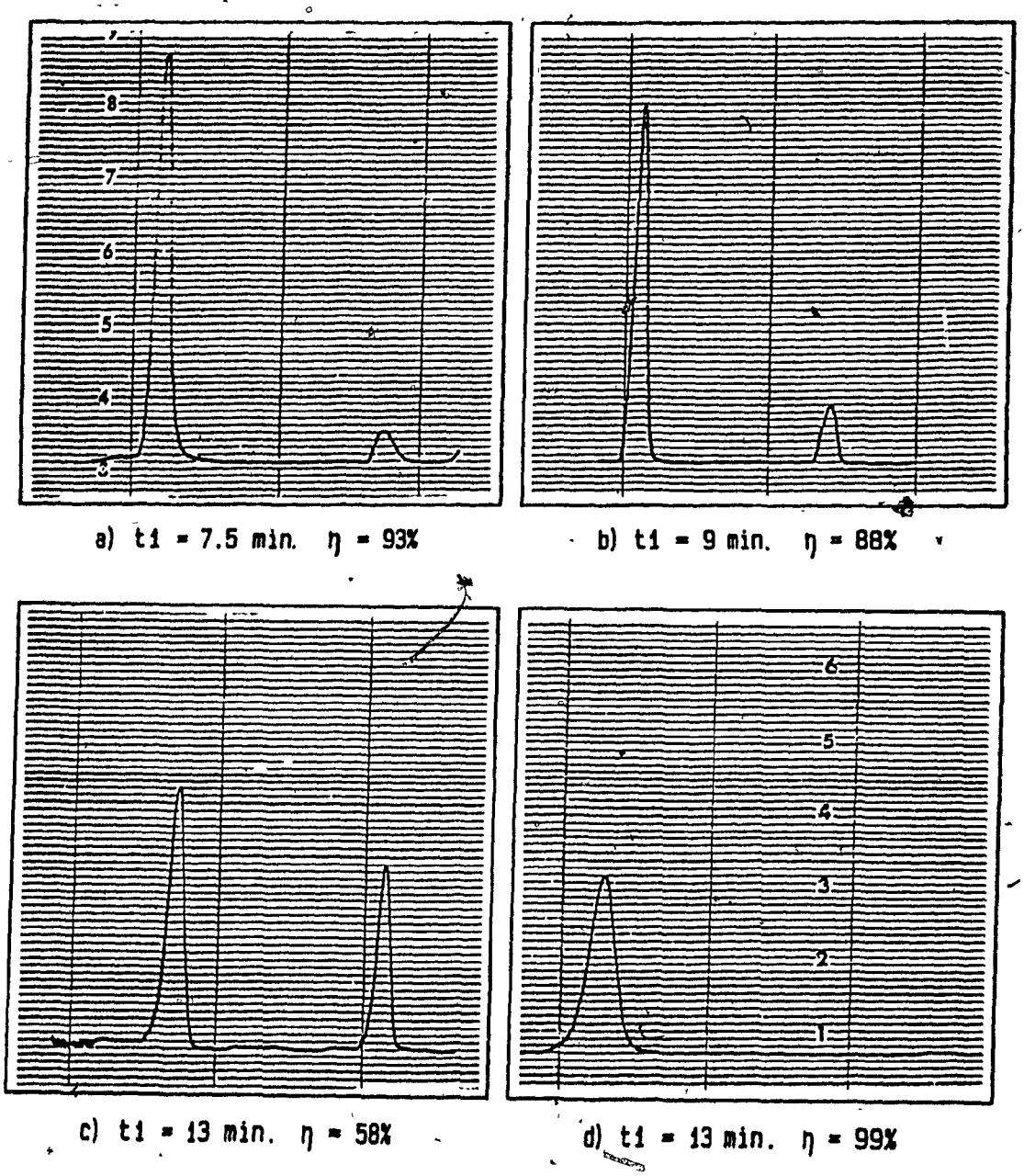

Figure 8-6. Typical lateral power distributions for 3P devices, a),b),c) TM polarization, d) TE polarization.

alone, although 4P devices did show quite a bit of it at the output (Figure 8-5). However, some of the waves scattered in the input section stand a good chance of being recoupled (or "re-scattered") at discontinuities of the output branches (Figure 8-7). The slightest difference in input beam alignment or in the geometry of the branches of the DC would result in different amounts of power ending up in the output branches. This effect is believed to be the main cause of the problem. Again, the fact that a planar guide confines the scattered light in the depth direction facilitates this recoupling effect. Other channel waveguides do not have this problem because scattered light leaks into the substrate.

Secondly, the transfer efficiency η for multimode devices ($t_1 > 10'$) can be adjusted by changing the angle of entry and the spot size of the input beam. This has the effect of varying the amount of power carried by each mode. Higher-order modes are less confined and couple more strongly to the adjacent channel, giving higher η values than the predictions of the calculations. This is shown by the results of measurements on the device fabricated with $t_1 = 13'$.

As can be seen from Figures 8-5 and 8-6, the 3P devices showed significantly less scattering, and especially so for the TM polarization. These results are more reliable for a comparison with theory (Figure 8-8). We see that the agreement is excellent for the TM modes (decreasing slightly at smaller

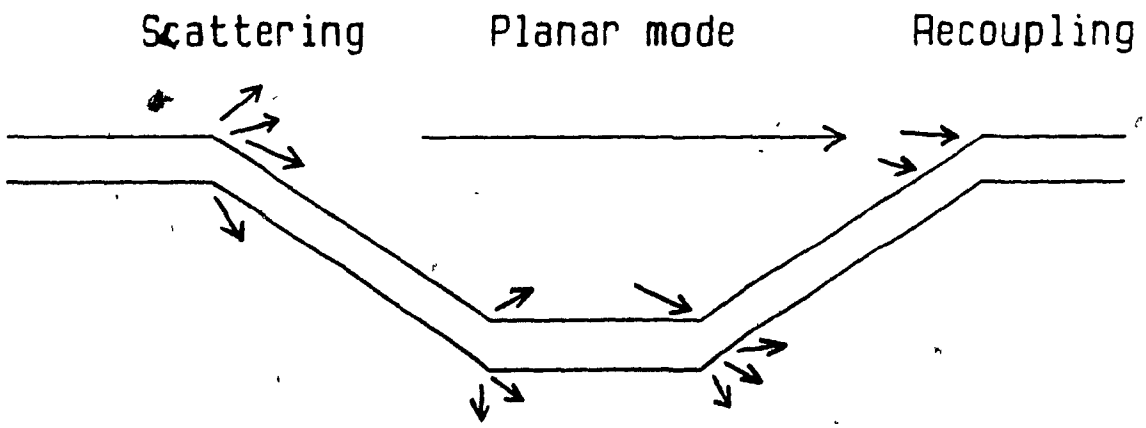

Figure 8-7. Diagram showing scattering points, planar modes and possible recoupling points at downstream bends in the channels.

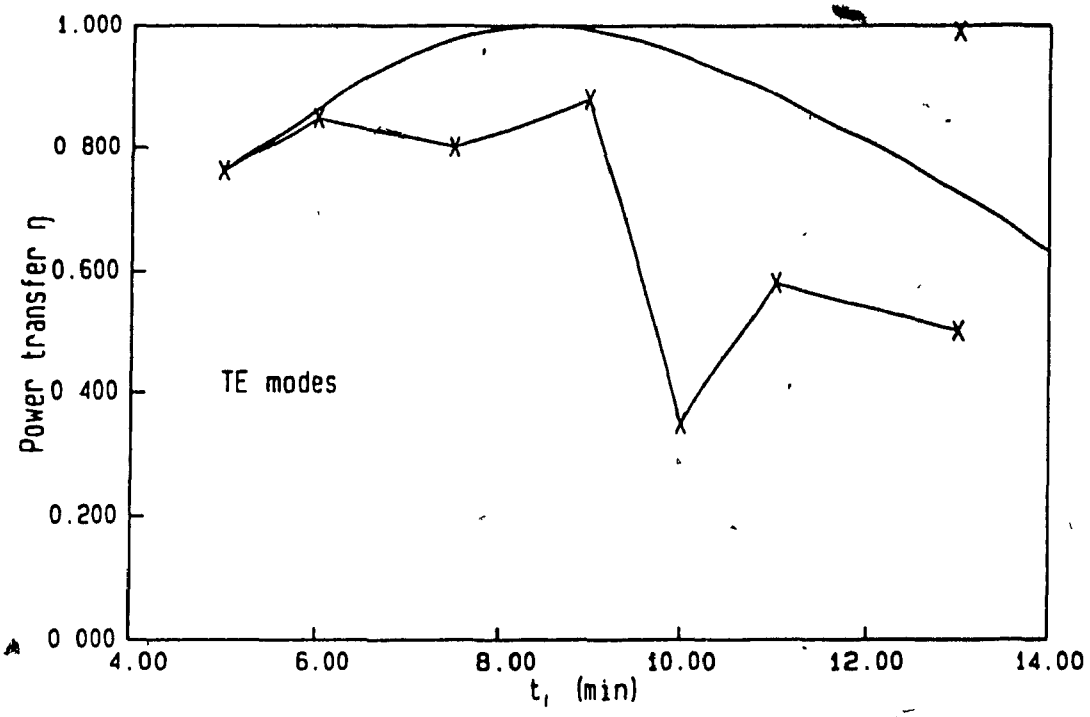

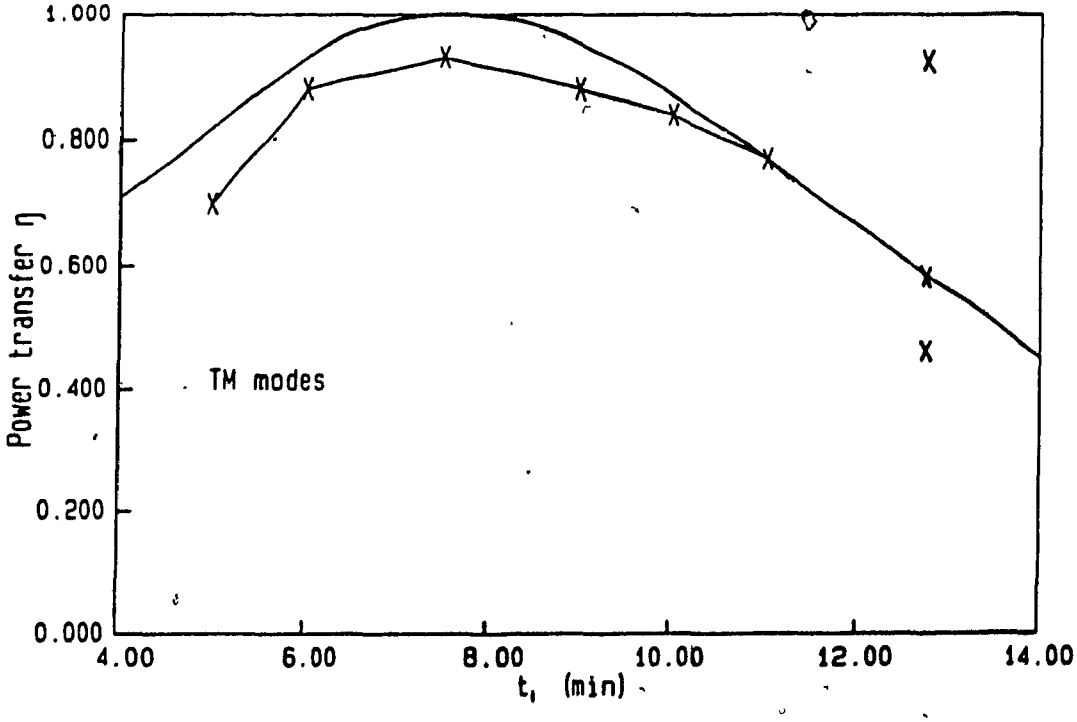

Figure 8-8. Experimental power transfer values (x's), and theoretical prediction (continuous line), versus t_1. $3P_0$ design.
a) TE polarization. b) TM polarization.

values of t_1 as predicted by (8-24), because of the loss of confinement). For TE modes on the other hand (Figure 8-8), the agreement is less accurate, probably due to the already observed occurrence of more scattering for that polarization. The cause of that phenomenon is not understood at the present time because the lateral confinement of the TM modes is only marginally better (as evidenced by the larger ΔN values). It must have arisen from some increased sensitivity to scattering for that polarization.

To conclude on these results, we can say that when the proper experimental conditions are met, the agreement between predicted and measured values of power transfer is excellent. In short, these conditions are those for which the confinement is maximal (i.e. t_1 as large as possible), while keeping the individual waveguides in the single-mode regime (which places an upper limit on t_1) to get a unique transfer coefficient η. Also, the adjustability of device performance allowed by the two-step method with varying relative times of exchange has been demonstrated, as well as the feasibility of single-mode optical circuits with channels of wide lateral dimensions.

On the other hand, these advantages come with a structure which is very weakly guiding and inherently susceptible to crosstalk (unwanted and uncontrolled coupling) due to lateral scattering. This introduces constraints on the geometry of the

devices that can be expected to perform according to the theoretical predictions.

TABLE 8-1

EXPERIMENTAL RESULTS FOR η, 4-PORT DEVICES

t_1 input	TE a	TE b	TE TH	TM a	TM b	TM TH
5	.45	.43	.80	.41	.43	.82
6	.59	.59	.87	.65	.82	.93
7.5	.56	.44	.97	.67	.61	1.0
9	.43	.27	1.0	.36	.19	.92
10	.83	.66	.98	.71	.80	.84
11	.45	.48	.92	.25	.39	.76

"TH" stands for theoretical calculation.
"input a" means that light is launched in branch "a" and power transfer to branch "b" is measured (opposite for "input b").

TABLE 8-2

EXPERIMENTAL RESULTS FOR η, 3-PORT DEVICES

t_1	TE	TH	TM	TH
5	.70	.80	.70	.82
6	.85	.87	.88	.93
7.5	.80	.97	.83	1.0
9	.88	1.0	.88	.92
10	.85	.98	.84	.84
11	.85	.92	.77	.76
13	.88	.78	.92	.58
15	.50	*	.58	*
17	.86	.43	.90	.23

"TH" stands for theoretical calculation. For t_1 = 13' and 17', the measured efficiencies are the maximum ones obtained.
* Other input conditions change the transfer result (see text).

CHAPTER 9. CONCLUSION

The work presented in this thesis can be conveniently split up into two main aspects.

It is possible to summarize the net accomplishment of chapters 2 to 5 as the gain of a better understanding of the process of potassium-sodium ion-exchange in glass for the purposes of making optical waveguides. The methods used to achieve this are fairly general and can be used in the study of other types of ion-exchange. In fact, the characterization procedure of chapter 4, apart from yielding essential design parameters, has been repeated by another group to study K^+-Na^+ in other types of glass [Gortych 1986a, 1986b].

Also, while we were not the first to solve numerically the non-linear diffusion equations of ion-exchange [Helfferich 1958], [Wilkinson 1978], nor the last [Houde-Walter 1985], our main contribution in this area was the use of an analytical approximation for the resulting concentration profile and its correlation with the single independent parameter of these equations (α). This provides a clarification of the problem of deciding which approximate profile provides the best fit for different types of exchange. Furthermore, the approach consisting of presenting analytical approximations to numerical results is believed to be more useful to other workers, especially experimentalists, in the field because they do not

have to reproduce the computer programs and entire calculations to adapt the results to their specific problems.

Finally, the stress analysis of chapter 5 helped to solve two important problems, i.e. first, the inconsistency between the Huggins-Fantone model and the measurements of the maximum index change Δn_s and second, the influence of the exchange temperature and glass composition on the magnitude of the index change.

As in all scientific endeavours, it is from a better understanding of some basic phenomena that advances and breakthroughs become possible. In the case of K^+-ion exchange in glass, the process had been used quite frequently in the past 15 years or so for device work; mainly because of its simplicity and potential for low propagation losses and good index match to single-mode optical fibers, but generally with very approximate knowledge of waveguide parameters (diffusion depth and index change).

The results presented here provide a much firmer basis for the development of waveguide features that will bring this technology toward more practical and commercial applications. It was already noted that the great potential of these waveguides lies probably in passive waveguide functions where low insertion and throughput losses are essential. Measurements have shown that propagation losses as low as 0.2 dB/cm are possible in

planar and multimode channel waveguides [Findakly 1985, Findakly 1980]*. Also, it can be seen from Figure 8-6 that very little additional losses are caused by bends in the guides when they are well designed. Therefore, the main problem left to be solved is that of the insertion losses at the fiber-waveguide junction. For multimode waveguides, great progress has occurred in this area recently, with propagation losses lower than .05 dB/cm and coupling losses of .25 dB/facet [Cline 1986]. For single-mode waveguides, the coupling is much more difficult in view of the small sizes involved. A way to avoid that difficulty is to increase the size of the single-mode channel waveguides and to "symmetrize" their index profile in the depth direction, to improve the refractive-index match with fibers [Chartier 1980, Findakly 1980, Parriaux 1982, Voges 1983, Tangonan 1983, Ctyroky 1984a]. As an example of how the results of this work can be used in this context, studies of refractive index modifications for the purposes of lowering throughput losses and improving mode matching to optical fibers , can be undertaken with the methods of Chapter 2 and 5. In particular, it is possible to run the 2-D ion-exchange numerical model with different boundary conditions to get quite interesting predicted profile shapes (Figures 9-1 to 9-3).

The second part of the thesis deals with the realization of single-mode passive optical circuits in glass. The basic element of these circuits is a channel waveguide fabricated by a two-

---

*Note: it was not our goal in this work to determine the losses of these particular waveguides, but rather to prove certain concepts and find methods of analysis. Loss measurements are necessary at a later stage in device development.

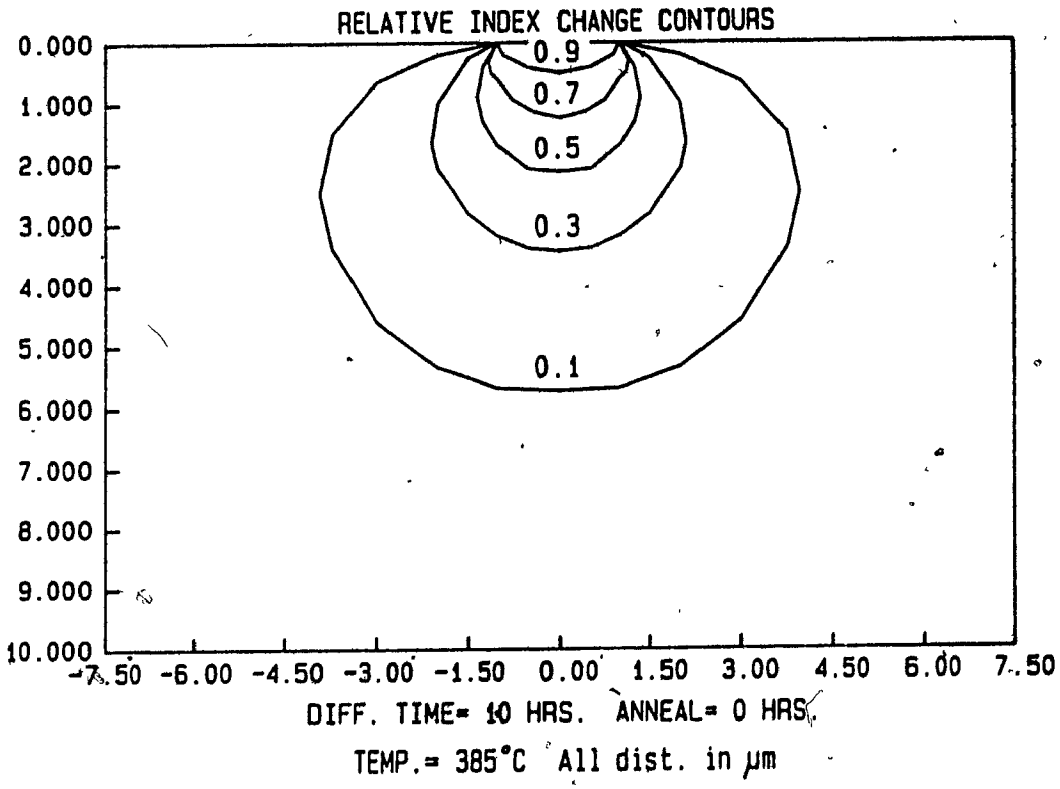

Figure 9-1. Refractive index contours for a narrow aperture and long exchange time.

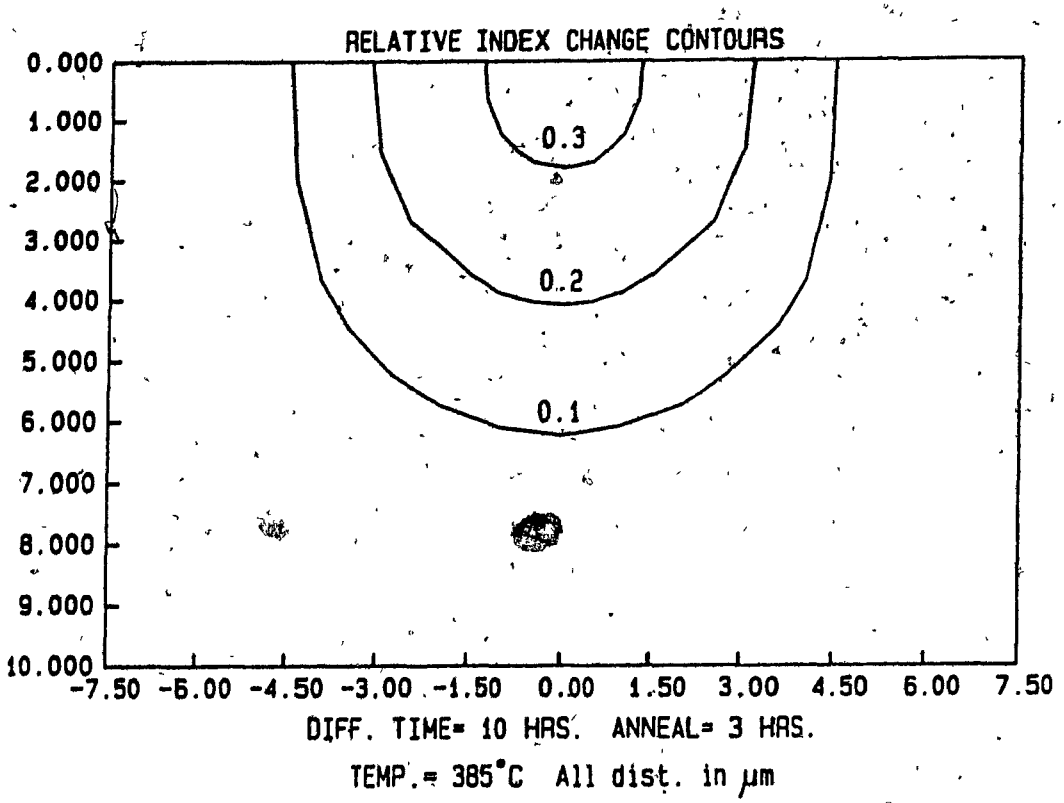

Figure 9-2. Result of annealing the profile of Figure 9-1 for 3 hours outside of the melt (at the same temperature).

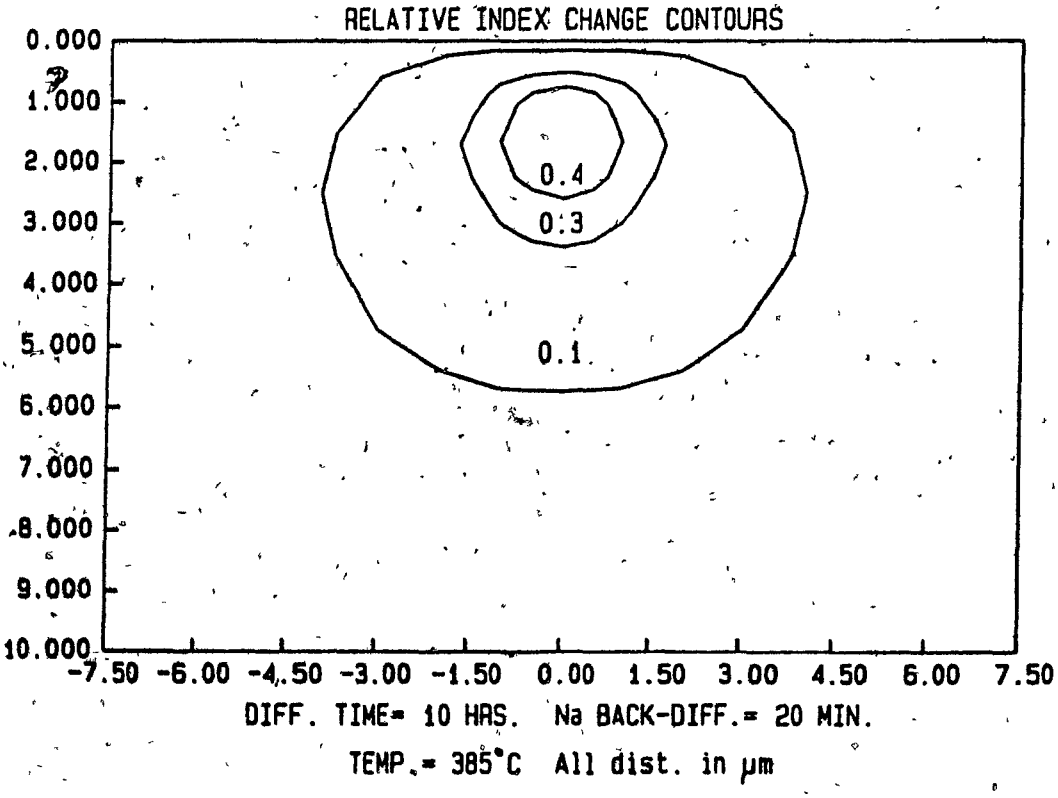

Figure 9-3. Result of performing a second ion-exchange in <u>sodium</u> nitrate on the profile of Figure 9-1 to bury it below the surface of the substrate.

step ion-exchange method, for which we have presented the first detailed analysis. The main line of thought, here, was that of having a self-contained design procedure, as general as possible, and simple to carry out without losing accuracy.

This was achieved with the help of the "effective-index method", in itself a standard procedure by now, but with the more novel approach of fitting local values of effective index (calculated on the exact refractive index profile with an accurate numerical method) with a simple analytical function. The parameters of this analytical model have been shown to be derivable from planar waveguide data exclusively. Therefore, with the fabrication and measurement of a minimum of two planar waveguides, from which Δn_s and D_e can be calculated at a given temperature, a full model for a channel waveguide made by two-step ion-exchange can be written down directly.

Furthermore, we have shown that Hermite-Gaussian functions provide excellent approximations to the lateral dependence of the two lowest modes of these channels, allowing the use of a particularly simple variational method to the solution of the dispersion equation.

Finally, a design example for a simple circuit was presented, along with experimental verification of the results. These showed that the two-step channel guides provide good adjustability of performance because their "cladding" index can

be controlled by changing the relative times of exchange of the two steps.

This is a lot simpler than the alternative approaches available for lateral mode control, such as using a planar cladding [Haruna 1985] (which requires an additional step of high vacuum processing), or a raised strip on top of a planar guide [Hocker 1976] (which is difficult to fabricate with precision and yields a non-planar structure).

It is worth noting that the methods of Chapter 6 are adaptable to other types of waveguide fabrication (titanium in-diffusion or proton exchange in lithium niobate for instance [Warren 1983]).

Again for this part of the thesis, we can say that the groundwork has been established for further developments. In fact, the analytical model for the lateral effective-index profile can be used for other geometries than straight channels. This is because this model is essentially a fit of the transition between two planar regions of different depths (Figure 6-4). Therefore, it can be used to model structures of arbitrary geometry in the plane of the substrate, such as: prisms, lenses, tapers, etc... [Hinkov 1982, Tamir 1979, p.133], which are needed for signal processing as wavelength-division (de-)multiplexers, Fourier transform elements, or mode transformers respectively.

Finally, on a more speculative note, some of the particular properties of the two-step ion-exchanged channels in glass that were highlighted in this work could be exploited in sensor devices. In particular, the directional couplers of Chapter 8 were seen to be very weakly guiding with a ΔN as small as $2\text{-}5 \times 10^{-4}$.

Therefore, an externally induced index perturbation of the same magnitude (e.g. from a temperature change, or from an index change in the cladding of the guide) would have a strong influence on measurable optical properties. This is also true of externally applied stresses since the index change of these guides is almost entirely due to stress already.

APPENDIX A

In this section, equations (2-30) and (2-31) are derived explicitly, following (and expanding on) [Crank 1956]. Note that most of the symbols (β, ϕ, etc...) used here do not have the same definitions as in the core of the thesis; they will be defined as we go along and as needed.

First, let's define:

$$s = \frac{\ln(1 - \hat{\alpha}c)}{\ln(1 - \hat{\alpha})} \qquad (A-1)$$

which means that:

$$c = \frac{1 - e^{s\ln(1 - \hat{\alpha})}}{\hat{\alpha}} \qquad (A-2)$$

$$\frac{dc}{d\eta} = -\frac{1}{\hat{\alpha}} \ln(1 - \hat{\alpha})\, e^{s\ln(1 - \hat{\alpha})} \frac{ds}{d\eta} \qquad (A-3)$$

and (2-29) becomes:

$$-2\eta\frac{dc}{d\eta} = -\frac{1}{\hat{\alpha}} \frac{d}{d\eta}\left(e^{-s\ln(1 - \hat{\alpha})}\ln(1 - \hat{\alpha})\, e^{s\ln(1 - \hat{\alpha})}\frac{ds}{d\eta}\right) \qquad (A-4)$$

$$-2\eta\left(-\frac{\ln(1 - \hat{\alpha})}{\hat{\alpha}} e^{s\ln(1 - \hat{\alpha})}\frac{ds}{d\eta}\right) = -\frac{\ln(1 - \hat{\alpha})}{\hat{\alpha}} \frac{d^2s}{d\eta^2} \qquad (A-5)$$

$$\frac{d^2s}{d\eta^2} = -2\eta\, e^{s\ln(1 - \hat{\alpha})} \frac{ds}{d\eta} \qquad (A-6)$$

$$s(0) = 1 \quad ; \quad \left.\frac{ds}{d\eta}\right|_{\eta=\infty} = 0 \qquad (A-7)$$

(note: $c \geq 0$, $\hat{\alpha} \leq 1 \Rightarrow 1 \geq s \geq 0 \Rightarrow \left| e^{s\ln(1 - \hat{\alpha})} \right| < \infty$ in (A-3)

Transforming again:

$$\phi = -\frac{ds}{d\eta} \qquad (A-8)$$

$$\beta = -\ln(1 - \hat{\alpha}) \qquad (A-9)$$

$$q = \frac{e^{-\beta s}}{\beta} \qquad (A-10)$$

Equation (A-6) becomes:

$$\frac{d\phi}{d\eta} = -2\eta\ \beta q \phi \qquad (A-11)$$

and we also get:

$$\frac{dq}{d\eta} = -e^{-\beta s}\frac{ds}{d\eta} = \beta q \phi \qquad (A-12)$$

so that:

$$\frac{d\phi}{d\eta} = \frac{dq}{d\eta}\frac{d\phi}{dq} = \beta q \phi \frac{d\phi}{dq} \qquad (A-13)$$

which transforms (A-11) into:

$$\frac{d\phi}{dq} = -2\eta \qquad (A-14)$$

We differentiate with respect to q:

$$\frac{d^2\phi}{dq^2} = -2\frac{d\eta}{dq} = \frac{-2}{\beta\phi q} \qquad (A-15)$$

Now, posing:

$$z = \frac{\phi}{\sqrt{q}} \qquad (A-16)$$

we get:

$$\frac{d^2\phi}{dq^2} = \frac{-1}{4q\sqrt{q}}\, z + \frac{1}{\sqrt{q}}\frac{dz}{dq} + \sqrt{q}\,\frac{d^2z}{dq^2} \qquad (A-17)$$

which, replaced in (A-15), gives:

$$q\left(q\,\frac{d^2z}{dq^2} + \frac{dz}{dq}\right) = \frac{z}{4} - \frac{2}{\beta z} \qquad (A-18)$$

$$q\,\frac{d}{dq}\left(q\,\frac{dz}{dq}\right) = \frac{z}{4} - \frac{2}{\beta z} \qquad (A-19)$$

$$\frac{d}{du}\left(\frac{dz}{du}\right) = \frac{z}{4} - \frac{2}{\beta z} \qquad (A-20)$$

with $u = \ln(q)$. (A-21)

Equation (A-20) is integratable if we can find a function "g" whose derivative with respect to "u" gives the right-hand side. Such a function is:

$$g = \left(A + \frac{z^2}{4} - \frac{4}{\beta}\ln(z)\right) \tag{A-22}$$

since:

$$\frac{dg}{du} = \left(\frac{z}{2} - \frac{4}{\beta z}\right)\frac{dz}{du} \tag{A-23}$$

Replacing (A-23) in (A-20):

$$\frac{d}{du}\left(\frac{dz}{du}\right) = \frac{1}{2\left(\frac{dz}{du}\right)}\frac{dg}{du} \tag{A-24}$$

rearranging:

$$2\frac{dz}{du}\frac{d}{du}\left(\frac{dz}{du}\right) = \frac{dg}{du} \tag{A-25}$$

$$\frac{d}{du}\left(\frac{dz}{du}\right)^2 = \frac{dg}{du} \tag{A-26}$$

integrating once:

$$\left(\frac{dz}{du}\right)^2 = g + B \tag{A-27}$$

and upon regrouping constants and using (A-22):

$$\frac{dz}{du} = \pm\sqrt{a + \frac{z^2}{4} - \frac{4}{\beta}\ln(z)} \tag{A-28}$$

which is a separable ODE. We get:

$$u + b = \pm\int_0^z \frac{dz'}{\sqrt{a + \frac{z'^2}{4} - \frac{4}{\beta}\ln(z')}} \tag{A-29}$$

where a and b are the constants of integration. Replacing q and ϕ we get:

$$\ln(q) + b = \pm\int_0^{\frac{\phi}{\sqrt{q}}} \frac{dz'}{\sqrt{a + \frac{z'^2}{4} - \frac{4}{\beta}\ln(z')}} \tag{A-30}$$

and from (A-7), (A-9), (A-10) $\phi \to 0$ as $q \to 1/\beta$. Of course, $s \to 0$ because $c(\eta \to \infty) = 0$ as well as $\frac{dc}{d\eta}$; so that:

$$b = -\ln\left(\frac{1}{\beta}\right) \tag{A-31}$$

and (A-30) becomes:

$$\ln(\beta q) = \pm \int_0^{\frac{\phi}{\sqrt{q}}} \frac{dz'}{\sqrt{a + \frac{z'^2}{4} - \frac{4}{\beta}\ln(z')}} \qquad (A-32)$$

Now from (A-14), (A-7), (A-10) we get that:

$$\frac{d\phi}{dq} \to 0 \Rightarrow \eta \to 0 \Rightarrow s \to 1 \Rightarrow q \to \frac{e^{-\beta}}{\beta} \qquad (A-33)$$

In order to use condition (A-33) to fix "a", we must differentiate (A-32) with respect to "q". But at first we note that:

$$\ln(\beta q) = -\beta s < 0 \text{ (since } s, \beta \geq 0),$$

which means that we must take the negative sign on the RHS of (A-32) (since the integrand and the upper limit are positive). So:

$$\frac{d}{dq}(\ln(\beta q)) = \frac{1}{q} = -\frac{d}{dq}\int_0^{\frac{\phi}{\sqrt{q}}} \frac{dz'}{\sqrt{a + \frac{z'^2}{4} - \frac{4}{\beta}\ln(z')}} \qquad (A-34)$$

$$\frac{1}{q} = -\frac{d}{dq}\left(F\left(\frac{\phi}{\sqrt{q}}\right) - F(0)\right) \qquad (A-35)$$

where F is a primitive of the integral, which implies that:

$$\frac{1}{q} = -\frac{dF(\phi/\sqrt{q})}{dq} = -\frac{\frac{1}{\sqrt{q}}\frac{d\phi}{dq} - \frac{\phi}{2q\sqrt{q}}}{\sqrt{a + \frac{\phi^2}{4q} - \frac{4}{\beta}\ln(\frac{\phi}{\sqrt{q}})}} \qquad (A-36)$$

Applying condition (A-33) to (A-36), we get:

$$\frac{1}{q} = \frac{\phi/(2q\sqrt{q})}{\sqrt{a + \frac{\phi^2}{4q} - \frac{4}{\beta}\ln(\frac{\phi}{\sqrt{q}})}} \text{ at } q \to \frac{e^{-\beta}}{\beta} \qquad (A-37)$$

which imposes:

$$a = \frac{4}{\beta}\ln\left(\frac{\phi}{\sqrt{q}}\right) \text{ evaluated at } q = \frac{e^{-\beta}}{\beta} \qquad (A-38)$$

With this value of "a", (A-32) becomes:

$$\ln(\beta q) = -\int_0^{\frac{\phi}{\sqrt{q}}} \frac{dz'}{\sqrt{\frac{z'^2}{4} - \frac{4}{\beta}\ln(\frac{z'}{\epsilon})}} \qquad (A-39)$$

where $\epsilon = \left(\frac{\phi}{\sqrt{q}}\right)_{q=\frac{e^{-\beta}}{\beta}}$ (A-40)

To simplify (A-39) even further, we must introduce some more transformations:

$$r = \sqrt{q\beta} \qquad (A-41)$$

$$\theta = \frac{\phi}{\epsilon\sqrt{q}} \qquad (A-42)$$

$$\theta_1 = \frac{z'}{\epsilon} \qquad (A-43)$$

$$\mu = \frac{8}{\beta\epsilon^2} \qquad (A-44)$$

to arrive at:

$$\ln(r^2) = 2\ln(r) = -2\int_0^{\epsilon\theta} \frac{dz'}{\sqrt{z'^2 - \frac{16}{\beta}\ln(z'/\epsilon)}} \qquad (A-45)$$

$$\ln(r) = -\int_0^{\theta} \frac{\epsilon\, d\theta_1}{\sqrt{\epsilon^2\theta^2 - \frac{8}{\beta}\ln(\theta_1^2)}} \qquad (A-46)$$

$$\ln(r) = -\int_0^{\theta} \frac{d\theta_1}{\sqrt{\theta_1^2 - \mu\ln(\theta_1^2}} \qquad (A-47)$$

Now we must replace condition (A-40) by a condition on μ, which is equivalent according to (A-44). Putting (A-40) into (A-42), we see that when $q = (e^{-\beta}/\beta)$, $\theta = 1$, which transforms (A-47) for this particular case to:

$$\beta = 2\int_0^{1} \frac{d\theta_1}{\sqrt{\theta_1^2 - \mu\ln(\theta_1^2)}} \qquad (A-48)$$

which is a completely deterministic equation for μ since β is a known constant and θ_1 a dummy variable. We will now

return to the original variables to find c(η). First from (A-14), (A-42):

$$\eta = -\frac{1}{2}\frac{d\phi}{dq} = -\frac{1}{2}\frac{d}{dq}(\epsilon\theta\sqrt{q}) \tag{A-49}$$

$$\eta = -\frac{\epsilon}{2}\left(\frac{\theta}{2\sqrt{q}} + \sqrt{q}\frac{d\theta}{dq}\right) \tag{A-50}$$

$$\eta = -\frac{1}{2}\sqrt{\frac{8}{\beta\mu}}\left(\frac{\theta\sqrt{\beta}}{2r} + \frac{r}{\sqrt{\beta}}\left(\frac{\beta}{2r}\right)\frac{d\theta}{dr}\right) \tag{A-51}$$

$$\eta = \frac{-1}{\sqrt{2\mu}}\left(\frac{\theta}{q} + \frac{d\theta}{dr}\right) \tag{A-52}$$

where:

$$r = \exp\left(-\int_0^{\theta}\frac{d\theta_1}{\sqrt{\theta_1^2 - \mu\ln(\theta_1^2)}}\right) \tag{A-53}$$

giving:

$$\frac{dr}{d\theta} = -\frac{r}{\sqrt{\theta^2 - \mu\ln(\theta^2)}} \tag{A-54}$$

or:

$$\frac{d\theta}{dr} = -\frac{\sqrt{\theta^2 - \mu\ln(\theta^2)}}{r} \tag{A-55}$$

and putting in (A-52):

$$\eta = \frac{-1}{\sqrt{2\mu}}\left(\theta - \sqrt{\theta^2 - \mu\ln(\theta^2)}\right)\exp\left(\int_0^{\theta}\frac{d\theta_1}{\sqrt{\theta_1^2 - \mu\ln(\theta_1^2)}}\right) \tag{A-56}$$

We also have, from (A-10), (A-41):

$$\frac{e^{-\beta s}}{\beta} = q \Rightarrow -\beta s = \ln(\beta q) \Rightarrow s = \frac{\ln(r^2)}{-\beta} \tag{A-57}$$

giving, by (A-47):

$$s = \frac{-2\ln(r)}{\beta} = \frac{2}{\beta}\int_0^{\theta} \frac{d\theta_1}{\sqrt{\theta_1^2 - \mu\ln(\theta_1^2)}} \qquad \text{(A-58)}$$

and s is related to c by (A-1), giving:

$$c = \frac{1 - e^{s\ln(1-\hat{\alpha})}}{\hat{\alpha}} = \frac{1 - e^{-\beta s}}{\hat{\alpha}} \qquad \text{(A-59)}$$

so that:

$$c = \frac{1}{\hat{\alpha}}\left(1 - \exp\left(-2\int_0^{\theta} \frac{d\theta_1}{\sqrt{\theta_1^2 - \mu\ln(\theta_1^2)}}\right)\right) \qquad \text{(A-60)}$$

Equations (A-60) and (A-56) together form a parametric solution for $c(\eta)$ as $c(\theta)$ with $\eta(\theta)$.

APPENDIX B

FLOW CHARTS OF MAIN COMPUTER PROGRAMS WRITTEN FOR THIS WORK

A. PROGRAM DBLDFS to calculate the concentration profile resulting from ion-exchange.

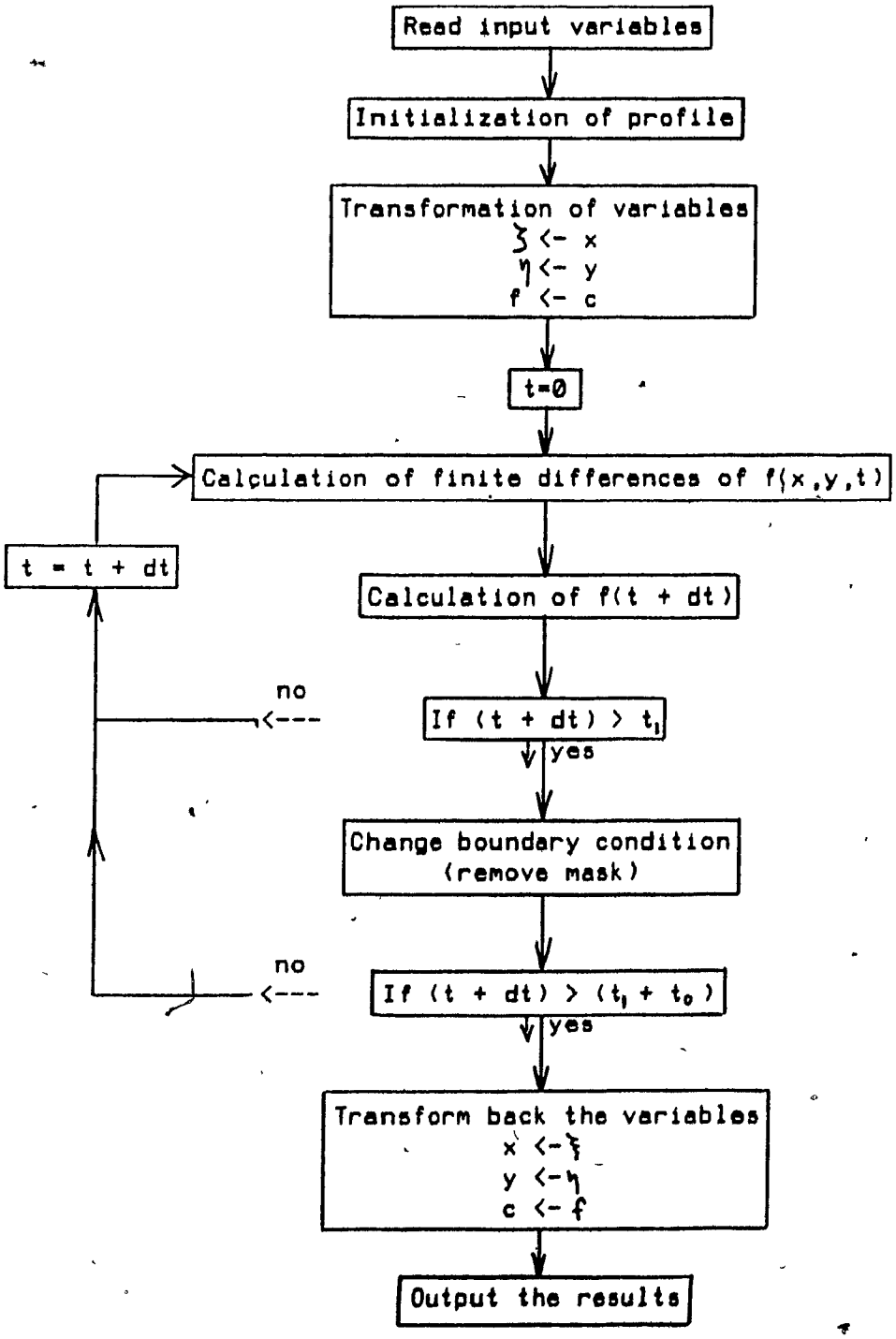

B. PROGRAM BETA2D to calculate the mode and propagation constant of a channel guide by the Rayleigh-Ritz method

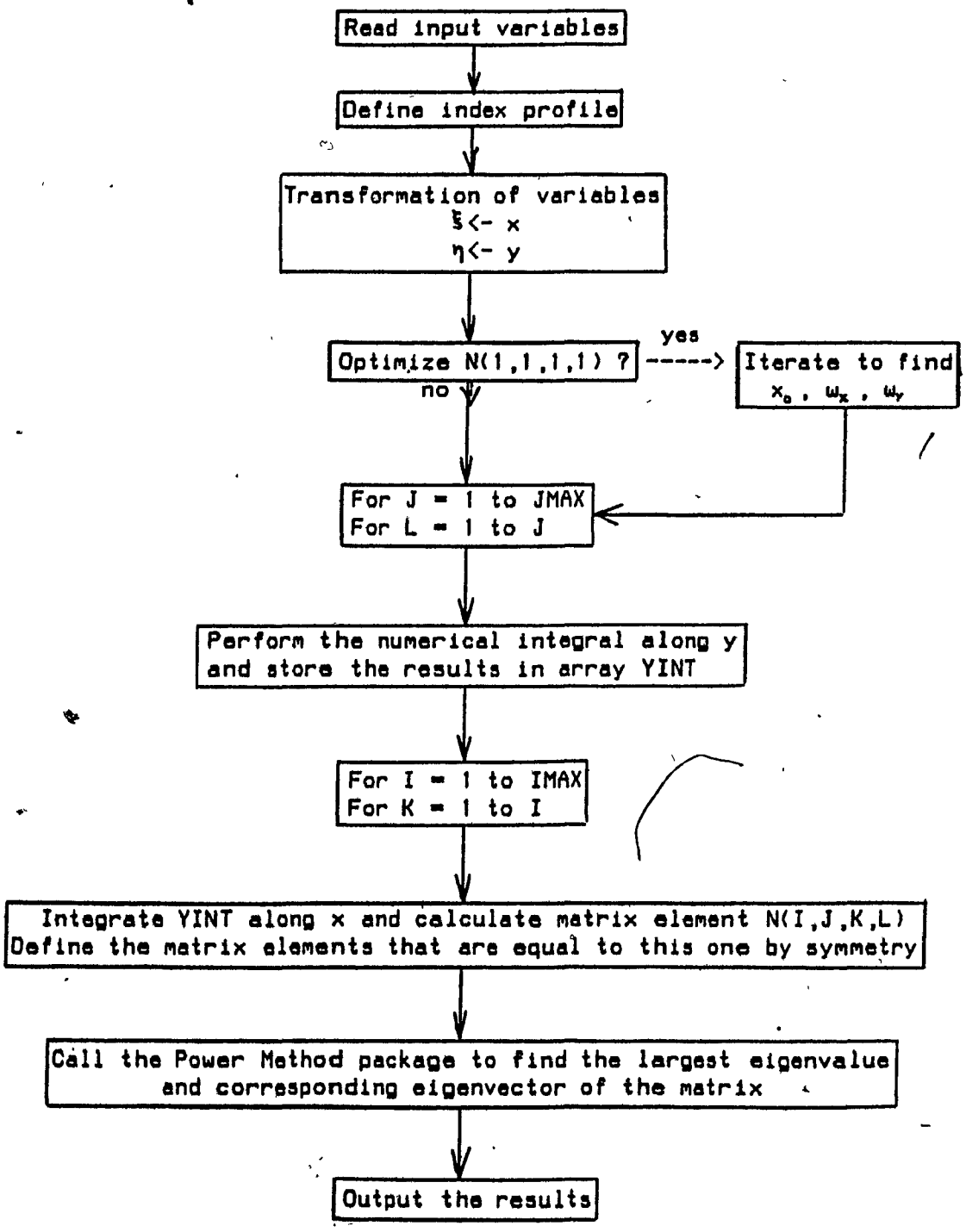

Note: In the one-dimensional equivalent of this program, the integration along y is not performed and the array XINT is defined by the values of the integrand at the corresponding x positions.

REFERENCES

a) General recent references

- Special journal issues: IEEE J. Quantum Electron. QE-22, no.6, June 1986 and J. Lightwave Technol. LT-4, no.10, October 1986

- Conference proceedings: Technical Digest of the Topical Meeting on Integrated and Guided-Wave optics, 26-28 February 1986, Atlanta GA, and Technical Digest of the Optical Fiber Communication Conference, February 1987, Reno NV

- Books: [Hunsperger 1984, Jeunhomme 1983], see below

b) Specific references

Abramovitz, M. and I. A. Stegun. 1965. *Handbook of mathematical functions with formulas, graphs and mathematical tables.* National Bureau of Standards Applied Mathematics Series, Vol. 55, National Bureau of Standards, Washington, D. C.

Adams, M. J. 1981. *An Introduction to Optical Waveguides.* John Wiley and Sons, New York

Aksenov, E. T., A. V. Kukharev, A. A. Lipovskii, and A. V. Pavlenko. 1982. "Fabrication of optical waveguides in glasses by diffusion from nitrate melts," Sov. Phys. Tech. Phys. 27, pp.1472-1475

Aksenov, E. T., A. A. Lipovskii, and A. V. Pavlenko. 1981. "Fabrication of low-mode optical waveguides of increased

thickness in glass," Sov. Phys. Tech. Phys. 26, pp.136-137

Albert, J. and G. L. Yip. 1987a."Wide single-mode channels and directional coupler by two-step ion-exchange in glass," accepted for publication in: IEEE J. Lightwave Technol.

Albert, J. and G. L. Yip. 1987b."Stress-induced index change for K^+-Na^+ ion exchange in glass," Electron. Lett. 23, pp.737-738

Albert, J. and G. L. Yip. 1987c."Theoretical analysis of single-mode channel optical waveguides made by two-step ion exchange in glass," International IEEE AP-S Symposium and URSI Radio Science meeting, June 15-19 1987, Blacksburg, Virginia

Albert, J. and G. L. Yip. 1986. "Wide-channel passive single-mode directional couplers in glass with adjustable power transfer," Technical Digest of the 12th European Conference on Optical Communication, Barcelona (Spain), pp.373-376

Albert, J. and G. L. Yip. 1985. "Refractive index profiles of planar waveguides made by ion-exchange in glass," Appl. Opt. 24, pp.3692-3693

Anderson, I. 1979. "On the coupling of degenerate modes on non-parallel dielectric waveguides," Microwaves, Opt. and Acoust. 3, pp.56-58

Auracher, F. 1983. "Principles and performance of access couplers for multimode fibers and devices for wavelength division multiplexing," in *Integrated Optics*, S. Martellucci and A. N. Chester (eds.), Plenum, New York,

pp.123-138

Baba, K., K. Shiraishi, O. Hanaizumi, and S. Kawakami. 1984. "Buried ion-exchanged optical waveguides with refractive index profiles controlled by rediffusion," Appl. Phys. Lett. 45, pp.815-817

Bartholomew, R. F. and H. M. Garfinkel. 1980. "Chemical strengthening of glass," in *Glass: Science and technology*, vol. 5, D. R. Uhlmann and N. J. Kreidl (eds.), Academic Press, New York

Bergh, R. A., G. Kotler, and H. J. Shaw. 1980. "Single mode fiber optic directional coupler," Electron. Lett. 16, pp.260-261

Born, M. and E. Wolf. 1980. *Principles of Optics*. 6th ed. Pergamon Press, Oxford

Bradenburg, A. 1986. "Stress in ion-exchanged glass waveguides," IEEE J. Lightwave Technol. LT-4, pp.1580-1593 .

Campbell, J. C. 1979. "Tapered waveguides for guided wave optics," Appl. Opt. 18, pp.900-902

Chartier, G., P. J. R. Laybourn, and A. Girod. 1986. "Masking process for double-ion-exchanged glass optical waveguides," Electron. Lett. 22, pp.925-926

Chartier, G. 1983. "Fabrication of surface optical waveguides," in *Integrated Optics*, S. Martellucci and A. N. Chester (eds.), Plenum, New York, pp.49-72

Chartier, G., P. Collier, A. Guez, P. Jaussaud, and Y. Won.

1980. "Graded-index surface or buried waveguides by ion-exchange in glass," Appl. Opt. 19, pp.1092-1095

Chartier, G., P. Jaussaud, A. D. de Olivera and O. Parriaux. 1978. "Optical waveguides fabricated by electric-field controlled ion exchange in glass," Electron. Lett. 14, pp.132-134

Chang, S. 1987. "A coupled mode formulation by reciprocity and a variational principle," J. Lightwave Technol. LT-5, pp.5-15

Cline, T. W. 1986. "Diffused channel glass waveguide optical splitters," Technical Digest of the 1986 Integrated and guided-wave optics meeting IGWO'86, Atlanta, Georgia, paper FDD4

Cochrane, P., R. D. Hall, J. P. Moss, R. A. Betts and L. Bickers. 1986. "Local-line single-mode optics - Viable options for today and tomorrow," IEEE J. Select. Areas Commun. SAC-4, pp.1438-1445

Conte, S. D. and C. de Boor. 1980. *Elementary Numerical Analysis*. McGraw-Hill, New York

Crank, J. 1975. *The Mathematics of Diffusion*. 2nd ed. Clarendon Press, London

Crank, J. 1956. *The Mathematics of Diffusion*. Oxford University Press, London

Ctyroky, J. 1984a. "Theory of coupling loss of an ion exchanged multimode channel waveguide to optical fibers," J. Opt.

Commun. 5, pp.93-99

Ctyroky, J., M. Hofman, J. Janta, and J. Schrofel. 1984b. "3-D analysis of $LiNbO_3$: Ti channel waveguides and directional couplers," IEEE J. Quantum Electron. QE-20, pp.400-409

Cullen, T. J. and C. D. W. Wilkinson. 1984. "Radiation losses from single-mode optical Y junctions formed by silver-ion exchange in glass," Opt. Lett. 10, pp.134-136

Cullen, T. J., C. N. Ironside, C. T. Seaton, and G. I. Stegeman. 1986. "Semiconductor-doped glass ion-exchanged waveguides," Appl. Phys. Lett. 49, pp.1403-1405

Danko, J. J. and J. R. Haavisto. 1985. "Modal conversion in a gradient-index channel waveguide due to boundary perturbations," J. Lightwave Technol. LT-3, pp.176-183

Donnelly, J. P., N. L. DeMeo and G. A. Ferrante. 1983. "Three-guide optical couplers in GaAs," J. Lightwave Technol. LT-1, pp.417-424

Doremus, R. H. 1973. *Glass Science*. Wiley, New York

Doremus, R. H. 1969. "Ion exchange in glasses," in *Ion-Exchange*, Vol. 2, J. A. Marinsky, ed., Dekker, New York

Dwight, H. B. 1961. *Tables of integrals and other mathematical data*. Fourth ed. 1961. Macmillan, New York

Fantone, S. D. 1983. "Refractive index and spectral models for gradient-index materials," Appl. Opt. 22, pp.432-440

Feit, M. D., J. A. Fleck Jr. and L. McCaughan. 1983. "Comparison

of calculated and measured performance of diffused channel-waveguide couplers," J. Opt. Soc. Am. 73, pp.1296-1303

Finak, J., H. Jerominek, Z. Opilski and K. Wojtala. 1982. "Planar diffusion glass waveguides obtained by immersing in molten KNO_3," Opt. Appl. 12, pp.11-17

Findakly, T. 1985. "Glass waveguides by ion-exchange: a review," Opt. Eng. 24, pp.244-250

Findakly, T. and B. Chen. 1982. "Single-mode integrated optical 1×N star coupler," Appl. Phys. Lett. 40, pp.549-550

Findakly, T. and E. Garmire. 1980. "Reduction and control of optical waveguide losses in glass," Appl. Phys. Lett. 37, pp.855-856

Findakly, T. and C. Chen. 1978. "Optical directional couplers with variable spacing," Appl. Opt. 17, pp.769-773

Forrest, K., S. J. Pagano and W. Viehmann. 1986. "Channel waveguides in glass via silver-sodium field-assisted ion exchange," J. Lightwave Technol. LT-4, pp.140-150

Frederikse, H. P. R. 1981. "Solid state physics," in *Physics Vade Mecum*, H. L. Anderson (ed.), American Institute of Physics, New York

Frischat, G. H. 1975. *Ionic Diffusion in Oxide Glasses*. Trans Tech Publications, Bay Village, Ohio

Garmire, E. M. and K. Honda. 1986. "Depolarization in channel glass waveguides," J. Lightwave Technol. LT-4, pp.220-227

Garmire, E. M. 1979. "Semiconductor component for monolithic applications," in *Integrated Optics*, T. Tamir (ed.), Springer Verlag, New York

Gedeon, A. 1974. "Comparison between rigorous theory and WKB-analysis of modes in graded-index waveguides," Opt. Comm. 12, pp.329-332

Gerald, C. F. 1970. *Applied Numerical Analysis*, Addison-Wesley, Reading MA

Giallorenzi, T. G., E. J. West, R. Kirk, R. Ginther, and R. A. Andrews. 1973. "Optical waveguides formed by the thermal migration of ions in glass," Appl. Opt. 12, pp.1240-1245

Gortych, J. E. and D. G. Hall. 1986a. "Fabrication of planar optical waveguides by K^+-ion exchange in BK7 and Pyrex glass," IEEE J. Quantum Electron. QE-22, pp.892-895

Gortych, J. E. and D. G. Hall. 1986b. "Fabrication of planar optical waveguides by K^+ ion exchange in BK7 glass," Opt. Lett. 11, pp.100-102

Gould, S. H. 1966. *Variational methods for eigenvalue problems*. 2nd ed. University of Toronto Press, Toronto

Griffiths, G. and P. J. Khan. 1981. "Analysis of planar optical waveguide fabrication by ion exchange in glass," IEEE J. Quantum Electron. QE-17, pp.529-535

Hammer, J. M. 1979. "Modulation and switching of light in dielectric waveguides," in *Integrated Optics*, T. Tamir

(ed.), Springer Verlag, New York

Hardy, A. and W. Streifer. 1985. "Coupled-mode theory of parallel waveguides," J. Lightwave Technol. LT-3, pp.1135-1146

Haruna, M., M. Belanger and G. L. Yip. 1985. "Passive 3-branch optical power divider by K^+-ion exchange in glass," Electron. Lett. 21, pp.535-536

Haruna, M. and J. Koyama. 1984. "Thermo-optic waveguide interferometric modulator/switch in glass," IEE Proc. pt. H 31, pp.322-324

Haus, H., W. P. Huang, S. Kawakami and N. A. Whitaker. 1987. "Coupled-mode theory of optical waveguides," J. Lightwave Technol. LT-5, pp.16-23

Helfferich, F. and M. S. Plesset. 1957. "Ion exchange kinetics. A nonlinear diffusion problem," J. Chem. Phys. 28, pp.418-424

Hinkov, V. 1982. "In-diffused passive elements of integrated optics in ion-exchanged waveguides," Wave Electron. 4, pp.147-152

Hocker, G. B. and W. K. Burns. 1977. "Mode dispersion in diffused channel waveguides by the effective index method," Appl. Opt. 16, pp.113-118

Hocker, G. B. 1976. "Strip-loaded diffused optical waveguides," IEEE J. Quantum Electron. QE-12, pp.232-236

Hocker, G. B. and W. K. Burns. 1975. "Modes in diffused optical

waveguides of arbitrary index profile," IEEE J. Quantum Electron. QE-11, pp.270-276

Honda, K., E. M. Garmire, and K. E. Wilson. 1984. "Characteristics of an integrated optics ring resonator fabricated in glass," IEEE J. Lightwave Technol. LT-2, pp.714-718

Houde-Walter, S. N. and D. T. Moore. 1985. "Gradient-index profile control by field-assisted ion exchange in glass," Appl. Opt. 24, pp.4326-4333

Huggins, M. L. 1940."The refractive index of silicate glasses as a function of composition," J. Opt. Soc. Am. 30, pp.495-504

Hunsperger, R. G. 1984. *Integrated optics*. 2nd ed. Springer Verlag, New York

Izawa, T. and H. Nakagome. 1972. "Optical waveguide formed by electrically induced migration of ions in glass plates," Appl. Phys. Lett. 21, pp.584-586

Jackel, J. L., K. Y. Lee and F. J. Favire. 1985. "Do glass waveguides depolarize?," J. Lightwave Technol. LT-3, pp.818-819

Jahnke, E. and F. Emde. 1945. *Tables of Functions with Formulae and curves*. 4th ed. Dover Publications, New York

Janta, J. and J. Ctyroky. 1978. "On the accuracy of WKB analysis of TE and TM modes in planar graded-index waveguides," Opt.

Comm. 25, pp.49-52

Jeunhomme, L. B. 1983. *Single-mode fiber optics.* Dekker, New York

Kapron, F. P., D. B. Keck and R. D. Maurer. 1970. "Radiation losses in glass optical waveguides," Appl. Phys. Lett. 17, pp.423-425

Kawasaki, B. S. and K. O. Hill. 1977. "Low-loss access coupler for multimode optical fiber distribution networks," Appl. Opt. 16, pp.1794-1795

Kirby, P. A. and G. H. B. Thompson. 1976. "Channelled substrate buried heterostructure GaAs-(GaAl)As injection lasers," J. Appl. Phys. 47, pp.4578-4589

Kistler, S. S. 1962. "Stresses in glass produced by nonuniform exchange of monovalent ions," J. Am. Ceram. Soc. 45, pp.59-68

Knox, R. M. and P. P. Toulios. 1970. "Integrated circuits for the millimeter through optical frequency range," in *Proceedings of the MRI Symposium on Submillimeter waves,* J. Fox (ed.), Polytechnic Press, New York, pp.497-516

Kogelnik, H. 1983. "Integrated optics devices for optical communications," in *Integrated Optics,* S. Martellucci and A. N. Chester (eds.), Plenum, New York, pp.1-10

Kogelnik, H. 1979. "Theory of dielectric waveguides," in *Integrated Optics,* T. Tamir (ed.), Springer Verlag, New York

Lagu, R. K. and R. V. Ramaswamy. 1986. "Process and waveguide parameter relationships for the design of planar silver ion-diffused glass waveguides," J. Lightwave Technol. LT-4, pp.176-181

Lagu, R. K. and R. V. Ramaswamy. 1984. "Fabrication of single mode glass waveguides by electrolytic release of silver ions," Appl. Phys. Lett. 45, pp.117-118

Landau, L. D. and E. M. Lifshitz. 1969. *Electrodynamique des milieux continus*. Mir, Moscou

Landau, L. D. and E. M. Lifshitz. 1965. *Quantum Mechanics*. 2nd ed. Pergamon Press, New York

Marcatili, E. A. J. 1969. "Dielectric rectangular waveguide and directional coupler for integrated optics," Bell Syst. Tech. J. 48, pp.2071-2102

Marcatili, E. A. J. 1986. "Improved coupled-mode equations for dielectric guides," IEEE J. Quantum Electron. QE-22, pp.988-993

Marcuse, D. 1982. *Light Transmission Optics*, 2nd ed. Van Nostrand, New York, New York

Marom, E., O. G. Ramer and S. Ruschin. 1984. "Relation between normal-mode and coupled-mode analyses of parallel waveguides," IEEE J. Quantum Electron. QE-20, pp.1311-1319

Martin, W. E. 1974. "Refractive index profile measurements of diffused optical waveguides," Appl. Opt. 13, pp.2112-2116

Mathews, J. and R. L. Walker. 1970. *Mathematical Methods of Physics*. 2nd ed. Benjamin-Cummings, Menlo Park, California

Matsuhara, M. and A. Watanabe. 1975. "Coupling of curved transmission lines and application to optical directional couplers," J. Opt. Soc. Am. 65, pp.163-168

Matsuhara, M. 1973. "Analysis of TEM modes in dielectric waveguides, by a variational method," J. Opt. Soc. Am. 63, pp.1514-1517

McHenry, M. A. and D. C. Chang. 1984. "Coupled-mode theory of two nonparallel dielectric waveguides," IEEE Trans. Microwave Theory Tech. MTT-32, pp.1469-1475

Meunier, J. P., J. Pigeon and J. N. Massot. 1983. "A numerical technique for the determination of propagation characteristics of inhomogeneous planar optical waveguides," Opt. Quant. Electron. 15, pp.77-85

Miller, S. E. 1954. "Coupled wave theory and waveguide applications," Bell Sys. Tech. J. 33, pp.661-720

Morey, G. W. 1938. *The Properties of Glass*. Reinhold, New York

Mueller, C. T. and E. Garmire. 1985. "Coupling characteristics of $LiNbO_3$ directional couplers," Appl. Opt. 24, pp.2846-2850

Okamura, Y., S. Sato and S. Yamamoto. 1985. "Simple method of measuring propagation properties of integrated optical

waveguides: an improvement," Appl. Opt. 24, pp.57-60

Okuda, E., I. Tanaka and T. Yamasaki. 1984. "Planar gradient-index glass waveguide and its application to a 4-port branched circuit and star coupler," Appl. Opt. 23, pp.1745-1748

Parriaux, O., J. L. Coutaz, A. Girod, G. H. Chartier and V. Neuman. 1982. "Buried single-mode waveguides in glass," IEEE Trans. Comp. Hybrids Manuf. Technol. CHMT-5, pp.209-211

Pfaender, H. G. 1983. *Schott guide to glass*. Van Nostrand Reinhold, New York

Rahman, B. M. A. and J. B. Davies. 1984. "Finite-element solution of integrated optical waveguides," J. Ligthwave Technol. LT-2, pp.682-687

Rapp, D. 1971. *Quantum Mechanics*. Holt, Rinehart and Winston, New York

Richmond, O., W. C. Leslie, and H. A. Wriedt. 1964. "Theory of residual stresses due to chemical concentration gradients," Trans. ASM 57, pp.294-300

Saad, S. M. 1985. "Review of Numerical methods for the analysis of arbitrarily-shaped microwave and optical dielectric waveguides," IEEE Trans. Microwave Theory Tech. MTT-33, pp.894-899

Schaefer, G. and H. Nassenstein. 1953. "Bestimmung der photoelastischen Konstanten p und q optischer Glaser," Z.

Naturforschg. 8a, pp.90-96

Schiff, L. 1968. *Quantum Mechanics*. 3rd ed. McGraw Hill, New York

Schlaak, H. F., A. Brandenburg and and G. Sulz. 1986. "Integrated optical couplers with circular waveguides," Technical Digest of the 1986 Integrated and guided-wave optics meeting IGWO'86, Atlanta, Georgia, paper THCC8

Schmidt, R. V. 1983. "Integrated optics switches and modulators," in *Integrated Optics*, S. Martellucci and A. N. Chester (eds.), Plenum, New York, pp.181-210

Schulze, G. 1913. "Versuche uber die Diffusion von Silber in Glas," Ann. Physik 40, pp.335-367

Shand, E. B. 1958. *Glass engineering handbook*, 2nd ed. McGraw Hill, New York

Sharma, A., E. Sharma, I. C. Goyal and A. K. Ghatak. 1980. "Variational analysis of directional couplers with graded index profile," Opt. Comm. 34, pp.39-42

Stewart, G. and P. J. R. Laybourn. 1978. "Fabrication of ion-exchanged optical waveguides from dilute silver nitrate melts," IEEE J. Quantum Electron. QE-14, pp.930-934

Stewart, G., C. A. Millar, P. J. R. Laybourn, C. D. W. Wilkinson, and R. M. De LaRue. 1977. "Planar optical waveguides formed by silver migration in glass," IEEE J. Quantum Electron. QE-13, pp.192-200

Suematsu, Y. and K. Kishino. 1977. "Coupling coefficient in

strongly coupled dielectric waveguides," Rad. Sci. 12, pp.587-592

Suhara, T., Y. Handa, H. Nishihara and J. Koyama. 1979. "Analysis of optical channel waveguides and directional couplers with graded-index profile," J. Opt. Soc. Am. 69, pp.807-815

Tamir, T. 1979. "Beam and waveguide couplers," in *Integrated Optics*, T. Tamir (ed.), Springer Verlag, New York

Tangonan, G. L. 1983. "Planar tees and couplers for multimode devices," in *Integrated Optics*, S. Martellucci and A. N. Chester (eds.), Plenum, New York, pp.155-180

Taylor, H. F. 1976. "Dispersion characteristics of diffused channel waveguides," IEEE J. Quantum Electron. QE-12, pp.748-752

Tien, P. K. 1977. "Integrated optics and new wave phenomena in optical waveguides,"Rev. Mod. Phys. 49, pp.361-420

Tsutsumi, K., H. Hirai and Y. Yuba. 1986. "Characteristics of swelling of sodium-potassium ion-exchanged glass waveguides," Electron. Lett. 22, pp.1299-1300

Voges, E. 1983. "Planar tees and star couplers," in *Integrated Optics*, S. Martellucci and A. N. Chester eds., Plenum, New York, pp.139-154

Walker, R. G. and C. D. W. Wilkinson. 1983a."Integrated optical ring resonators made by silver ion-exchange in glass," Appl.

Opt. 22, pp.1029-1035

Walker, R. G., C. D. W. Wilkinson and J. A. H. Wilkinson. 1983b. "Integrated optical waveguiding structures made by silver ion-exchange in glass. 1: The propagation characteristics of stripe ion-exchanged waveguides; a theoretical and experimental investigation," Appl. Opt. 22, pp.1923-1928

Walker, R. G. and C. D. W. Wilkinson. 1983c. "Integrated optical waveguiding structures made by silver ion-exchange in glass. 2: Directional couplers and bends," Appl. Opt. 22, pp.1929-1936

Warren, C., S. Forouhar and W. S. C. Chang. 1983. "Double ion exchanged chirp grating lens in lithium niobate waveguides," Appl. Phys. Lett. 43, pp.424-426

Wilkinson, C. D. W. and R. Walker. 1978. "The diffusion profile of stripe optical waveguides formed by ion exchange," Electron. Lett. 14, pp.599-600

White, J. M. and P. F. Heidrich. 1976. "Optical waveguide refractive index profiles determined from measurement of mode indices: a simple analysis," Appl. Opt. 15, pp.151-155

Wood, V. E. 1976. "Diffusion profiles in ion-exchanged waveguides," J. Appl. Phys. 47, p.3370

Yariv, A. 1973. "Coupled-mode theory for guided-wave optics," IEEE J. Quantum Electron. QE-9, pp.919-933

Yariv, A. 1975. *Quantum Electronics*. 2nd ed. John Wiley and Sons, New York

Yeh, C., K. Ha, S. B. Dong and W. P. Brown. 1979. "Single-mode optical waveguides," Appl. Opt. 18, pp.1490-1504

Yip, G. L. and J. Albert. 1986. "Optical waveguides by K^+-ion exchange in glass," Technical Digest of the Sino-British joint meeting on Optical fiber Communication, Beijing (China), pp.167-171

Yip, G. L. and J. Albert. 1985. "Characterization of planar optical waveguides by K^+-ion exchange in glass," Opt. Lett. 10, pp.151-153

Yip, G. L. and J. Finak. 1984. "Directional-coupler power divider by two-step K^+-ion exchange," Opt. Lett. 9, pp.423-425

Zernike, F. 1979. "Fabrication and measurement of passive components," in *Integrated Optics*, T. Tamir (ed.), Springer Verlag, New York

Zienko, A. A., N. M. Lyndin, V. A. Sychugov, A. V. Tishchenko and G. P. Shipulo. 1979. "Investigation of the parameters of planar optical waveguides fabricated by ion exchange in glass," Sov. J. Quantum Electron. 9, pp.611-613